공 학 박 사 학 위 논 문

Development of High-flux and Anti-fouling Polyamide Thin-film Nanocomposite RO/PRO Membrane through Coating and Embedding of TiO_2 Nanomaterials

타이타니아 나노물질의 코팅 및 첨가를 통한 고투과, 내오염성의 역삼투, 압력지연삼투 폴리아마이드 나노복합막 개발

2016년 8월

서울대학교 대학원

화학생물공학부

김 정 찬

Development of High-flux and Anti-fouling Polyamide Thin-film Nanocomposite RO/PRO Membrane through Coating and Embedding of TiO_2 Nanomaterials

by

Jungchan Kim

under the supervision of

Professor Jeyong Yoon, Ph. D.

A dissertation submitted in partial fulfillment of the requirements for the Degree of
Doctor of Philosophy

AUGUST 2016

SCHOOL OF CHEMICAL AND BIOLOGICAL ENGINEERING
SEOUL NATIONAL UNIVERSITY

Abstract

In this dissertation, development of high performance and fouling resistant PA TFC membrane was implemented by coating and embedding of TiO_2 nanomaterial for RO and PRO applications.

Firstly, the surface of PA TFC membrane was coated with TiO_2 nanoparticles (TNPs) via a sol-gel-derived spray coating method. The optimum TiO_2 nanoparticle coating layer, which is dense and durable without blocking the pore or surface, was formed by base-catalyzed (ammonium hydroxide) TiO_2 sol-gel-derived spray coating. Through this optimized coating condition, the active and support layer of a commercial TFC was coated with TiO_2 nanoparticles (TNPs) for RO and PRO application, respectively. This TNP coating imparted hydrophilic properties and a negative charge to the membrane surface. These modified surface properties reduced the interaction force between humic acid and membrane surface and resulted in the enhancement of fouling resistance in RO and PRO process. The less favorable foulant-membrane interaction of the TNP-coated membrane was confirmed by a lower interaction force between a humic acid-tethered AFM tip and the membrane surface. A TNP coating of support layer increased water flux and reduced reverse salt flux in PRO process, while water flux and salt rejection were maintained when the proper amounts of TiO_2 sol was coated in RO process.

Secondly, TiO_2 nanomaterials embedded polyamide thin-film nanocomposite membrane was fabricated for enhancement of water flux and fouling resistance. In addition, the effect of structure and surface property of nanomaterial on water flux was evaluated by comparison of TiO_2 nanotube (TNT) and TiO_2 nanoparticle (TNP) embedded PA TFN membrane. The TFN RO membranes containing TNT or TNP exhibited similarly high hydrophilicities and enhanced water permeability compared with a conventional RO membrane. Although TNP TFN RO membrane has similar surface hydrophilicity with TNT TFN RO membrane when the same amount of TNP and TNT are embedded, the TNT TFN RO membranes had better water permeability than the TNP TFN RO membranes. Compared with non-porous TNP, nanochannels of TNT provided additional enhanced water permeability by serving as water transport passageways.

From these results, it is expected that the addition of TiO_2 nanomaterials in PA TFC membrane can enhance the performance and fouling resistance in RO and PRO process.

Keywords: TiO_2 sol-gel-derived spray coating; surface modification; TiO_2 nanocomposite membrane; pressure retarded osmosis; reverse osmosis

Student number: 2009-23948

Table of contents

List of Figures

List of Tables

1. Introduction

1.1. Research background

Conventional energy generation depends on nuclear, oil, coal or natural gas [1, 2]. However, the consumption of these fossil fuel-based sources and nuclear energy has been associated with various environmental problems, such as emission of harmful chemicals and greenhouse gases, and the generation of nuclear waste[3-5]. Furthermore, A World Resources Institute forecasted that water scarcity will be severe owing to extreme growth of world population [6]. Consequently, demands for renewable energy and new sources of fresh water have increased [7].

In order to solve these problems, reverse osmosis (RO) process and pressure retarded osmosis (PRO) process have been developed for producing of fresh water and renewable energy, respectively [8-10]. RO process is a pressure-driven process that uses a semi-permeable membrane to produce fresh water by removing salt from saline water. Currently, no less than 15,000 desalination plants have been constructed, and RO process comprises approximately 50% of those plants [11]. Pressure retarded osmosis (PRO) is a type of membrane-based, salinity-gradient energy generation process. PRO can theoretically produce 2,000 TWh/year, assuming a 0.8 kWh/m^3 power density at 2.9 × 10^9 m^3/h of productivity when using fresh water and seawater as feed and draw solutions, respectively [12].

Polyamide (PA) thin-film composite (TFC) membrane comprise over 90% of

the market for RO/NF process [13]. Moreover, PA TFC membrane has been studied as an alternative to cellulose acetate membrane for pressure retarded osmosis (PRO) process [14]. PA TFC membrane typically consists of polyester non-woven fabric acting as structural support (120~150 μm), a micro porous inter layer (40~50 μm), and polyamide active layer (0.2 μm). PA TFC membrane has many advantages compared to cellulose acetate membrane, such as high water flux and salt rejection, strong mechanical strength, wide operation pH and temperature ranges and resistance to biological decomposition [13]. In spite of these advantages, membrane fouling and relatively high energy consumption are considered as the main obstacles of PA TFC membrane [15, 16]. The major factor of total cost for water desalination is energy consumption. In RO process, the specific energy consumption (The energy cost per volume of produced permeate) is substantially high since its high pressure requirement reaches up to approximately 70 bar [17]. On the other hand, membrane fouling is referred to deposition of foulants such as particulate or dissolved organic matter, dissolved solids and microorganism at the membrane surface or inside pore [11]. Deposition of foulants increase hydraulic resistance, reduce water flux and increase concentration polarization which lead to decrease of salt rejection. Fouled membrane requires washing with chemicals to recover membrane performance. Frequent chemical cleaning and irreversible membrane fouling shorten membrane life and replacement period of membrane [18]. These frequent chemical cleaning and reduced membrane life, consequently, results in increase of operation cost.

Addition of nanomaterials, such as zeolite, CNT, graphene, SiO_2, silver and TiO_2 on surface or inner layer of PA TFC membrane have been studied to overcome the energy consumption and membrane fouling problems [19]. Among reported nanomaterials for membrane application, TiO_2 nanomaterials have been frequently used to enhance membrane performance factors, such as water permeability and anti-fouling properties. Titanium dioxide (TiO_2) is a cost-effective, biocompatible, and photocatalytic material that has been applied to dye-sensitized solar cells, photoelectrolytic cells and also has been used in water treatment membranes [20-23]. An amino-functionalized TiO_2 nanotube (TNT)-embedded PA thin-film nanocomposite membrane demonstrated high water permeability and organic fouling resistance due to the hydrophilic properties and nanoporous structure of TNT [24]. The addition of TiO_2 nanoparticles (TNPs) in the active layer or the support layer of PA TFC membranes have been shown to enhance surface hydrophilicity, which results in increased water flux in RO and FO processes [25, 26]. The TNPs were self-assembled on the PA TFC membrane surface by a dip coating method. Under UV light, organic foulants were detached via a self-cleaning effect, and microorganisms were inactivated [27-29]. In case of TiO_2 coating on membrane, only dip coating method was used in previous studies. Through dip coating, large surface can be easily coated with TiO_2. However, the typically slow coating rate (e.g., a few millimeters per second) could be an obstacle for the large-scale manufacturing of such membranes [30-32]. Moreover, to my best knowledge, the effect of TiO_2 nanoparticle coating of PA

TFC membrane in PRO process have not yet been investigated. It is hypothesized that TiO_2 coating of PA TFC membrane support layer can enhance performance of PRO process, since the surface hydrophilicity of support layer is also very important factor affecting water flux and fouling property in PRO process. Therefore, the development of novel coating method for fast and facile membrane coating with TiO_2 is required for RO and PRO applications.

In addition, the effects of structural properties of embedded nanomaterial on membrane performance has yet to be verified. Furthermore, the effects of the embedded nanomaterials and their hydrophilic and void space contributions on performance enhancement in TFN RO membranes have to be identified. Therefore, the effect of structural properties of embedded nanomaterial on membrane performance was evaluated using TiO_2 nanoparticle and TiO_2 nanotube.

1.2. Objectives

In this dissertation, the enhancement of water flux and fouling resistance of PA TFC membrane in reverse osmosis (RO) and pressure retarded osmosis (PRO) process was implemented by addition of TiO_2 nanoparticles and nanotubes. For this purpose, following two topic of studies were conducted.

Firstly, polyamide (PA) thin-film composite (TFC) membrane was coated with TiO_2 nanoparticle (TNP) and the effect of TNP coating on water flux, salt rejection, and fouling resistance were evaluated in RO/PRO processes. The optimum synthesis condition of TiO_2 sol for sol-gel-derived spray coating method was investigated by evaluating the effect of base material, solution, additive, and catalysts. To find the appropriate coating condition of TiO_2 sol on PA TFC membrane, the water flux and salt rejection changes were evaluated using lab-scale cross-flow osmotically or pressure driven membrane system with varying coating amount of TiO_2 sol. The surface morphology and property of TNP coated membranes were analyzed by SEM, EDS, XPS, FT-IR, contact angle, and zeta potential. Fouling resistance was evaluated as the degree of water flux reduction when humic acid was added to the feed solution.

Secondly, TiO_2 nanotube (TNT) and TiO_2 nanoparticle (TNP) embedded PA thin-film nanocomposite (TFN) membranes were synthesized to enhance the water flux of PA RO membrane. By using a same material, both the TNT and

TNP TFN RO membranes might have similar hydrophilicity which could independently evaluate the effect of the nanomaterial structure on the performance of the TFN RO membrane. The morphology of the TNT and TNP structures were analyzed by SEM and TEM. The TNT and TNP TFN RO membranes were fabricated by interfacial polymerization. The surface properties of these TFN RO membranes were analyzed by SEM, EDS, and contact angle measurement. Water flux and salt rejection were measured in a lab-scale cross-flow RO filtration system.

2. Literature review

2.1. Membrane fouling and surface property of antifouling membrane

Membrane fouling is defined as deposition of deposition of foulants such as particulate or dissolved organic matter, dissolved solids and microorganism at the membrane surface or inside pore [15, 16]. Deposited foulant increase hydraulic resistance and concentration polarization on membrane. These phenomena can result in reduction of the water flux and salt rejection in RO process or power generation in PRO process.

Membrane fouling can be divided in two types: surface fouling and internal (pore) fouling. Since there is no distinguishable pores on active layer of PA TFC membrane, surface fouling is dominantly observed in RO process. In case of PRO process, foulants retained in feed water can be deposited not only on surface but also inner pore of porous support layer. Therefore, more severe membrane fouling have been reported to occur on porous support layers in PRO processes [33, 34].

Deposition of foulant on membrane is initiated from interaction between foulant and membrane surface, hence the fouling characteristics of a membrane is affected by its surface property such as hydrophilicity, morphology, and surface charge [35]. Fig. 2-1 shows surface property factors for anti-fouling membrane. In

general, hydrophilic, smooth, and negatively charged membranes are known to have resistance to the fouling because foulant (i.e. protein and humic acid) naturally has the hydrophobic and negatively charged surface property [36]. However, in case of biofouling, our previous study suggested that surface property has no correlation with membrane surface property since the biofilm is formed on membrane surface after organic foulant covered the membrane surface [37].

Surface hydrophilicity

It is generally accepted that as hydrophilicity of membrane increases, membrane show better fouling resistance. Hydrophobic membrane tends to be fouled more easily than hydrophilic membrane because most foulants exist in water such as natural organic matter (NOM) or protein have hydrophobic surface property [36]. In addition, it is insisted that a formation of pure water layer via hydrogen bond on hydrophilic membrane surface can prevent the attachment and the deposition of hydrophobic foulant [38].

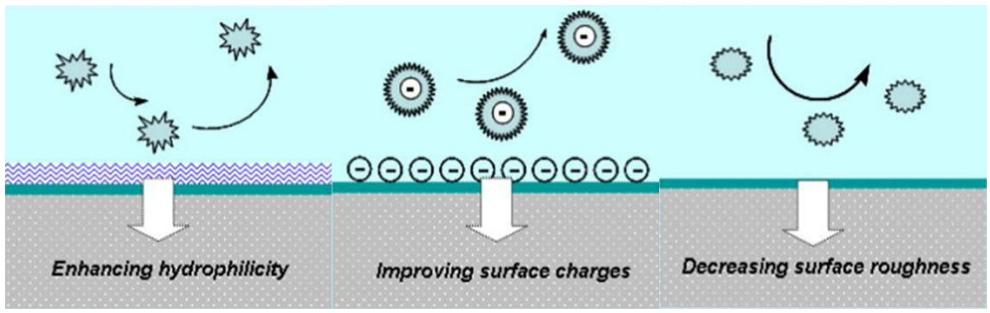

Fig. 2-1. Schematic diagrams of surface properties affecting on membrane fouling [38].

Surface charge

Surface charge is also regarded as important surface property for fouling resistance of membrane. Charged membrane surface repulses co-ion by electrostatic repulsive force. Humic acid is a representative type of NOM and has negatively charged surface due to its abundant phenolic and carboxylic functional groups in chemical structure. Moreover, microorganism also have negatively charged surface property. Therefore, synthesis or modification of membrane to have charged surface can prevent the deposition of co-ionically charged foulant by electrostatic repulsive force. Note that a charged membrane surface can repulse a co-ionically charged foulant, on the contrary, draw a counter-ionically charged foulant. Thus, the charge property of membrane should be considered according to target foulant of feed water [38].

Surface roughness

In terms of surface roughness, it is commonly regarded that a smoother surface has less fouling tendency than rough surface because a foulant is more likely to be entrapped in rough surface compared to smoother surface. Elimelech et al. compared the fouling characteristics of cellulose acetate and PA TFC membranes [39]. In colloidal fouling experiment, PA TFC membrane showed higher fouling tendency than cellulose acetate membrane due to higher surface roughness.

However, surface roughness is still remained as controversial factor. For instance, Riedl et al. and Yan et al. reported opposite result to common expectation [40, 41]. The rougher surface represented less fouling tendency under organic particle filtration. Moreover, there are few studies reporting the effect of surface fouling by the deposition of molecules smaller than the surface roughness scale. However, based on intuition, rough and heterogeneous surface is more favorable for attachment of organic particle than a smoother surface. Therefore, in many studies the reduction of surface roughness are generally known to reduce fouling tendency [36].

On the basis of these understanding of membrane fouling mechanism, development of anti-fouling membrane has been implemented via enhancement of surface hydrophilicity or surface charge and reducing surface roughness.

2.2. Surface modification of membrane

Surface modification of conventional membrane is efficient and feasible method for enhancement of fouling resistance. Surface properties (i.e., hydrophilicity, roughness, and surface charge) can be easily modified via surface modification and relevant results have been reported in numerous articles [38]. Surface modification method can be divided to physical and chemical method.

In physical method, surface modification via surface adsorption and surface coating were reported. In previous studies, hydrophilic surfactant and polyelectrolyte were used in surface adsorption method and hydrophilic polymer were commonly used for surface coating method.

Surface adsorption is very simple modification method which absorb surfactant or electrolyte on membrane surface. Wilbert et al. [42] modified commercial cellulose acetate RO/NF membrane and polyamide thin-film composite RO/NF membrane with T-X type and P type surfactants consist of hydrophobic head group and hydrophilic tail. Surfactants were absorbed on membrane surface by soaking method and the effect of the HLB value (ratio of hydrophobic head group length and hydrophilic tail length), and the length of hydrophilic tail on surface property were evaluated. Surfactant absorbed PA membrane showed reduced roughness and enhanced fouling resistance against vegetable broth.

Surface coating is one of the physical modification method and very simple and facile method. Due to its technical convenience, this method have been adapted by many researchers and membrane manufacturers. Hydrophilic polymer (i.e., poly(vinyl alcohol) (PVA) and poly(ethylene glycol) (PEG)) was used for surface coating.

Louie et al. used highly hydrophilic block copolymer as coating material of membrane surface [43]. Figs 2-2(a), (b) and (c) displays chemical structure of PEBAX 1657 which is highly hydrophilic block copolymer, roughness change of SWC4 membrane after PEBAX coating, and fouling property of PEBAX coated SWC4 under oil/surfactant filtration condition, respectively. A commercial membrane was prepared via dip-coating using PEBAX 1657 dissolved *n*-butanol solution. Although the formation of continuous PEBAX 1657 coating layer greatly reduced surface roughness, the water flux of ESPA1, and ESPA3 membrane was largely reduced after coating. PEBAX 1657 coated low flux RO membrane (SWC4) demonstrated significantly enhanced fouling resistance under oil/surfactant/water emulsion filtration condition and showed stable fouling resistance during long-term (106-day) fouling test.

Kim and Lee coated PA RO/NF membrane with PVA to enhance fouling resistance in dyeing waste water treatment process [44]. PVA coating reduced surface roughness and negative charge, increased hydrophilicity and fouling resistance.

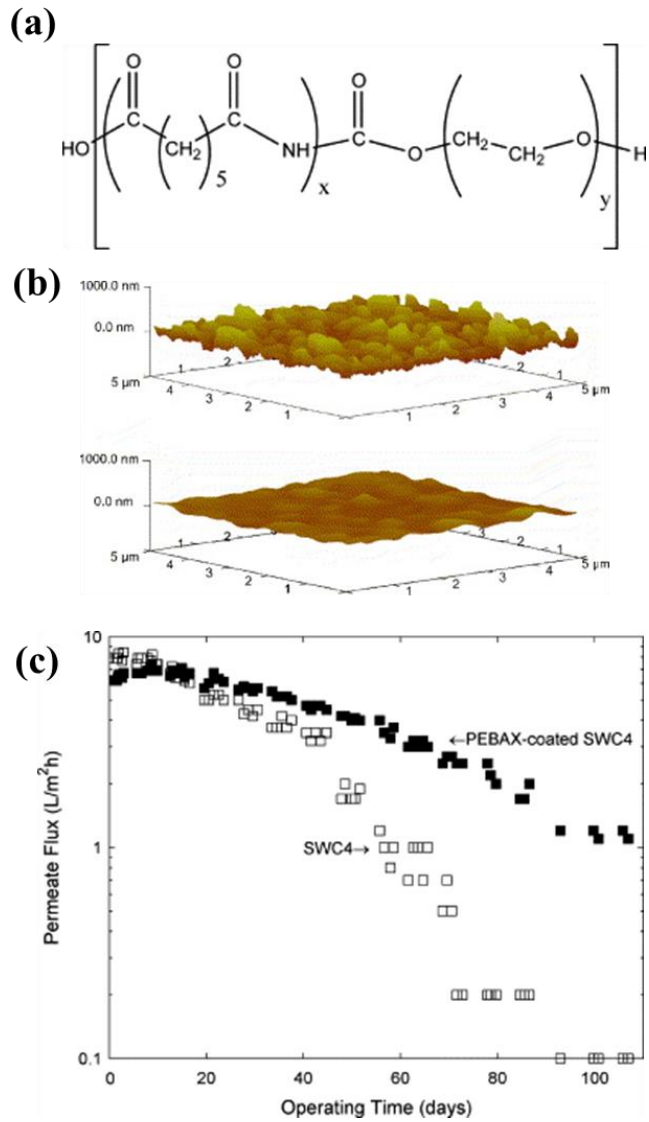

Fig. 2-2. (a) Structure of PEBAX 1657 (b) roughness change of SWC4 membrane after PEBAX coating (c) fouling property of PEBAX coated SWC4 under oil/surfactant filtration condition [43]

Surface modification through chemical method also have been focused on increasing surface hydrophilicity or charge and reducing the roughness. In chemical method, coating of hydrophilic and charged materials are linked to the polymer chain of membrane via chemical treatment such as redox initiating and plasma treatment. Surface hydrophilization treatment, radical grafting, chemical coupling were reported as chemical modification.

Surface hydrophilization treatment is carried out via chemical treatment of membrane with acid or alcohol to enhance surface hydrophilicity and water flux of membrane. Kulkarni et al. treated commercial PA RO membrane (HR95PP, HR 98PP) with hydrofluoric, hydrochloric, sulfuric, phosphoric, nitric acids, ethanol and 2-propanol [45]. The acid treatment caused a partial hydrolysis on membrane surface and resulted in enhancement of surface hydrophilicity. Treatment with ethanol, 2-propanol, hydrofluoric acid, and hydrochloric acid increased water flux without salt rejection loss, while other acids reduced salt rejection.

Radical grafting is an effective method for modification of polymer. Fig. 2-3 shows a schematic diagram of radical grafting procedure [38]. In radical grafting process, an active site—produced by free radical or initiator—reacts with monomer and a branch chain is synthesized at polymer chain. Belfer group reported surface modification of RO/NF membrane via redox initiation and grafting method in several articles [46-49]. The advantage of this method is that various water-soluble monomer can be used since this process is conducted in

water at room temperature. A membrane was soaked in a aqueous solution containing 10 ~ 20% of monomer (acrylic acid (AA), methacrylic acid (MA), polyethylene glycol methacrylate (PEGMA), 3-sulfopropyl methacrylate (SPM), vinylsulfonic acid (VSA) and 2-acrylamido-2-methylpropane-sulfonic acid (AMPS)) with redox initiator ($K_2S_2O_8$ and $Na_2S_2O_5$). After a certain soaking time, membrane was washed with DI water until all residual monomer was removed. Fig. 2-4 shows TEM images of cross-sectional area of NF270 membrane modified with AA. As membrane soaking time increased, thicker polymer layer was formed. The modified membrane demonstrated enhanced hydrophilicity, and negatively charged surface and foulants were more easily removed than the bare membrane.

Chemical coupling method is carried out via chemical reaction of polymer chain-end groups of membrane and epoxy functional group of coating material. The conventional PA membrane contains free carboxylic acid and primary amine groups in its end of polymer chain [50]. These chain end groups can be a reactive site for chemical reaction or chemical coupling. Based on this point, Van Wagner et al. modified commercial PA RO membrane by grafting reaction of uncrosslinked trimesoyl chloride and free primary amine with epoxy end groups of poly(ethylene glycol) diglycidyl ether (PEGDE) [51]. Although modified membrane exhibited no significant change of surface property, enhanced fouling resistance was observed against *n*-decane and SDS.

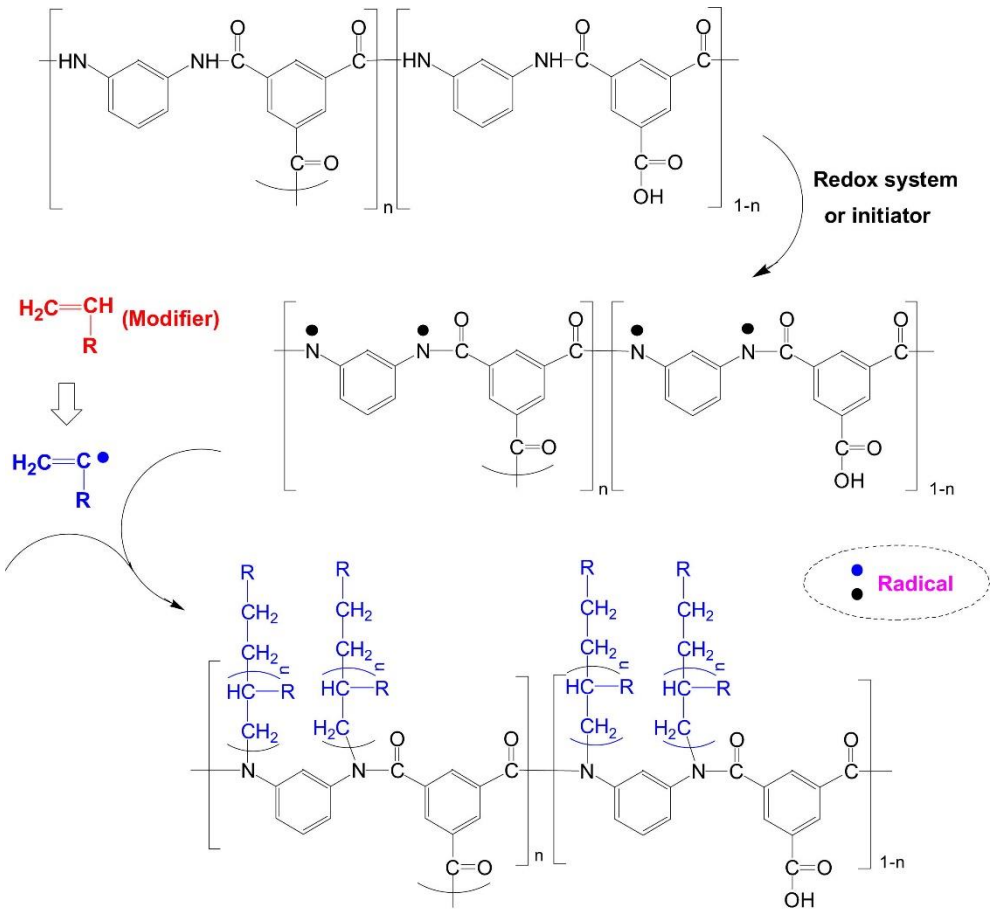

Fig. 2-3. Schematic diagram of radical grafting procedure [38]

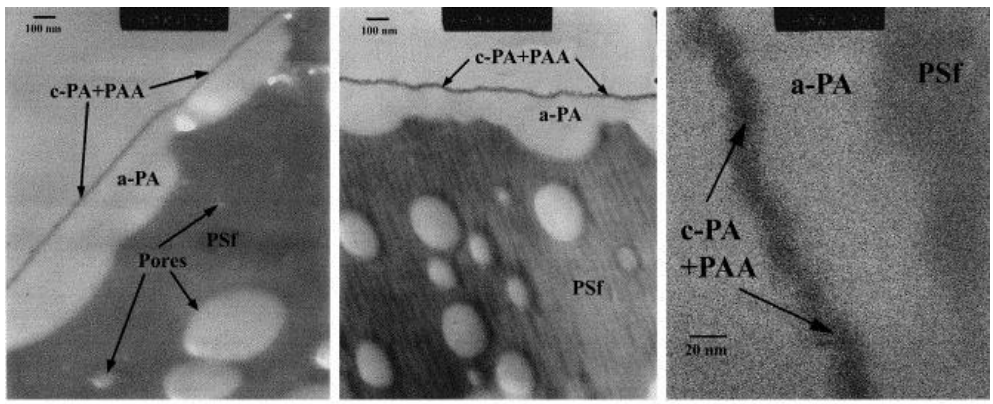

Fig. 2-4. TEM images of cross-sectional area of NF270 membrane (a) very low modification, (b) moderate modification, (c) enlarged image of (b) [48].

2.3. Nanomaterial coated and embedded membranes

Nanomaterial have been used as coating and embedding material for membrane to overcome membrane fouling and high energy consumption owing to high pressure operation in RO process. It is reported that the coating and embedding of nanomaterial enhances fouling resistance through changing surface into hydrophilic and highly charged. Moreover, the embedding of porous nanomaterial into membrane layer enhance permeate flux and fouling resistance of membrane by providing a passageway for water transport. In this dissertation, some articles using TiO_2 nanotube, TiO_2 nanoparticle, zeolite, carbon nanotube and graphene—showed outstanding enhancement in performance and anti-fouling property—were reviewed.

Titanium dioxide (TiO_2) is a cost-effective, biocompatible, and photocatalytic material that has been applied to dye-sensitized solar cells and photoelectrolytic cells and has been used in water treatment membranes [20-23]. In previous studies, TiO_2 nanomaterial (i.e., nanotube and nanoparticle) was used as coating and embedding material for enhancement of water flux and fouling resistance of membrane. Kwak et al. fabricated TiO_2 nanoparticle coated hybrid organic/inorganic PA TFC RO membrane [27, 29]. Polyamide active layer was synthesized via interfacial polymerization of *m*-phenylenediamine (MPD) 2 wt% DI water and trimesoyl chloride (TMC) 0.1 wt% hexane solution. TiO_2 nanoparticle (TNP) was synthesized by sol-gel process. Then, PA TFC RO

membrane was dipped in TNP dispersed solution for 1 h and TNPs were deposited on PA TFC RO membrane surface. Fig. 2-5 shows self-assembly mechanism of TNP on PA membrane. As shown in Fig. 2-5, self-assembling of TNP can be formed by a bidentate coordination of oxygens of carboxyl group to Ti^{4+}, and hydrogen bond between carbonyl group and to a TiO_2 surface hydroxyl group. TiO_2 hybrid PA TFC RO membrane demonstrated enhanced water flux than neat PA TFC RO membrane. Kwak et al. explained this enhanced water flux by following two reasons. Firstly, during the soaking of PA TFC RO membrane in TNP dispersed solution, PA TFC RO membrane was exposed in nitric acid (added as acid catalyst for sol-gel reaction). It is reported that nitric acid hydrolyze membrane surface, increase hydrophilicity, consequently, enhance water flux. Secondly, TiO_2 nanoparticles—attached on membrane surface—might enhance water uptake of membrane. The viability of *E. coli* on TiO_2 hybrid- and neat PA TFC RO membrane was evaluated under dark condition and UV irradiation. TiO_2 hybrid PA TFC RO membrane showed significantly enhanced bactericidal effect under UV irradiation, while showed no difference compared to neat PA TFC RO membrane under dark condition.

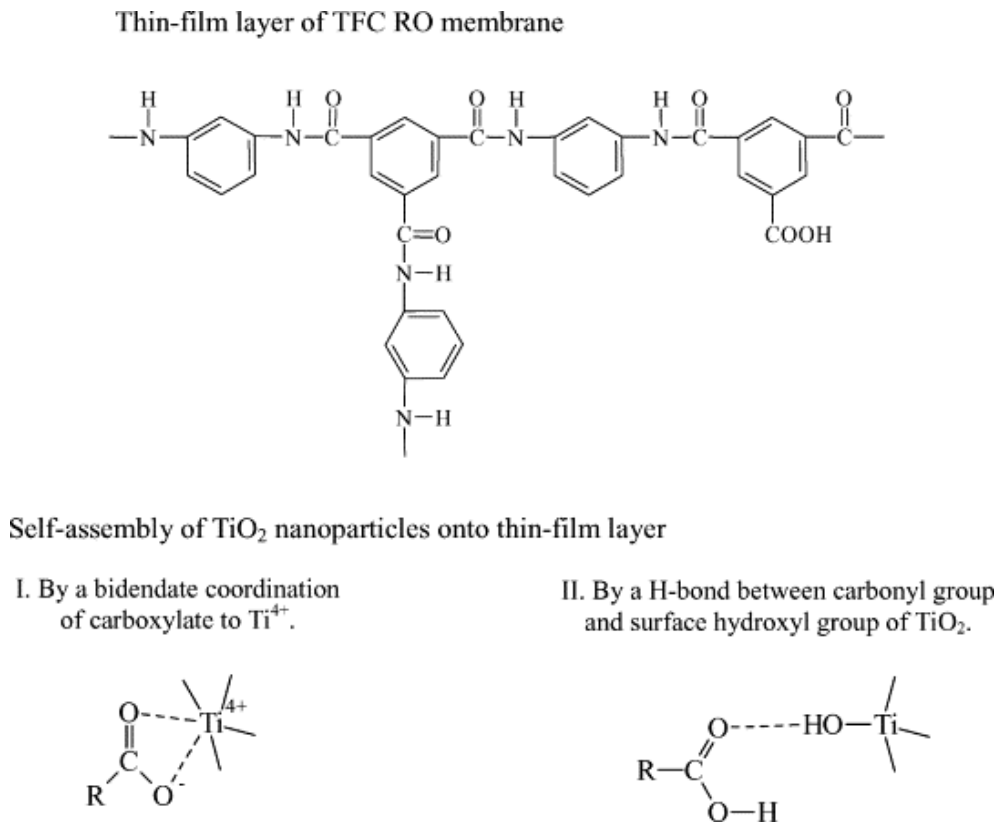

Fig. 2-5. Self-assembly mechanism of TiO_2 nanoparticle on PA membrane [29].

Emadzadeh et al. synthesized NH_2-TiO_2 nanotube (amine functionalized-TNT) embedded PA TFN RO membrane for enhancement of water flux and fouling resistance of conventional PA TFC RO membrane (Fig. 2-6) [24]. TNT was synthesized via hydrothermal reaction using commercial TiO_2 nanoparticle (Degussa P25) and amine functional group was attached on TNT surface through silane coating. The TNT embedded PA TFN RO membrane displayed increased hydrophilicity and fouling resistance in bovine serum albumin filtration test. Moreover, water flux increased with embedding amount of TNT and this result implies that the pore structure of TNT contributed to flux enhancement by serving as water transport passageways.

Jeong et al. used nano-scale zeolite-A as an embedding material for PA TFN RO membrane for water flux enhancement (Fig. 2-7) [52]. The role of zeolite-A was to change surface into hydrophilic and more negatively charged, and act as molecular sieve which provide preferential passageway for water molecule while not allowing a salt molecule to pass. Fig. 2-8 shows TEM images of cross-sectional area and EDX analysis result of plain zeolite-A PA TFN membrane. As we can see from Fig. 2-8(c), a zeolite-A nanoparticle was located in approximately 200 nm thickness of PA layer. As zeolite-A loading increased, hydrophilicity and negative charge increased and surface roughness degreased. The water flux was dramatically increased with loading amount of zeolite-A while salt rejection was maintained.

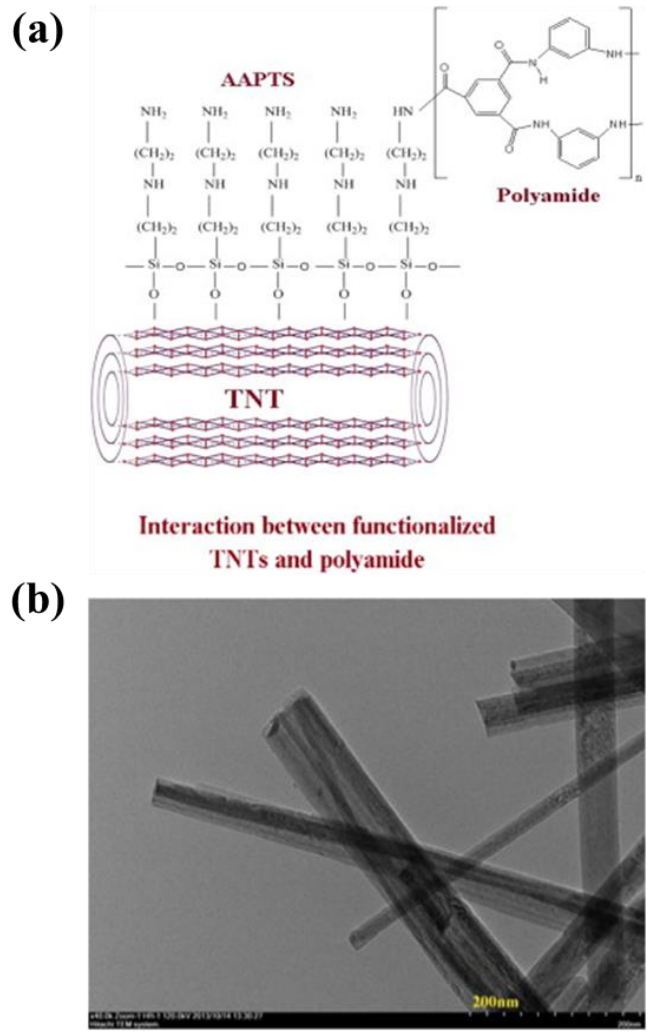

Fig. 2-6. (a) The illustrated schematic formation of polyamide (PA) with NH_2-TNTs (b) TEM image of self-synthesized TNTs which were prepared from TiO_2 nanoparticles via hydrothermal method Self-assembly mechanism of TiO_2 nanoparticle on PA membrane [24].

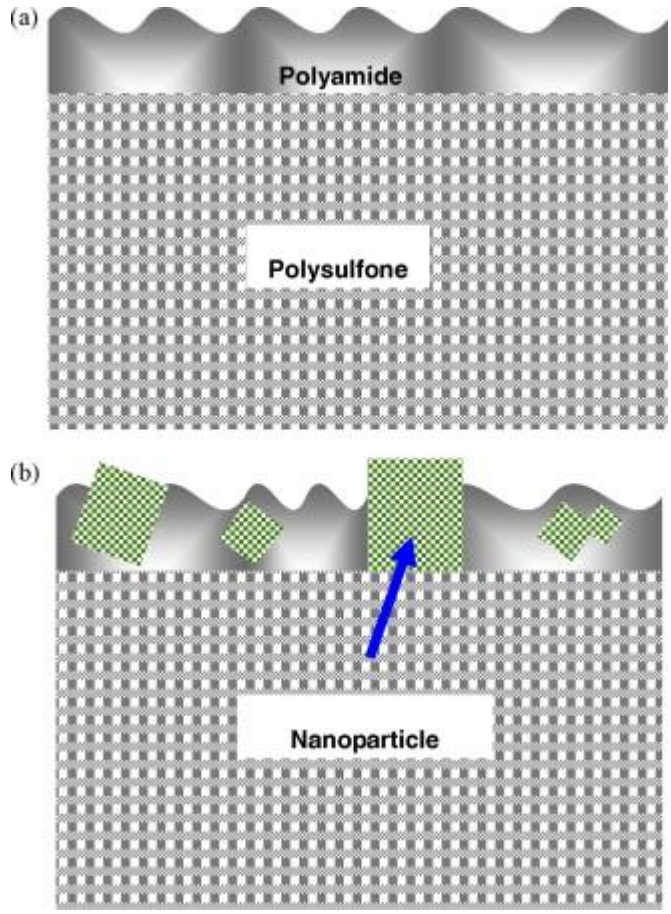

Fig. 2-7. Conceptual illustration of (a) plain PA TFC and (b) zeolite-A PA TFN membrane structures [52].

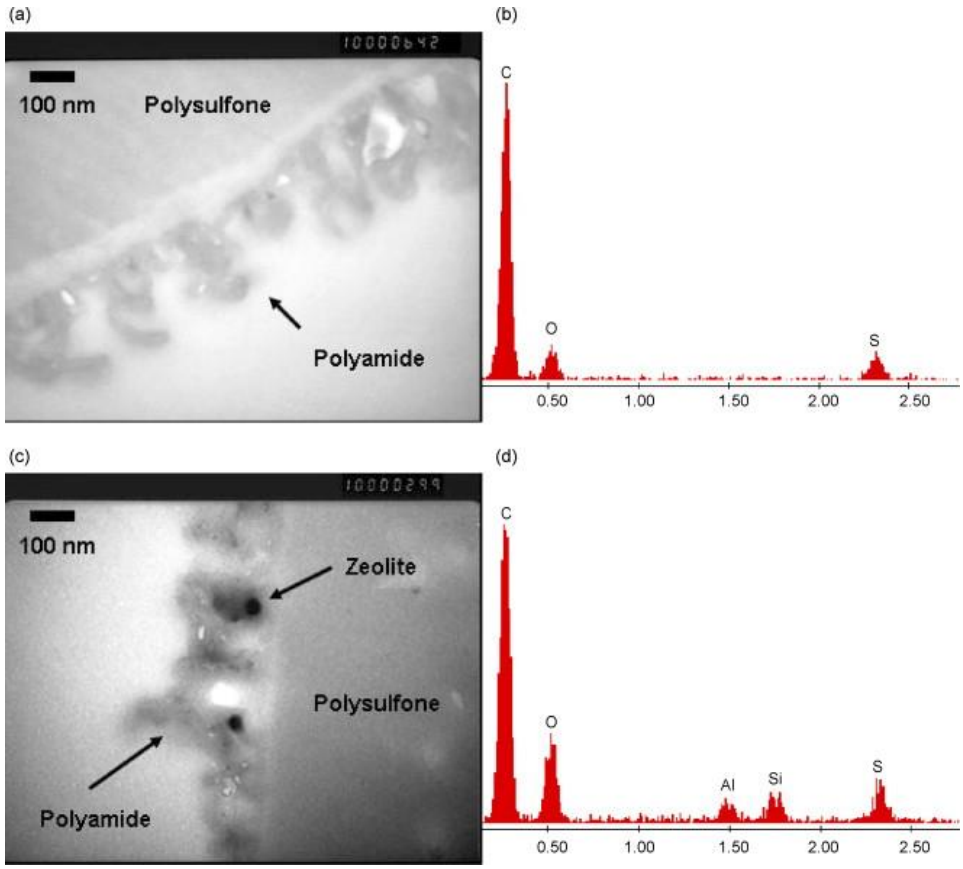

Fig. 2-8. Characterization of hand-cast thin film properties by TEM and EDX for (a–b) pure polyamide membrane and (c–d) nanocomposite membrane. Magnification is 100,000× in TEM images [52].

Kim et al. synthesized high performance PA TFN RO membrane by embedding of carbon nanotube (CNT) in PA active layer [53]. It was found that water molecule moves very fast through a very hydrophobic, narrow passageway of CNT in vertically aligned CNT membrane [54]. However, it is difficult to synthesis a vertically aligned CNT membrane with large area. In this article, CNT was chosen as embedding material to use its unique transport characteristics but relatively simple way. Acid treated CNT was dispersed in MPD aqueous solution and embedded into PA layer via interfacial polymerization. The effect of CNT acid treatment condition and concentration of MPD on membrane performance was evaluated to find the optimum performance. CNT embedded PA TFN membrane exhibited 30% increased water flux and reinforced mechanical strength. In their following study, graphene oxide (GO) was dispersed in MPD aqueous solution with CNT to improve dispersibility of CNT [55]. GO/CNT mixed solution showed improved dispersibility than CNT solution. Greatly enhanced water flux (58 LMH, 160% enhancement) and chlorine resistance were observed in GO/CNT embedded PA TFN membrane.

High efficient partially aligned zwitterion functionalized CNT embedded PA TFN membrane was reported [56]. Partially aligned CNT embedded PA membrane was prepared through following procedure (Fig. 2-9). The CNTs were deposited as bucky paper form on poly(ether sulfone) (PES) membrane through high-vacuum filtration of CNT dispersed solution. Then, PA layer was synthesized

via interfacial polymerization on CNT bucky paper layer. A molecular simulation results proved that zwitterion functional group increased salt rejection by electrostatic repulsion (Fig. 2-10(a)). In actual experiment, CNT embedded PA membrane represented 400% increased water flux with enhanced salt rejection (Fig. 2-10(b)). A remarkable result was that end-capped CNT embedded PA membrane also showed approximately 400% enhanced water flux with reduced salt rejection. This result was explained that enhanced water flux was also contributed by fast water transport through outer wall of CNT and this nanochannel allowed the pass of salt, consequently, resulted in reduction of salt rejection.

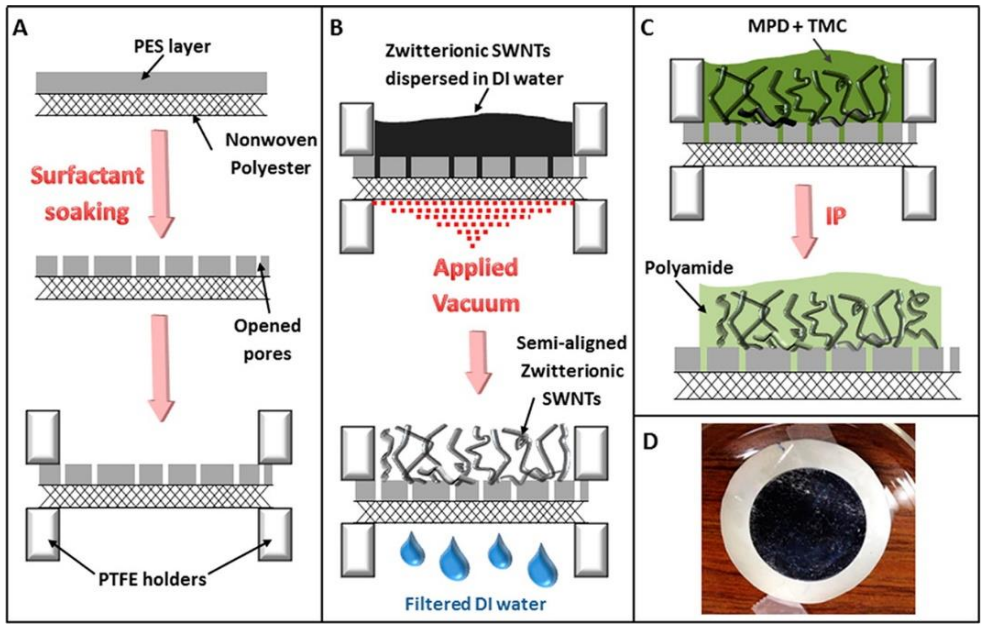

Fig. 2-9. Cross-sectional schematics of the fabrication procedure for CNT nanocomposite membrane [56].

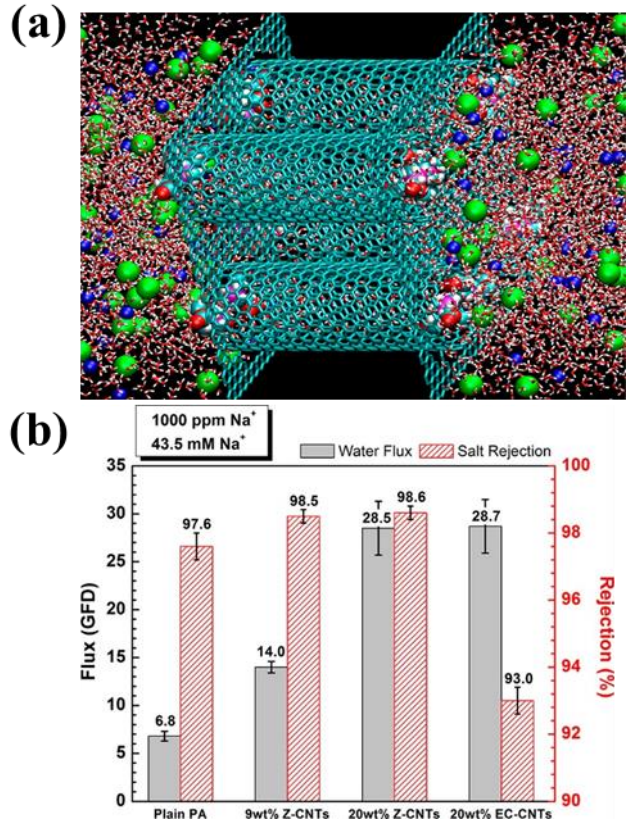

Fig. 2-10. (a) Molecular simulation of transport through zwitterion functionalized carbon nanotube (b) Water flux (solid) and salt rejection ratio (hatched) as a function of CNT concentration in the selective PA layer of the nanocomposite membrane [56].

3. TiO_2 nanoparticle coating on PA membrane for PRO, RO application via sol-gel derived spray coating method

3.1. Research background and strategies for finding an optimum condition of TiO_2 sol-gel derived spray coating

As mentioned in Chapter 2.3.1, coating or embedding of TiO_2 nanomaterial into PA TFC membrane enhance water flux and fouling resistance in RO, PRO, and FO process. Above all, TiO_2 nanoparticle (TNP) coating of PA TFC membrane via dip-coating method is very simple and do not require any other chemical treatment. Moreover, TNP coating layer endows PA TFC membrane with additional ability while maintaining its intrinsic characteristics. However, the typically slow coating rate (e.g., a few millimeters per second) could be an obstacle for the large-scale manufacturing of such membranes [30-32]. Recently, we reported a novel surface modification method via TiO_2 sol-gel-derived spray coating [57]. TiO_2 sol-gel-derived spray coating is a fast and simple method that can be carried out in room temperature. Moreover, selective layer (i.e., active or support layer only) coating is possible. Titanium butoxide (TiOBu) and isopropyl alcohol (IPA) were used as metal precursor and solution, respectively, for sol-gel reaction. TiO_2 coating layer was formed on surface via spray method using airbrush. TiO_2 coating layer was

formed in a very short time and deionization performance of capacitive deionization electrode was increased due to fast water uptake resulted from enhanced surface hydrophilicity.

Therefore, in this study, TiO_2 sol-gel derived spray coating was employed as alternative to dip-coating method to enhance water flux and fouling resistance in RO, PRO process.

3.1.1. TiO_2 coating via conventional sol-gel derived spray coating

Commercial PA TFC RO membrane (QfxSW400ES, NanoH2O Inc., USA) was coated with TiO_2 via suggested procedure in our previous study [57] and water flux and salt rejection change of QfxSW400ES were evaluated.

A 10 vol.% titanium butoxide (Aldrich Co. USA)-isopropyl alcohol (IPA, Aldrich Co., USA) coating solution was prepared. A certain volume (0.1 mL, 0.2 mL, 0.5 mL, and 1 mL) of coating solution was sprayed using airbrush on PA TFC RO membrane (10 cm × 10 cm). After evaporation of the coated solution, the membranes were rinsed with DI water. Water flux and salt rejection of the TiO_2 coated PA TFC RO membrane were evaluated in a lab-scale cross-flow RO filtration system. In this study, 6 L feed water containing 2,000 mg/L NaCl was used and an effective membrane area was 22.4 cm^2 (3.3 cm × 6.8 cm) with 0.3 cm of channel height. The membrane performance test was performed with 8 $cm \cdot s^{-1}$ of cross-flow velocity at 25°C.

From the results, it was found that previous TiO_2 sol-gel spray coating was not suitable for membrane, although it endowed CDI electrode with positive effect.

Fig. 3-1. The picture of TiO_2 sol-gel spray coated membrane after DI water rinsing.

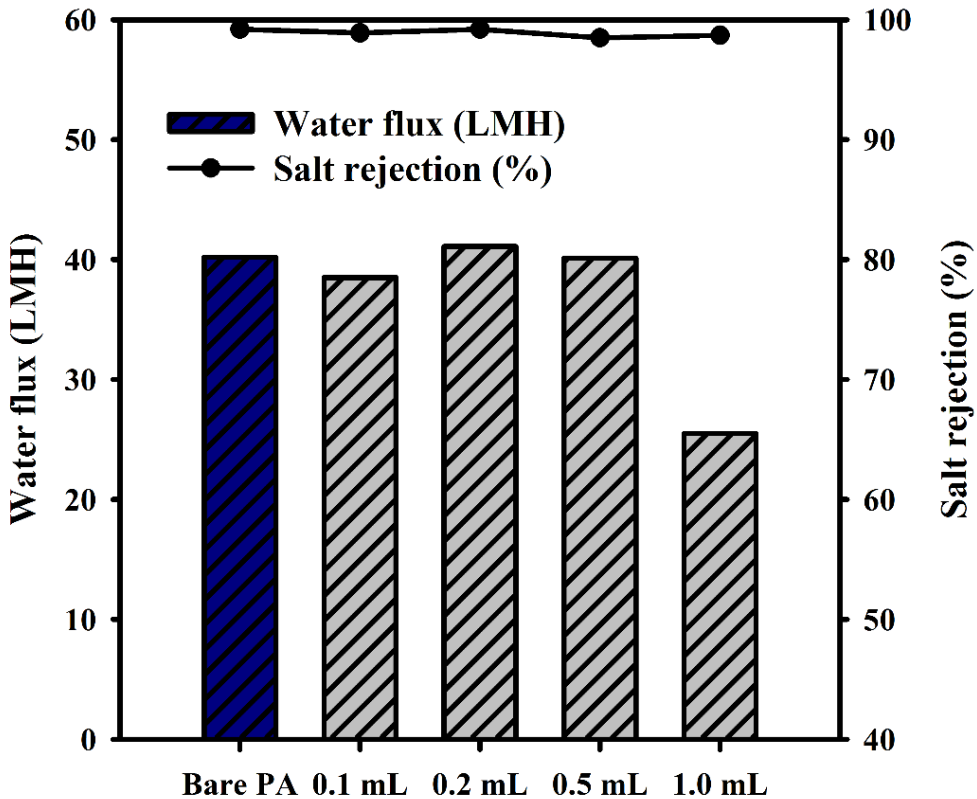

Fig. 3-2. Water flux and salt rejection change of TiO_2 coated membranes as function of the TiO_2 coating amount on QfxSW400ES PA TFC RO membrane (the test was carried out in cross-flow filtration system; cross-flow velocity and temperature: 8 $cm \cdot s^{-1}$ and 25°C; feed water: 2,000 mg/L NaCl).

Fig. 3-1 shows the image of 1.0 mL of TiO_2 coated PA TFC RO membrane after DI water washing. As shown in red circles of Fig. 3-1, coated TiO_2 layer was easily detached and floating on surface of the water. This implies that current TiO_2 sol-gel-derived spray coating forms very weak and vulnerable TiO_2 coating layer on PA membrane surface even to weak DI water washing. When stable TiO_2 coating layer was formed on membrane, it severely reduced water flux of membrane.

Fig. 3-2 displays water flux and salt rejection change of TiO_2 coated membranes as function of the titanium butoxide solution coating amount. As shown in Fig. 3-2, bare PA and TiO_2 coated membrane demonstrated over 98% of NaCl rejection regardless of TiO_2 coating amount. Salt rejection results confirmed that TiO_2 sol-gel-derived spray coating do not damage membrane surface. From the water flux result (bar chart in Fig. 3-2), the water flux was sharply dropped from 40 LMH to 25 LMH in 1.0 mL of TiO_2 coating amount, while it was maintained up to 0.5 mL of coating amount. To find out the cause of water flux reduction in TiO_2 coated membrane, surface morphology of TiO_2 coated membrane was observed using field emission scanning electron microscopy (FE-SEM; JSM-6701F, JEOL, Japan).

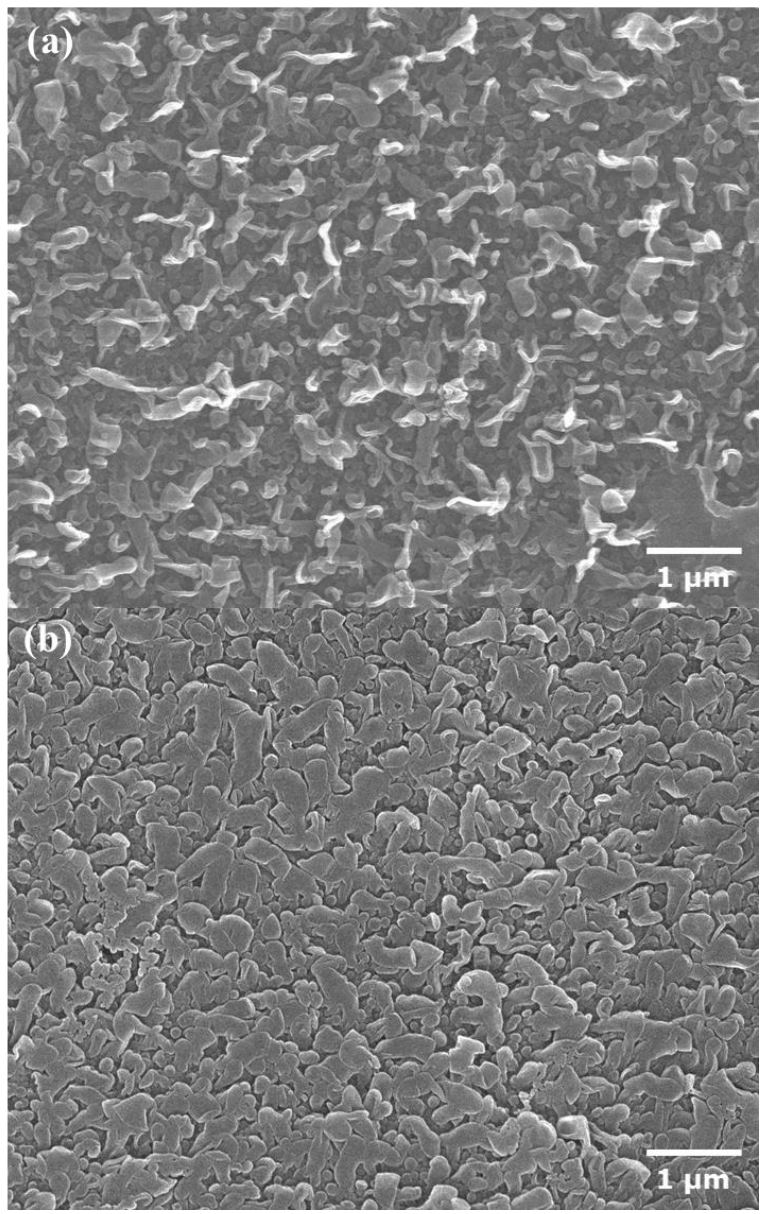

Fig. 3-3. SEM images of (a) bare and (b) 1.0 mL of TiO_2 coated PA RO membrane

Surface morphology of bare PA and 1.0 mL of TiO_2 coated PA membrane were represented in Fig. 3-3(a) and (b), respectively. As we can see from Fig. 3-3(a), bare PA membrane exhibited typical surface—ridge and valley—structure of PA, however, it was found that the surface structure of TiO_2 coated membrane was packed with dense TiO_2 coating layer (see Fig. 3-3(b)). This dense TiO_2 coating layer on membrane surface increased hydraulic resistance and resulted in reduction of water flux.

Therefore, optimization of TiO_2 sol-gel-derived coating method is required to complement the drawbacks of current method such as weak durability of coating layer and flux reduction, while making full use of advantages of TiO_2 coating such as hydrophilicity and negative charge.

3.1.2. Strategies for finding an optimum condition of TiO_2 sol-gel derived spray coating method

Fig. 3-4 represents the schematic diagram of strategy for TiO_2 sol-gel-derived spray coating method which is durable without flux loss, while making full use of advantages of TiO_2 coating layer. As expressed in Fig. 3-4, TiO_2 coating layer must be formed as porous or deposited particle structure and not as a dense film for favorable water transport. It is known that sol-gel reaction is affected by following factors: type of alcohol solvent and metal precursor, stabilizer, and catalyst [58, 59]. In this part, therefore, the effect of base material, stabilizer, and catalyst on TiO_2 sol-gel-derived coating was observed to achieve the optimization of TiO_2 coating layer.

Firstly, the effect of alcohol solvent for sol-gel reaction was examined. The TiO_2 sol-gel-derived spray coating was carried out using isopropyl alcohol (IPA), ethanol, methanol as solvent and their effect on coating layer was observed. In Fig. 3-4, the effect of alcohol solvent on TiO_2 sol-gel-derived spray coating was observed by FE-SEM. As shown in Figs 3-4(b) and (c), when the IPA and ethanol were used as solvent, no reaction was occurred in titanium butoxide solution (inset images of Figs 3-4(b) and (c)) and similar forms (dense film) of TiO_2 coating layer were formed on membrane surface. In case of methanol, TiO_2 sol was formed in titanium butoxide solution (inset images of Figs 3-4(d)).

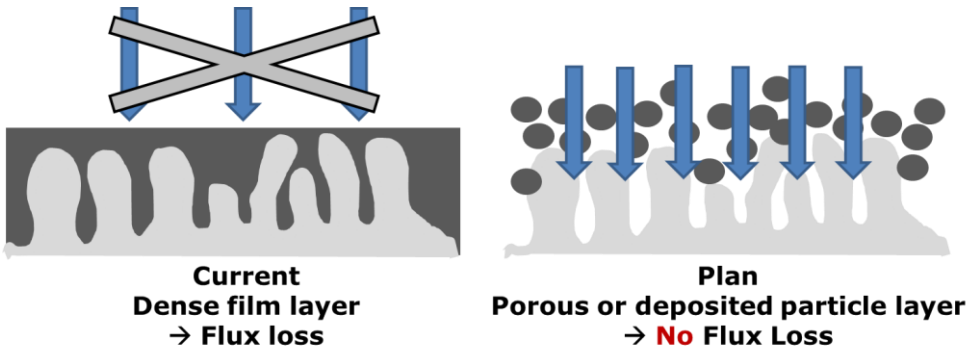

Fig. 3-4. Strategies for TiO_2 coating on membrane surface for performance enhancement without flux loss

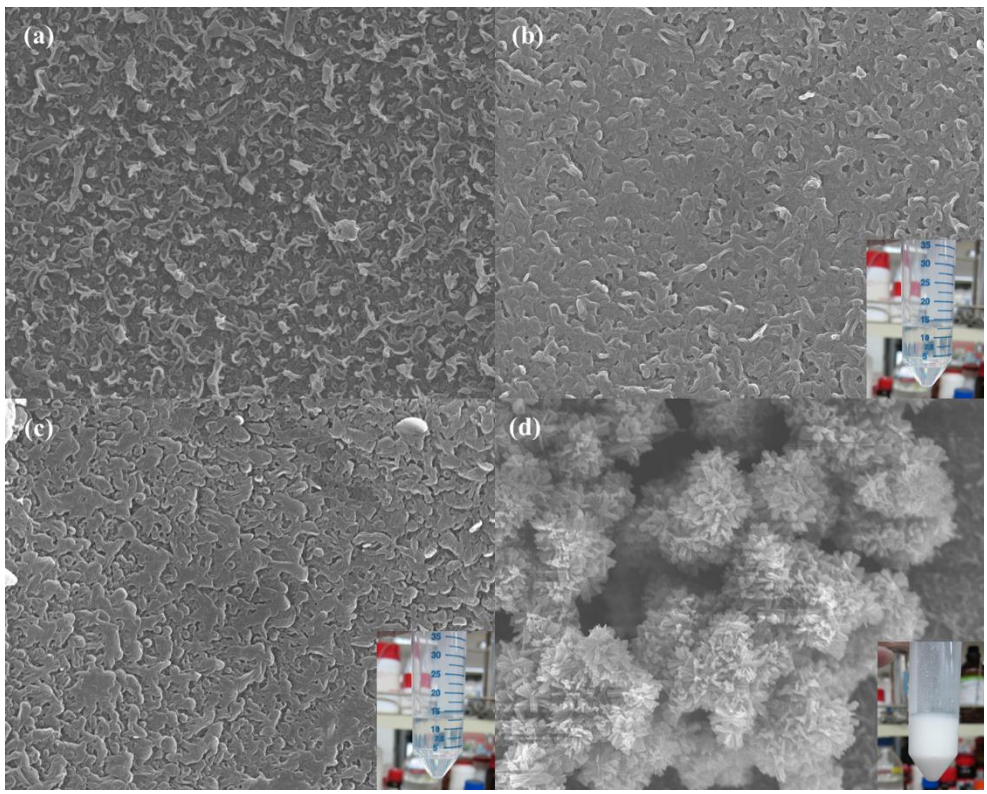

Fig. 3-5. Effect of alcohol solvent on sol-gel derived spray coating and its coating layer. (a) Bare PA, (b) ethanol, (c) IPA, and (d) methanol (inset images of (b), (c), and (d) represent the TiO_2 solution after mixing of titanium butoxide and (b) ethanol, (c) IPA, and (d) methanol, respectively)

After spray coating, it is observed that several μm size of TiO_2 particles were deposited on membrane surface (Figs 3-4(d)). As well as hydrolysis of titanium butoxide, alcoholysis (or alcohol interchange) reaction occur during sol-gel reaction. It is known that alcoholysis is occurred through S_N2 reaction and affected by steric factors [60]. It seems that alcoholysis of titanium butoxide was more readily caused in methanol which has smallest alkyl group. Then, TiO_2 sol was formed in titanium butoxide solution and membrane was coated with TiO_2 particles by spraying of this TiO_2 sol.

Secondly, the effect of type of titanium alkoxide was evaluated and titanium methoxide was chosen for metal precursor. Fig. 3-6 displays surface morphology of TiO_2 coated PA TFC RO membrane via TiO_2 sol-gel-derived spray coating using titanium methoxide as metal precursor. As we can find in inset image of Fig. 3-6(a), TiO_2 sol was formed in 10 vol.% titanium methoxide/IPA solution. In sol-gel reaction of titanium oxide, TiO_2 is synthesized via hydrolysis and condensation reaction. Since hydrolysis is also S_N2 reaction which have steric effect, hydrolysis rate decreased with alkyl chain length of metal alkoxide. From the SEM analysis, rod form with over 100 nm thickness TiO_2 particles were observed on membrane surface. From above results of solvent and titanium alkoxide effect, it was found that TiO_2 sol must be formed ahead spray coating to achieve particle form of TiO_2 coating layer.

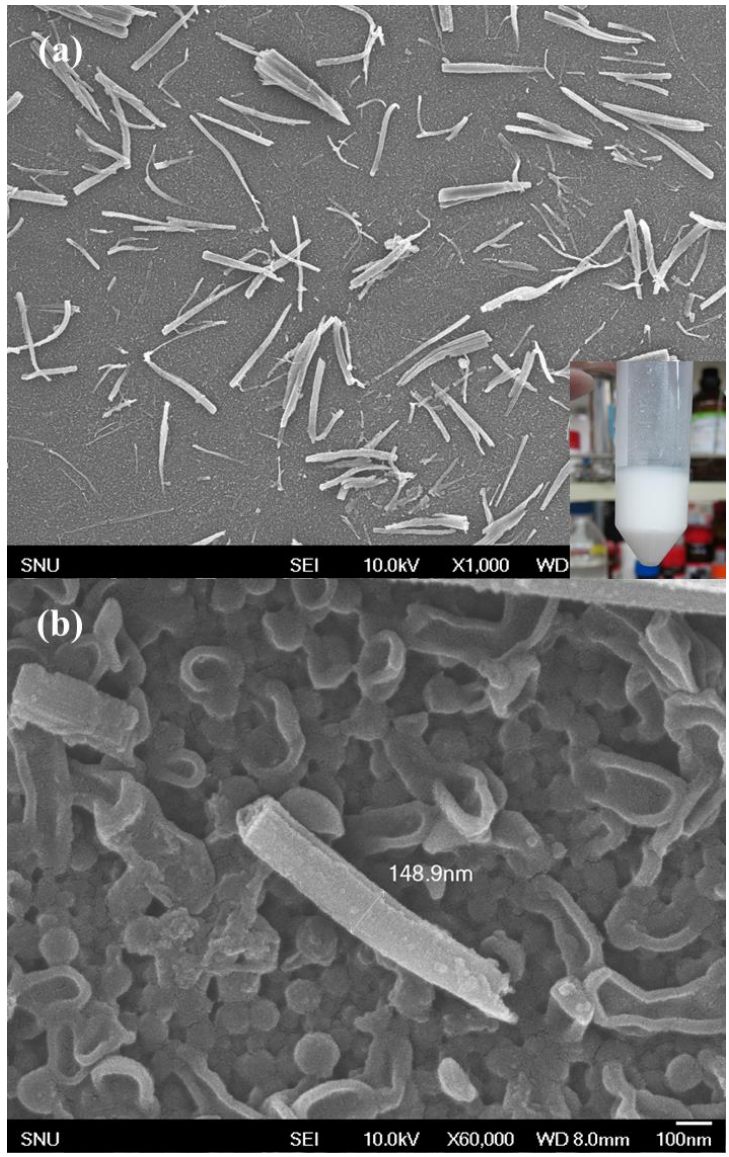

Fig. 3-6. Surface morphology of TiO_2 coated PA TFC RO membrane via TiO_2 sol-gel-derived spray coating using titanium methoxide as metal precursor.

However, it is difficult to expect enhancement of fouling resistance form above results, due to large particle size and wide uncoated area.

Thirdly, the effect of stabilizer on TiO_2 coating layer was evaluated. In sol-gel process, the role of stabilizer is stabilization of the sol and reducing hydrolysis and condensation reaction rate by forming complex intermediate [59]. Diethanolamine (DEA), diethylene-triamine, monoethanolamine, acetylacetone, acetic acid and polyethylene glycol have been used as stabilization, and chelation complexing agents [61-66]. Among them, DEA is most frequently employed stabilizer in sol-gel process [67-69]. In this study, DEA was used as stabilizer. After titanium alkoxide and alcohol solvent were mixed, 1 mL of 10 vol.% DEA in alcohol was added. Then, 1 mL of prepared mixture were sprayed on PA TFC RO membrane and surface morphology was observed by FE-SEM (Fig. 3-7). From surface SEM image in Fig. 3-7(b), it was shown that DEA added titanium butoxide-IPA solution made defect-free, dense, smooth TiO_2 coating layer on membrane. It could be explained that reduced hydrolysis and condensation rate by DEA was contributed to stable progress of TiO_2 formation and led to defect-free coating layer. No effect of the DEA on particle size was observed (see Figs 3-7(c), (d)) and defect-free, dense TiO_2 coating layer was also found around TiO_2 particles. It seems that unreacted residual titanium alkoxide was affected by DEA and formed this additional TiO_2 coating part.

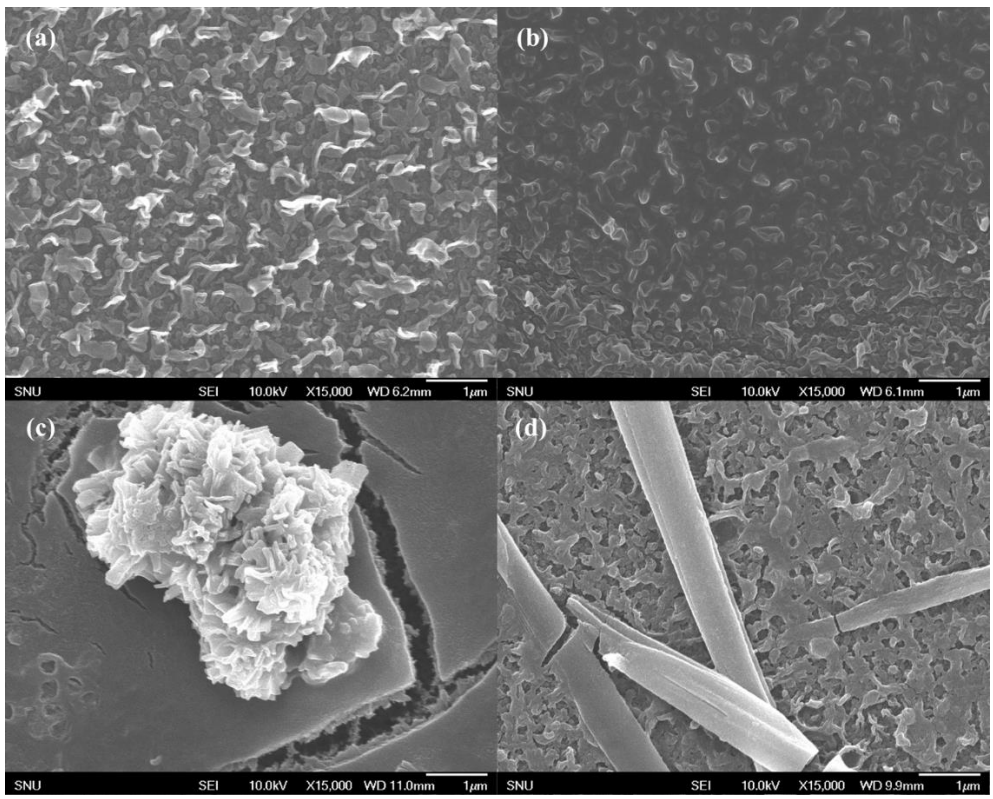

Fig. 3-7. Effect of diethanolamine on sol-gel derived spray coating and its coating layer. (a) Bare PA, (b) 1.0 mL of TiO_2 solution with diethanolamine (DEA) coated PA RO membrane, (c) titanium butoxide in methanol with DEA, and (d) titanium methoxide in IPA with DEA

Fourthly, the addition of acid and base catalyst was considered in this experiment. Fig. 3-8 represents the schematic diagram of expected effect of acid-base catalyzed TiO_2 sol-gel-derived spray coating on TFC membrane. It is known that acid and base catalysts affect the reaction rate of hydrolysis and condensation during sol-gel reaction [58]. Acid catalyst increases hydrolysis reaction rate and retards the condensation rate by producing good leaving groups resulted from protonation of negative charged alkoxide groups. On contrary, base catalyst enhances the condensation reaction rate and reduces the hydrolysis reaction rate by formation of strong nucleophiles resulted from deprotonation of hydroxo ligands [58]. Based on these role of acid and base catalyst in sol-gel reaction, the effect of the addition of acid and base catalyst on sol-gel reaction and TiO_2 coating layer were evaluated. In all experiment, the DI water was added into titanium butoxide solution for formation of TiO_2 sol and ethanol was used as solvent of sol-gel reaction for fast evaporation of sprayed TiO_2 sol. The hydrogen chloride and ammonium hydroxide were used as acid-catalyst and base-catalyst, respectively. Briefly, 100 μL hydrogen chloride and 1 mL DI water were injected into 10 vol.% titanium butoxide/ethanol 20 mL solution and 2 mL of titanium butoxide solution was sprayed on PA TFC RO membrane. Fig. 3-9 shows the change of titanium butoxide/ethanol solution after addition of hydrogen chloride and surface morphology of TiO_2 coated membrane via acid-catalyzed TiO_2 sol-gel-derived spray coating method.

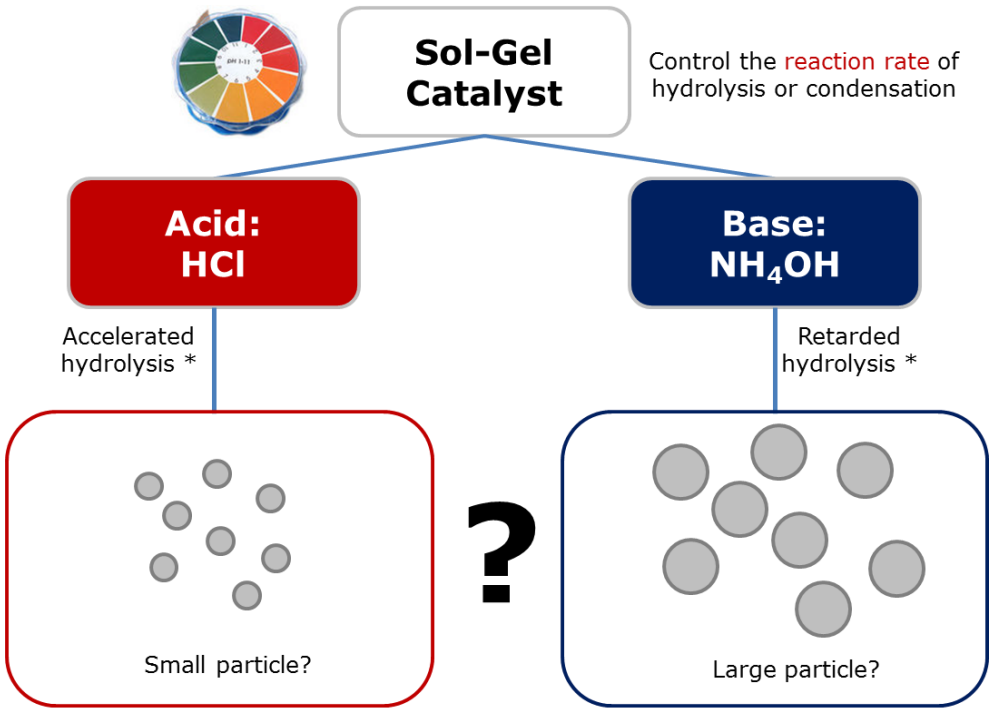

Fig. 3-8. Schematic diagram of predicted effect of acid-base catalyzed TiO_2 sol-gel-derived spray coating on TFC membrane [58].

Against my expectation which is that acid-catalyst enhances hydrolysis rate and leads to formation of nanoparticle, the results showed the addition of hydrogen chloride caused gelation of titanium butoxide/ethanol and transparent gel was formed (Fig. 3-9(a)). It can be assumed that most titanium butoxide were rapidly hydrolyzed and formed a gel via condensation. Hydrogen chloride added titanium butoxide/ethanol solution was sprayed on membrane before it was changed to a gel. As shown in Fig. 3-9(b), a dense film form with large cracks of TiO_2 coating layer was formed on membrane surface and the PA active layer was damaged by cracks (Fig. 3-9(c)). These results suggest that acid-catalyst is not suitable for TiO_2 sol-gel-derived spray coating.

To evaluate the effect of base-catalyst on TiO_2 sol-gel-derived spray coating, ammonium hydroxide was used as base-catalyst. Briefly, 200 μL (1 vol.%) of ammonium hydroxide and 1 mL of DI water were mixed with 16 mL ethanol and 2 mL of titanium butoxide was injected into the solution under vigorous stirring. After mixing for 10 min, 2 mL of TiO_2 sol was sprayed using airbrush on PA RO membrane. Fig. 3-10 displays the change of titanium butoxide/ethanol solution after addition of ammonium hydroxide and surface morphology of TiO_2 coated membrane via base-catalyzed TiO_2 sol-gel-derived spray coating method. After titanium butoxide was added into ethanol containing ammonium hydroxide and DI water, the solution was changed into a TiO_2 sol (Fig. 3-10 (a)).

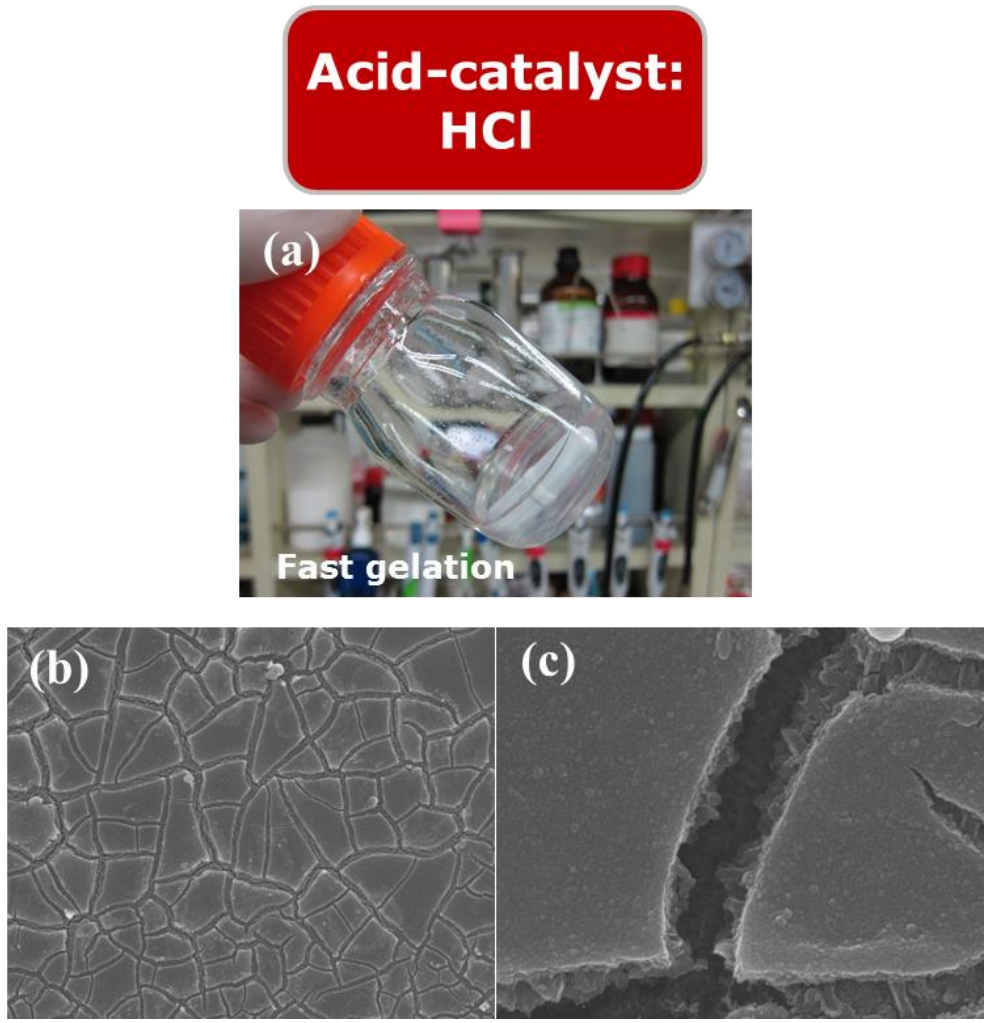

Fig. 3-9. Effect of hydrogen chloride as acid catalyst on TiO_2 sol-gel-derived spray coating (a) effect on titanium butoxide solution, (b) surface morphology of TiO_2 coating layer on PA TFC membrane, and (c) enlarged image of (b).

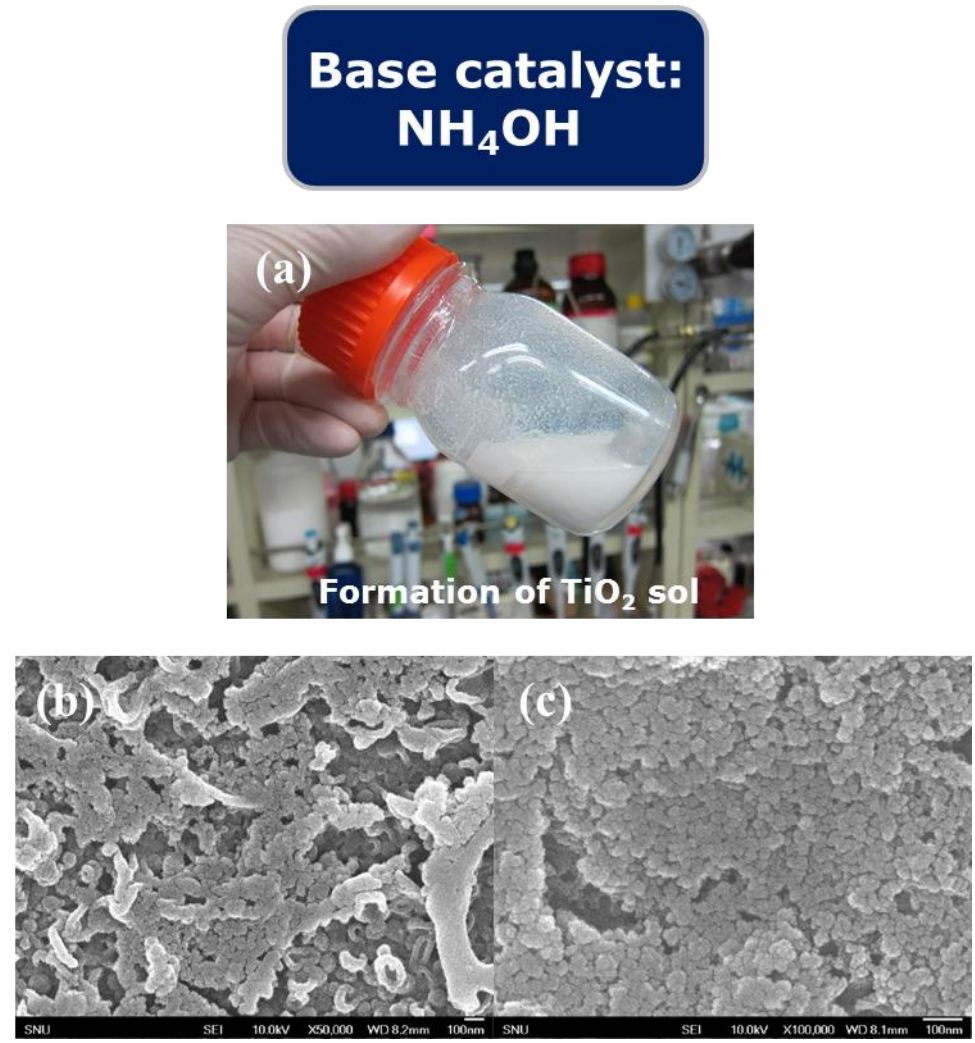

Fig. 3-10. Effect of ammonium hydroxide as base-catalyst on TiO_2 sol-gel-derived spray coating (a) effect on titanium butoxide solution, (b) surface morphology of TiO_2 coating layer on PA TFC membrane, and (c) enlarged image of (b).

As we can find from Figs 3-10(b) and (c), the most membrane surface was finely covered with TiO_2 nanoparticles with diameter approximately 30~40 nm. It seems that the ammonium hydroxide partially hydrolyzed the titanium butoxide in solution and nanoparticles were synthesized by condensation of partially hydrolyzed titanium hydroxide.

From above results evaluating the effect of acid and base catalyst, it can be concluded that base-catalyzed TiO_2 sol-gel-derived spray coating forms appropriate TiO_2 coating layer which finely covers membrane surface with TiO_2 nanoparticles. In this section, in order to optimize the coating condition of PA TFC RO membrane via base-catalyzed TiO_2 sol-gel-derived spray method, the diameter of coated TNP, the morphology of TNP coating layer, pure water flux of TNP coated PA TFC RO membrane, and the durability of TNP coating layer against cross-flow during RO operation were evaluated with varying the amount of ammonium hydroxide. Briefly, 1 mL of DI water was mixed with 16 mL ethanol and a certain volume (0 μL, 100 μL, 200 μL, 500 μL, and 1000 μL) of ammonium hydroxide was injected into solution. Then, 2 mL of titanium butoxide was injected into the solution under vigorous stirring. After mixing for 10 min, a 1 mL of 10 w/v% DEA/ethanol solution was added to neutralize the condensation reaction rate and stabilize the TiO_2 sol [59]. Finally, the TiO_2 sol was sonicated for 20 min. The prepared TiO_2 sol was deposited onto PA membrane with spray coating method. The PA RO membrane (10 cm × 10 cm, RE-SHF, Toray Chemical

Inc., Republic of Korea) was fixed on stainless plate and 2 mL of TiO_2 sol was sprayed using airbrush on PA RO membrane. After evaporation of the coated solution, the membranes were rinsed with DI water. Pure water permeability flux of TNP coated membranes were measured and compared with bare PA TFC RO membrane in a lab-scale cross-flow RO filtration system. A 6 L feed water containing 2,000 mg/L NaCl was used and an effective membrane area was 22.4 cm^2 (3.3 cm × 6.8 cm) with 0.3 cm of channel height. The membrane performance test was performed with 8 $cm \cdot s^{-1}$ of cross-flow velocity at 25°C. After the membrane compaction for 30 min at 15.5 bar, the permeated water was collected into bottle for 20 min under same pressure. The particle size of deposited TNPs and the morphology of TNP coating layer was observed by FE-SEM.

Fig. 3-11 and Fig. 3-12 exhibit the change of particle size of TNPs and morphology of TNP coating layer via base-catalyzed TiO_2 sol-gel-derived spray coating with varying the amount of ammonium hydroxide. As shown in Fig. 3-11, the particle size of TNPs apparently reduced from approximately 300 nm to 10 nm as the amount of ammonium hydroxide increased. A TNP with diameter of several nanometer was synthesized when using 1000 μL of ammonium hydroxide added base-catalyzed TiO_2 sol-gel-derived spray coating. On the other hand, over 100 nm size TNP was formed in case of no ammonium hydroxide.

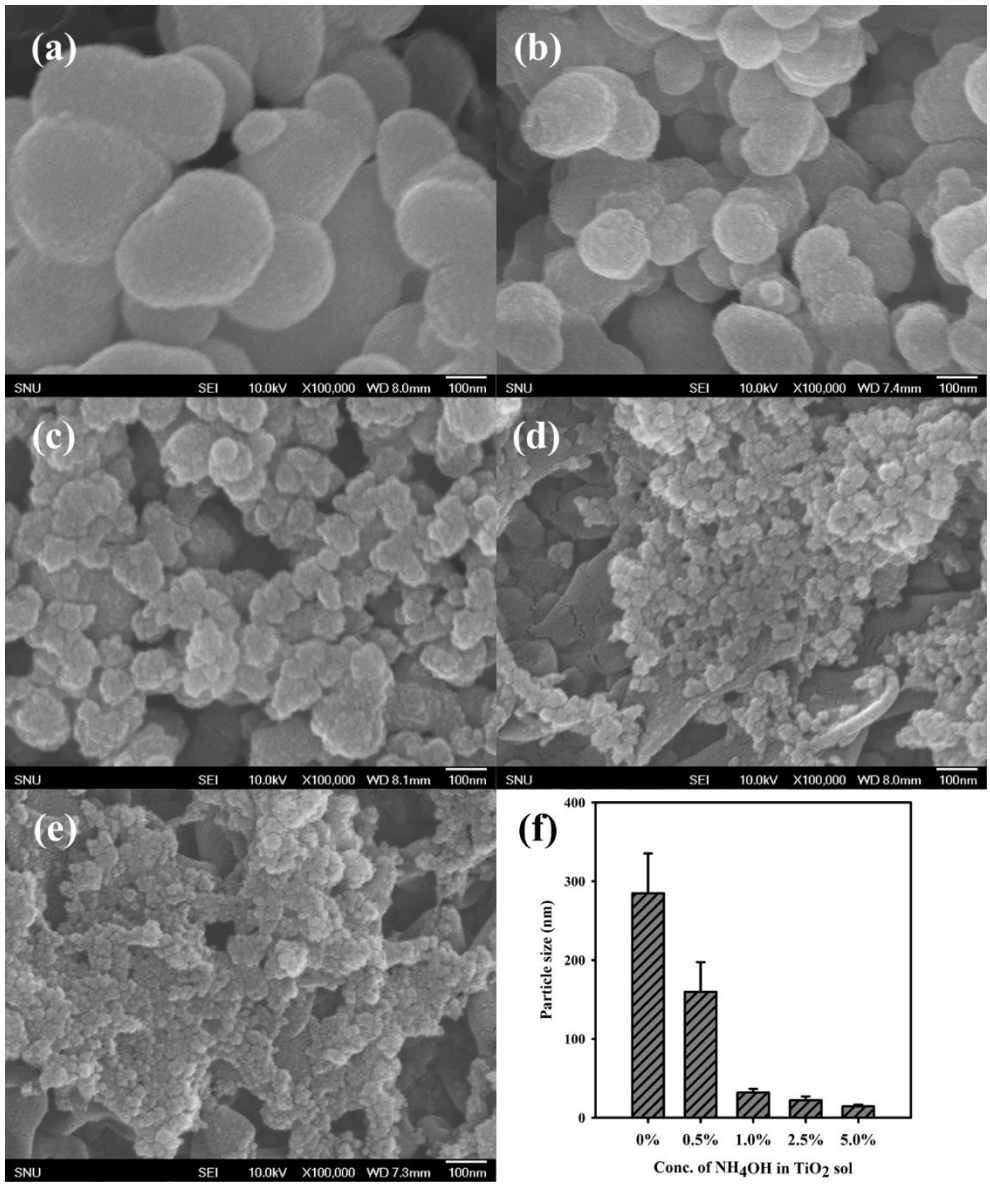

Fig. 3-11. Effect of ammonium hydroxide on size of TiO_2 nanoparticles via sol-gel-derived spray coating. (a) 0%, (b) 0.5%, (c) 1.0%, (d) 2.5%, (e) 5.0% of ammonium hydroxide added TiO_2 sol coated PA membrane, and (f) average diameter of TNPs in TiO_2 sol.

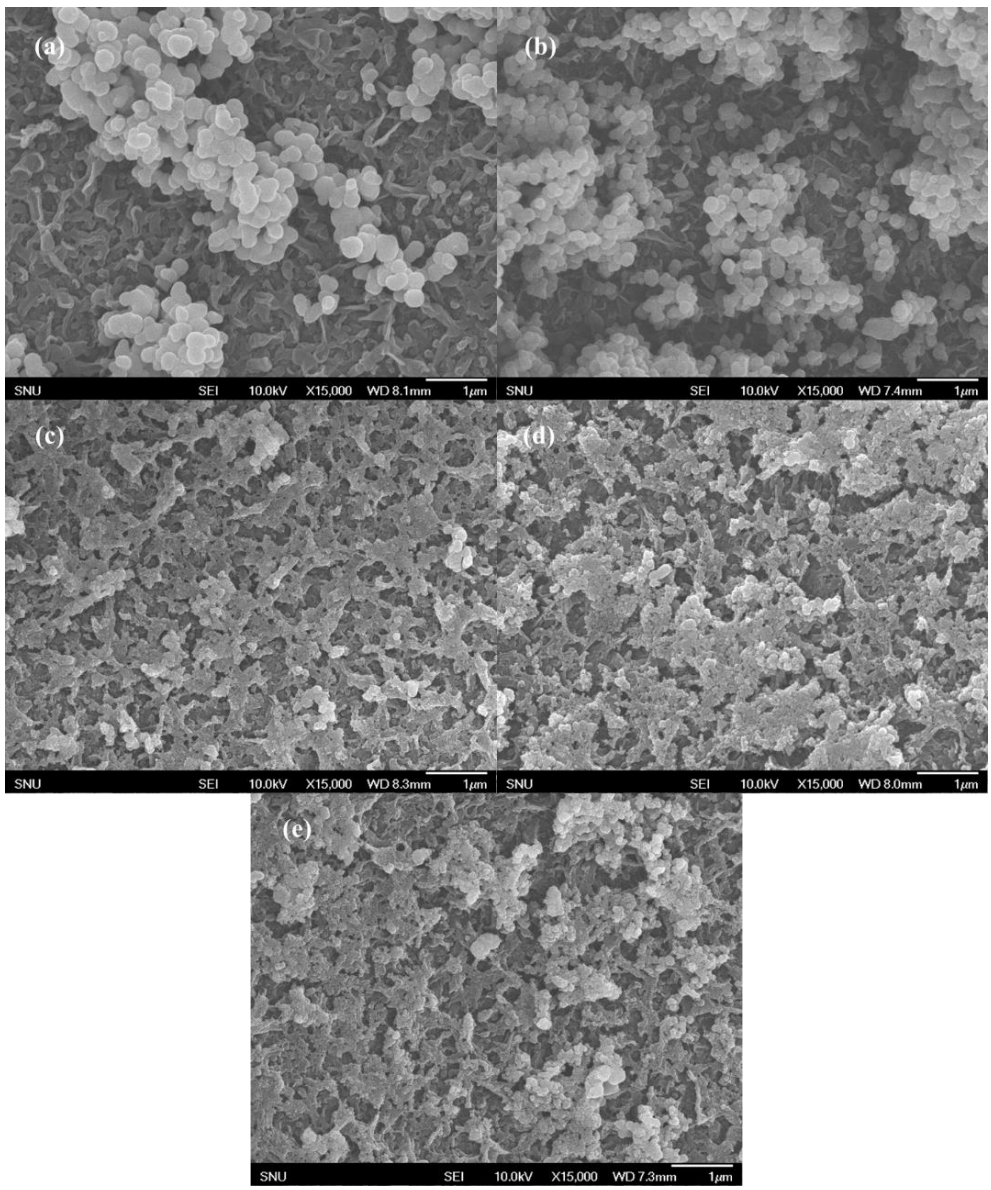

Fig. 3-12. Effect of ammonium hydroxide on TNP coating layer via sol-gel-derived spray coating. (a) 0%, (b) 0.5%, (c) 1.0%, (d) 2.5%, (e) 5.0% of ammonium hydroxide added TiO_2 sol coated PA membrane.

This result may be inferred that when the limited DI water—can hydrolyze a titanium butoxide—exist in solution, the number of generated TiO_2 nanoparticle increased and the particle size reduced with the amount of ammonium hydroxide by enhanced condensation rate. Fig. 3-12 shows the variation of the surface morphology of TNP coating layer. Without ammonium hydroxide, the large size of TNPs were sparsely deposited on membrane surface (Fig. 3-12(a)). On the other hand, as the amount of ammonium hydroxide increased, densely coated layer with more small size of TNPs were covered on membrane surfaces (Fig. 3-12(b)—(e)). A correlation between morphology of TNP coating layer and pure water flux was evaluated and displayed in Fig. 3-13. As indicated in Fig. 3-13, a severe water flux loss were caused in 500 μL and 1000 μL of ammonium hydroxide added TNP coating, while the pure water flux was maintained until 100 μL of ammonium hydroxide addition and slight flux loss was observed in 200 μL of ammonium hydroxide added TNP coating. This flux decline in 500 μL and 1000 μL of ammonium hydroxide added TNP coating is due to increased hydraulic resistance resulted from very densely packed TNPs on membrane surface.

We evaluated from Fig. 3-14 that the effect of ammonium hydroxide as base catalyst on durability of TNP coating layer with varying the adding amount of ammonium hydroxide.

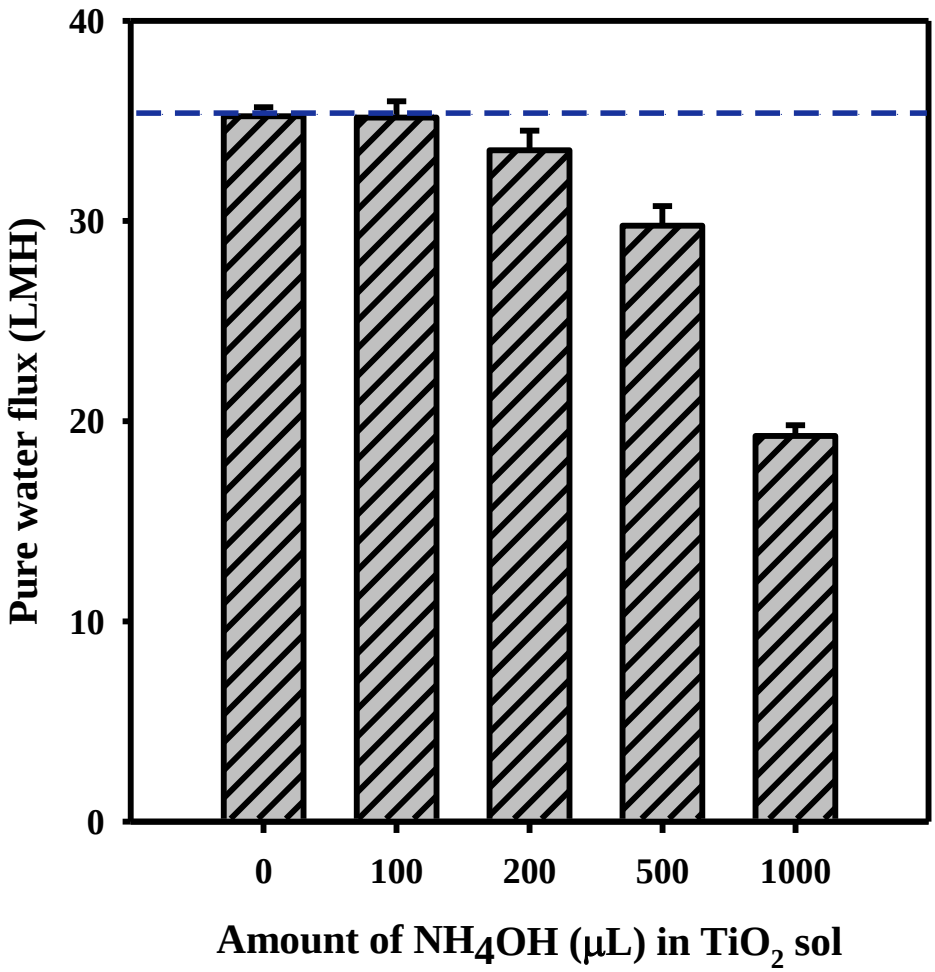

Fig. 3-13. Effect of ammonium hydroxide as base catalyst on pure water flux of 2 mL of TiO_2 sol coated PA RO membrane (the test was carried out in cross-flow filtration system; cross-flow velocity and temperature: 8 $cm \cdot s^{-1}$ and 25°C; blue dashed line: pure water flux of bare PA TFC membrane; n=3).

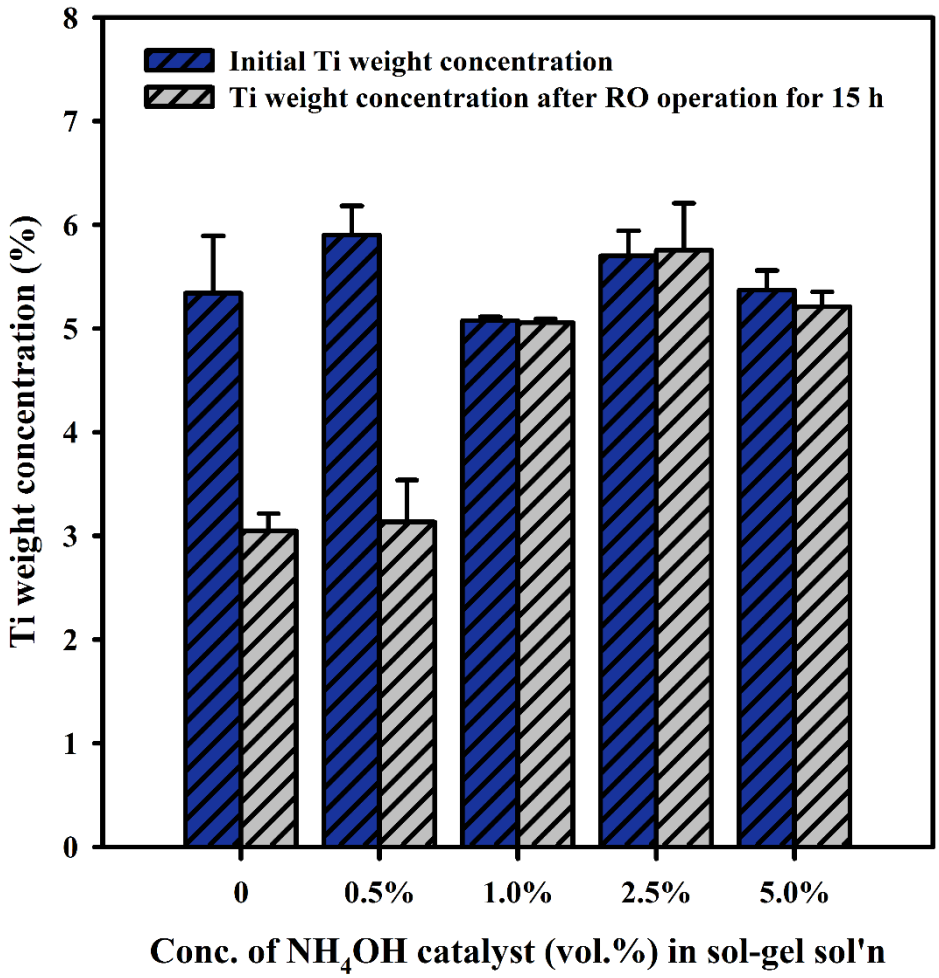

Fig. 3-14. Effect of ammonium hydroxide as base catalyst on durability of TNP coating layer (n=3).

The durability of TNP-coated membranes were examined by measuring the titanium weight concentrations using EDS (JSM-6701F, JEOL, Japan) after running the membrane in the lab-scale cross-flow RO filtration system for 15 h. From the EDS results, the initial Ti weight concentration of 2 mL of TiO_2 sol coated membranes were ranged in 5—6% regardless of ammonium hydroxide amount. The TiO_2 coating layers—from 200 μL, 500 μL, and 1000 μL ammonium hydroxide added TiO_2 sol—demonstrated excellent durability. These coating layer showed no difference in Ti weight concentration after 15 h of RO operation. However, no ammonium hydroxide and 100 μL of ammonium hydroxide added TiO_2 sol formed vulnerable coating layer and approximately 50% of TiO2 was lost after RO operation. This large loss of TiO_2 could be inferred that sparsely coated TiO_2 layer consist of large TiO_2 particle may have suffered from strong shear stress of cross-flow and resulted in detachment of TiO_2 particles. Meanwhile dense TiO_2 coating layer consist of small size of TNPs may have suffered from relatively weak shear stress.

From the optimization experiment results, the optimum TiO_2 nanoparticle coating layer, which is dense and durable without blocking the pore or surface, was formed by base-catalyzed (ammonium hydroxide 200 μL) TiO_2 sol-gel-derived spray coating. In the next section, PA TFC membrane was coated with TiO_2 via base-catalyzed sol-gel-derived spray coating and its effect on performance and fouling resistance were investigated in PRO and RO process.

3.2. A high-performance and fouling resistant thin-film composite membrane prepared via coating TiO_2 on a support layer by the sol-gel-derived spray method for pressure retarded osmosis applications

3.2.1. Introduction

Despite a high potential as a renewable energy source, PRO processes require suitable semipermeable membranes that are difficult to fabricate [70]. The support layers which typically consist of polyester non-woven fabric and a porous poly(sulfone) are known to have no significant effect on the overall membrane performance in reverse osmosis (RO) processes [50, 71]. However, these support layers negatively impact the performances of membranes in forward osmosis (FO) and PRO processes. The typically thick and bulky structures of support layers hinder effective osmotic flows between feed and draw solutions [72]. Additionally, support layers often have low membrane performance due to their hydrophobic nature hindering water transport near the membrane surface and causing the formation of air bubbles [73]. Severe membrane fouling have been reported to occur on porous support layers in PRO processes [33]. The membrane fouling of porous support layers, so called “internal fouling”, causes not only the formation of “cake layers”, but also clogging the pores of the membrane and decreases membrane performance. To overcome these problems, many studies have focused

on fabricating thin support layers or applying hydrophilic coatings to enhance water flux and reduce membrane fouling [74-81].

In this part, the high-performance and fouling-resistant properties of a thin-film composite membrane prepared by coating TNPs on a support layer by sol-gel-derived spray method for pressure retarded osmosis. TNPs were synthesized through a base catalyzed sol-gel process and deposited via spray coating on the support layer surface of a commercial TFC membrane with TNPs. Water flux and reverse salt flux performances of the TiO_2-coated membrane were evaluated in a lab-scale cross-flow osmotically driven system. Fouling resistance was evaluated as the degree of water flux reduction when humic acid was added to the feed solution.

3.2.2. Materials and methods

3.3.2.1. Materials

A commercial TFC FO membrane which has mesh-embedded support layer, was chosen for base membrane (Hydration Technology Innovations (HTI), Albany, OR) [39]. The base membrane was rinsed with DI water and stored in DI water at 4°C over two weeks. Titanium butoxide ($Ti(OC_4H_9)_4$, reagent grade, 97%), diethanolamine (DEA, $HN(C_2H_4OH)_2$, reagent grade, ≥ 98%), ammonium hydroxide (NH_4OH, 28% in water), sodium chloride (anhydrous, ≥ 99.0%), sodium sulfate (ACS reagent, anhydrous, ≥ 99.0%), magnesium chloride (anhydrous, ≥ 98.0%), magnesium sulfate (anhydrous, ≥ 99.5%), and humic acid (technical grade) were purchased from Sigma Aldrich. Ethanol (99.9%, Samchun Chemical Co., Ltd., Republic of Korea) was used as the solvent for the sol-gel process. Commercial TiO_2 nanoparticles (TNPs) (Aeroxide® P25, Evonik, Germany) were used for comparisons to synthesized TNPs.

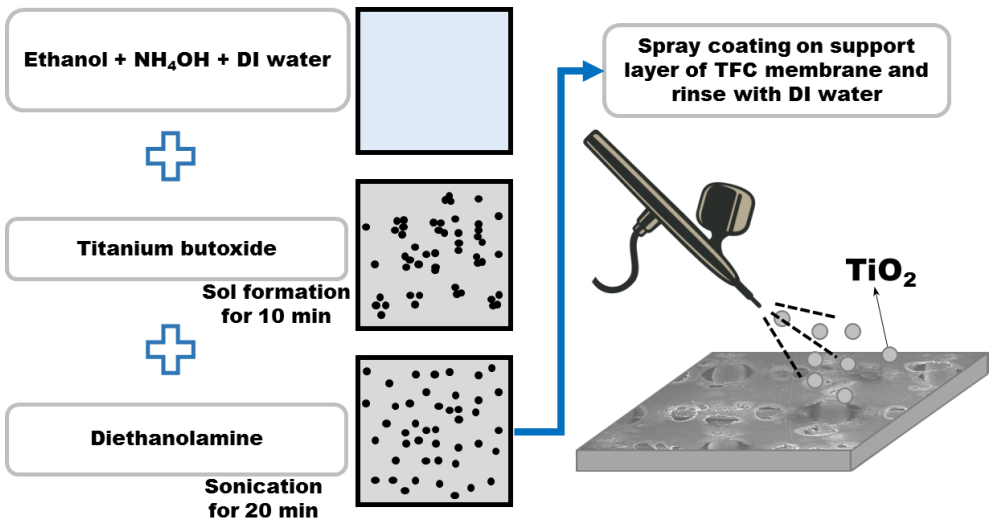

Fig. 3-15. Schematic procedure for preparing TNP-coated TFC membrane by sol-gel-derived spray coating method.

3.3.2.2. Preparation of TNP solution and TNP coated membrane

Fig. 3-15 shows a schematic of the TNP coating procedure on the membrane by spray method. TiO_2 nanoparticles (TNPs) were prepared by a sol-gel method. Briefly, 200 μL of ammonium hydroxide and 1 mL of DI water were added to 16 mL of ethanol. Then, 2 mL of titanium butoxide was injected into the solution under vigorous stirring. A TiO_2 sol was formed as the transparent mixture gradually became an opaque white color. After mixing for 10 min, a 1 mL of 10 w/v% DEA/ethanol solution was added to neutralize the hydrolysis and condensation reaction rate and stabilize the TiO_2 sol [59]. Finally, the TiO_2 sol sonicated for 20 min. The pH of the final solution was 11. The surface of the mesh and porous support layer was coated using a spray coating method. Briefly, a TFC membrane (3 cm × 6 cm) was placed on a stainless steel plate. Different amounts of TiO_2 sol (0.1 mL, 0.5 mL and 1.0 mL) were sprayed using an airbrush from an approximately 10-cm height. After the coating solution evaporated, the membranes were rinsed with DI water. The membranes coated with TiO_2 sol were identified as TNP0.1, TNP0.5 and TNP1.0, respectively, depending upon the volume of TiO_2 sol (0.1 mL, 0.5 mL, and 1.0 mL) sprayed on the surface. The membranes were subsequently compared with the uncoated TFC membrane.

3.3.2.3. Characterization of TNP coated membranes

The surface morphologies of the TNP-coated membranes were observed by field emission scanning electron microscopy (FE-SEM; JSM-6701F, JEOL, Japan). The membrane surface was coated with Pt to enhance the surface conductivity by sputtering at 20 mA for 80 s. Energy dispersive spectroscopy (EDS, JSM-6701F, JEOL, Japan) was used to analyze the elemental composition of the uncoated and TNP-coated TFC membranes. Contact angles via sessile drop method were measured to determine membrane surface hydrophilicity by using a contact angle analyzer (DSA100, KRÜSS, Germany). Briefly, membrane samples were prepared and dried at 40°C in a vacuum oven for 24 h and attached onto flat glass slides. Then, 6 μL of DI water were formed at the end of an 'I'-shaped needle, and the flat glass slide was carefully elevated toward the droplet to deposit the droplet on the membrane surface. Contact angle measurements were performed for at least three positions, and the mean values were reported with standard deviation. X-ray photoemission spectroscopy (XPS, SIGMA PROBE®, Thermo VG Scientific Co., Ltd.) analyses were performed. Carbon, oxygen, sulfur, and titanium elements were scanned at 0.10 eV steps. Surface zeta potential values of the TNP-coated membranes were measured by electrophoretic light scattering spectrophotometry (ELS-8000, Otsuka Electronics, Japan) at neutral pH.

The crystal structure of TNPs synthesized by the sol-gel method were analyzed by X-ray diffraction (XRD, Bruker D8 DISCOVER, Germany). The TNP solution

was prepared by drying in an oven at 70°C for over 12 h. The dried TNPs were deposited on a glass plate to a thickness of 2 mm. The crystal structure of the synthesized TNPs were compared with the commercial TNPs (Aeroxide P25). Attenuated total reflection Fourier-transform infrared (ATR-FTIR, Nicolet spectrophotometer 5700, Thermo Electron Corp., USA) spectroscopy was used to identify chemical bonds on the membrane surface.

3.3.2.4. Lab-scale cross-flow osmotically driven membrane system

Fig. 3-16 shows a schematic of a lab-scale cross-flow osmotically driven membrane system. More details about the system can be found in our previous study [82]. The feed and draw solutions were continuously circulated through a temperature controller and membrane cell. To evaluate the membrane performance and fouling resistance, all tests were conducted using a PRO mode (i.e., with the active layer facing the draw solution, AL-DS). The effective membrane area was 2.1 × 4.9 cm^2, the cross-flow velocity was fixed at 4 $cm \cdot s^{-1}$, the volumes of the feed and draw solution reservoirs were 4 L, and the solution temperature was maintained at 25 ± 1°C.

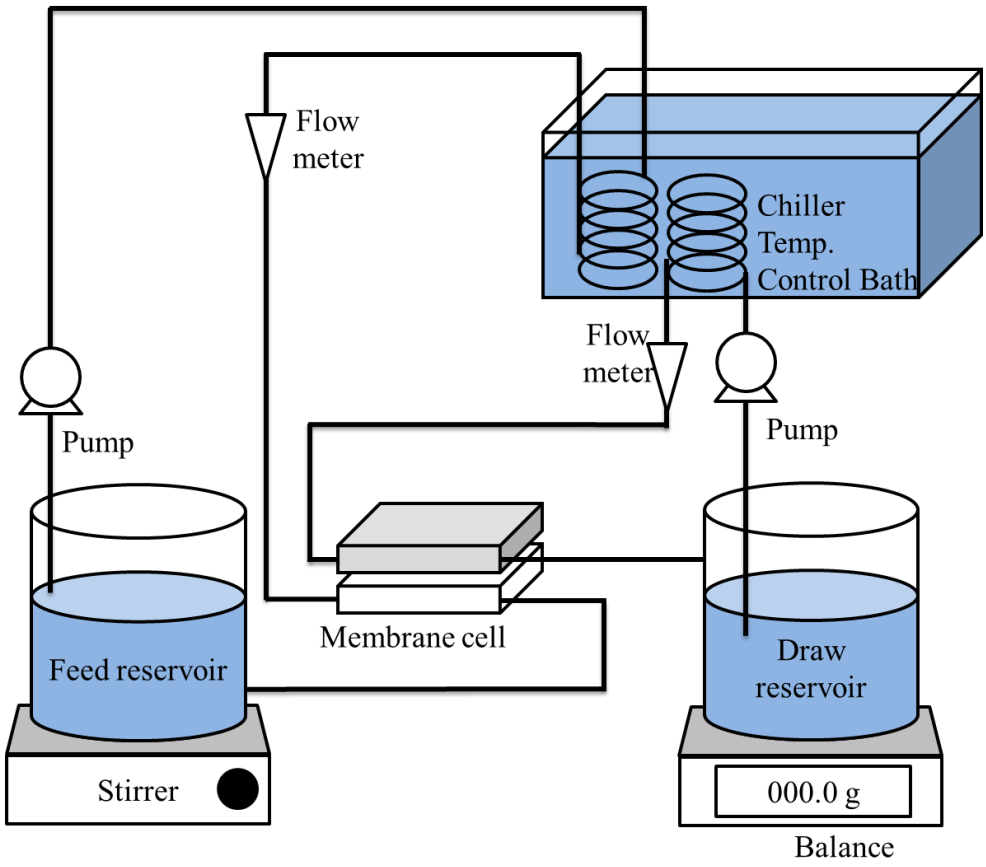

Fig. 3-16. Schematic diagram of lab-scale cross-flow osmotically driven membrane system (volumes of the feed and draw solution reservoirs: 4 L; effective membrane area: 2.1 × 4.9 cm^2).

3.3.2.5. Water permeability and reverse salt diffusion

Water permeability, reverse salt flux and fouling propensity were tested with the lab-scale cross-flow osmotically driven membrane system (Fig. 3-16). First, a membrane was placed in the membrane cell without spacers. Prior to the performance test, the cross-flow velocity and solution temperature were adjusted to 4 $cm \cdot s^{-1}$ and 25°C, respectively. After reaching a steady state, the water permeability and reverse salt flux were measured for 15 min. The water permeability and reverse salt flux were measured by monitoring changes in the draw solution weight and feed solution conductivity, respectively. The concentration of the draw solution was varied from 0.5 M to 2 M NaCl. Triplicate experiments for each membrane samples were employed for reproducibility. Mean values were reported with standard deviations.

To evaluate the effect of surface charge on reverse salt flux of PRO membrane, the reverse salt flux of TNP1.0 was measured at pH 4, 7 and 11. The pH of draw and feed solution was adjusted by addition of HCl and NaOH. The concentration of draw solution and cross-flow velocity were 1 M NaCl and 4 $cm \cdot s^{-1}$, respectively.

The salt rejection performances of the TFC and TNP1.0 membranes for various salts were tested in the dead-end filtration system. In this study, the tested membrane area was 14.6 cm^2 and 2 mM and 20 mM of NaCl, Na_2SO_4, $MgCl_2$, and $MgSO_4$ solutions were used in the feed solution. Membranes were mounted in a dead-end filtration test cell, and the feed solution was slowly pressurized by N_2

gas to 5 bar. During filtration, the water flux was maintained at approximately 1 LMH ($L \cdot m^{-2} \cdot h^{-1}$), and the salt rejection was measured by ion chromatography.

3.3.2.6. Evaluation of organic fouling characteristics

The feed solution consisted of 10 mM NaCl and 1 mM $CaCl_2$. The cross-flow velocity and initial water flux were adjusted to 4 $cm \cdot s^{-1}$ and 15 LMH, respectively, and the concentration of the draw solution was varied from 0.5 M to 1 M NaCl to maintain a consistent initial flux for the TNP-coated and TFC membranes. After a steady flux was reached, 40 mL of humic acid stock solution (10,000 $mg \cdot L^{-1}$) were added into the feed solution for so that the initial concentration of humic acid was 100 $mg \cdot L^{-1}$. The fouling experiment was performed for 6 h. The water flux was recorded every 30 min, and the water flux reduction was considered a criterion for membrane fouling.

Interaction forces between the TNP1.0 and TFC membrane surfaces and humic acid were evaluated by atomic force microscopy (AFM, Seiko Instrument, SPA-400, Japan) with a humic acid-immobilized AFM tip. The details for preparing the humic acid-immobilized AFM tips (Nanosensors, CONTR, 0.2 N m^{-1} spring constant) were described in our previous studies [83, 84]. Humic acid was immobilized onto the tip by treating the amine-terminated AFM tip with 1-ethyl-3-(3-dimethylaminopropyl)carbodiimide hydrochloride (EDC, 10 mM) and

humic acid (100 mM) solution for 2 h. The humic acid-immobilized AFM tip approached and retracted from the membrane surfaces at 0.1 $mm \cdot s^{-1}$, and the interaction forces were measured. All experiments were carried out in water at room temperature. Approximately 50 approach/retract cycles were performed for each membrane surface.

3.3.2.7. Evaluation of biofouling characteristics

To evaluate biofouling characteristics of TFC and TNP-coated membrane, cell attachment test was performed using CDC (Centers for Disease Control and Prevention) reactor. The detail experimental procedure can be found in our previous study [85, 86]. The flat sheet of TFC and TNP1.0 membranes (1 cm diameter) were attached on a round glass coupon of CDC reactor. PAO1 (*Pseudomonas aeruginosa*) tagged with green fluorescent protein (GFP) with an initial concentration of 1×10^6 CFU/mL in 0.01 wt.% tryptic soy broth (TSB) nutrient solution was filled to CDC reactor. The biofilm growth was carried out in batch mode (without nutrient flow) for 24 h, and then continuous mode for 24 h. After 48 h of biofilm growth, the volume and morphology of biofilm on membrane was observed by a confocal laser scanning microscope (CLSM, Leica Microsystems Inc., Bannockburn, IL) and the cell count was performed by plate counting method.

3.3.2.8. Durability test of TNP coating layer

The durability of TNP-coated membranes were examined by measuring the titanium weight concentrations using EDS (JSM-6701F, JEOL, Japan) after running the membrane in the cross-flow, osmotically driven membrane system for various operation times [27, 29]. Three sheets of the TNP1.0 membrane were prepared for the durability test. The membranes were tested under a 1 M NaCl draw solution and 4 $cm \cdot s^{-1}$ cross-flow velocity for 1 h, 12 h, 48 h and 168 h. The titanium weight concentrations of the membranes, which had surface areas of 800 μm × 600 μm, were obtained at three different points on each membrane.

3.2.3. Results and discussion

3.3.3.1. Surface morphology of TNP membranes

The surface morphology of TNP-coated and TFC membranes were observed using SEM and are shown in Fig. 3-17. Figs. 3-17(a) – (c) show dense TNP layers formed over porous surfaces and meshes in the TNP-coated membranes (TNP0.1, TNP0.5, and TNP1.0). The TNPs are relatively well distributed on TFC membrane, although not perfectly distributed. Fig 3-17(c) shows that the nature of heterogeneous coating becomes more visible at around a mesh-type of supporting layer. However, the membrane water flux was not affected significantly by this heterogeneous coating as observed in Fig. 3-22. Fig. 3-17(e) is an enlarged image of the TNP1.0 membrane and clearly shows the fine TNP particles with diameters of approximately 30-40 nm (compare with an enlarged image of the TFC membrane in Fig. 3-17(f)).

The thickness of the TNP coating layer varied from 0.3 μm to 1.9 μm (TNP 0.1, TNP0.5, and TNP1.0; refer to Fig. 3-18 in the Supporting Information). The thickness increased as the TiO_2 sol concentration increased, which was in good agreement with EDS analyses results (data not shown), for the TNP0.1, TNP0.5 and TNP1.0 membranes at 2.7%, 4.0% and 16%, respectively. The sol-gel-synthesized TNP appeared to have amorphous structures and showed no peaks in the XRD spectra (Fig. 3-19). Comparatively, the commercial TNP (Aeroxide P25) showed structures indicative of anatase and rutile.

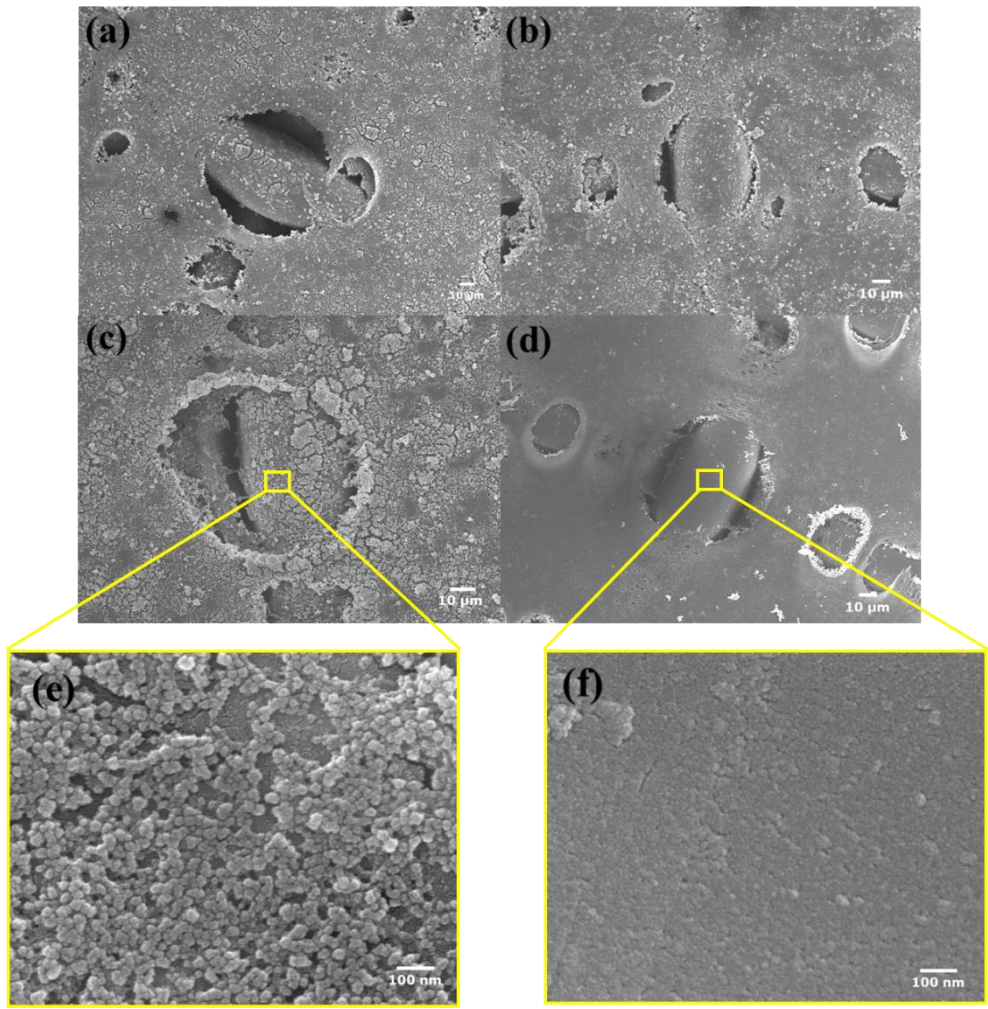

Fig. 3-17. SEM images of (a) TNP0.1, (b) TNP0.5, (c) TNP1.0, (d) TFC, enlarged images of (e) TNP1.0 and (f) TFC (note that TNP*X* indicates a membrane with TiO_2 sol (*X* mL) sprayed on the TFC membrane).

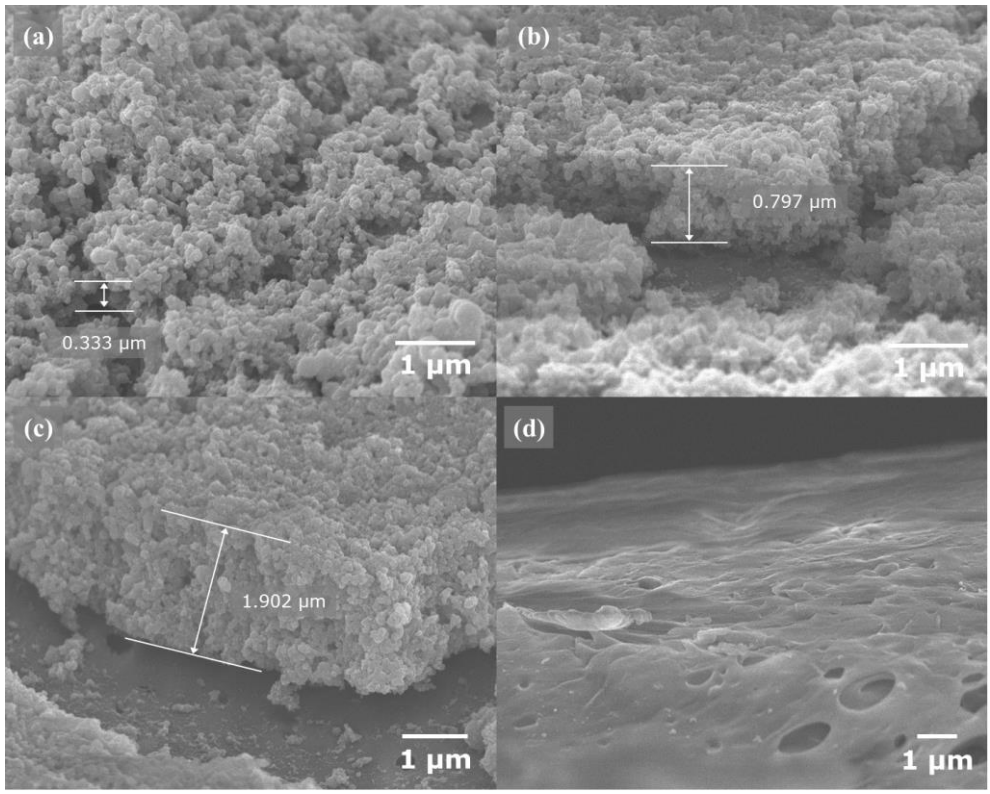

Fig. 3-18. SEM side view images of (a) TNP0.1, (b) TNP0.5 and (c) TNP1.0 and (d) TFC membranes (note that TNP*X* indicates a membrane with TiO_2 sol (*X* mL) sprayed on the TFC membrane).

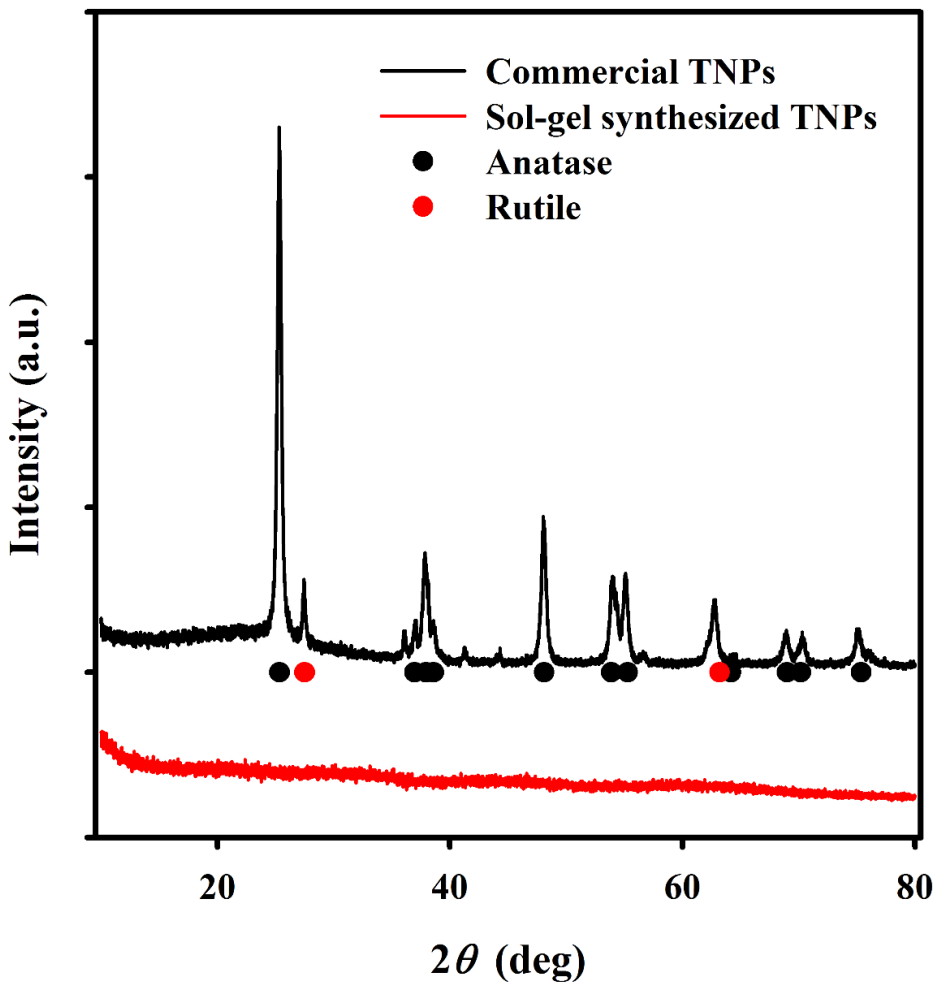

Fig. 3-19. XRD spectra of sol-gel synthesized TNPs and commercial TNPs (Aeroxide P25) (black and red dot represent anatase and rutile structure peaks).

3.3.3.2. X-ray photoelectron spectroscopy analysis

Fig. 3-20 compares the high resolution XPS spectra of the TNP1.0 and TFC membranes in terms of carbon, oxygen, sulfur and titanium presence. The XPS spectra of TNP1.0 and TFC shows Ti and Ti-O peaks, indicating that TiO_2 coating layers were successfully synthesized by the sol-gel method from the titanium butoxide precursor. As shown in Fig. 3-20(a), the TNP1.0 spectrum showed four titanium peaks: Ti 2p3/2 (457 – 459 eV), Ti 2p1/2 (463 – 464 eV), Ti^{3+} (457.2 eV & 462.8 eV), and Ti^{4+} (458.4 eV & 464.2 eV) [87, 88]. The oxygen spectrum of TNP1.0 shows that two Ti-O bond peaks were detected with the peaks (OH- and C-O-C) at 530.0 eV and 531.3 eV [89-91]. The peak intensity of C-O-C (532.0 eV) was reduced likely because the TNP coating layer weakened the peak intensity of the support layer. The carbon spectra show that a C-SO_2 peak (at 286.1 eV) and an aromatic ring peak at (291.0 eV) disappeared after the TNP layer was applied. The sulfur spectra show that C-S-C and SO_2 peaks were present in the TFC sample at 163.1 eV and 164.3 eV, respectively, but were missing in the TNP1.0 sample. The disappearance of these peaks after TNP coating is due to the limited penetration depth of XPS (~10 nm), which is much thinner than the thickness of TNP layer (~ 2 μm) [74, 92-94]. ATR-FTIR results confirmed the formation of a TiO_2 coating layer (Fig. 3-21) and showed Ti-O peaks at 561 cm^{-1} and 690 cm^{-1} [28, 95, 96].

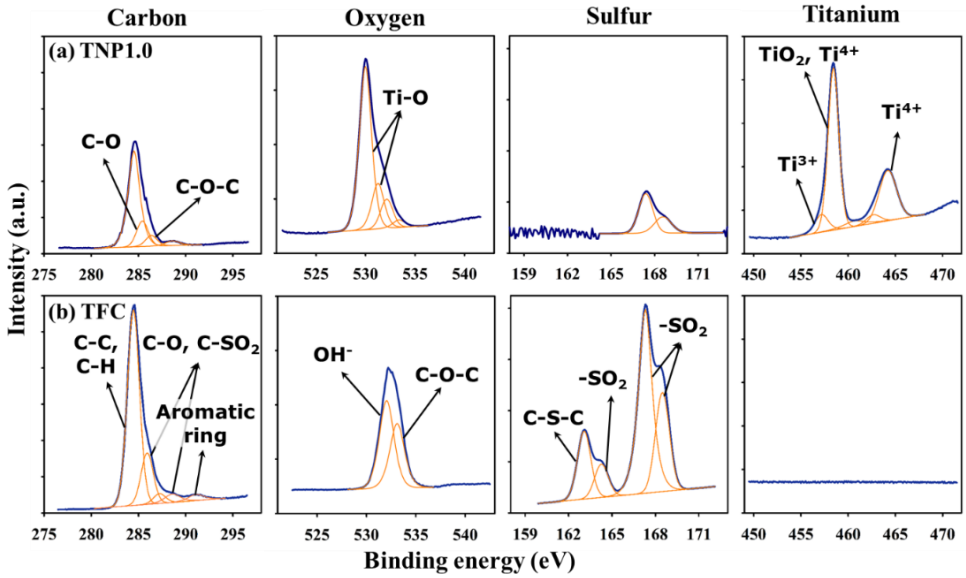

Fig. 3-20. High resolution X-ray photoelectron spectroscopy spectrum of (a) 1.0 mL of TiO_2 sol coated and (b) TFC membranes.

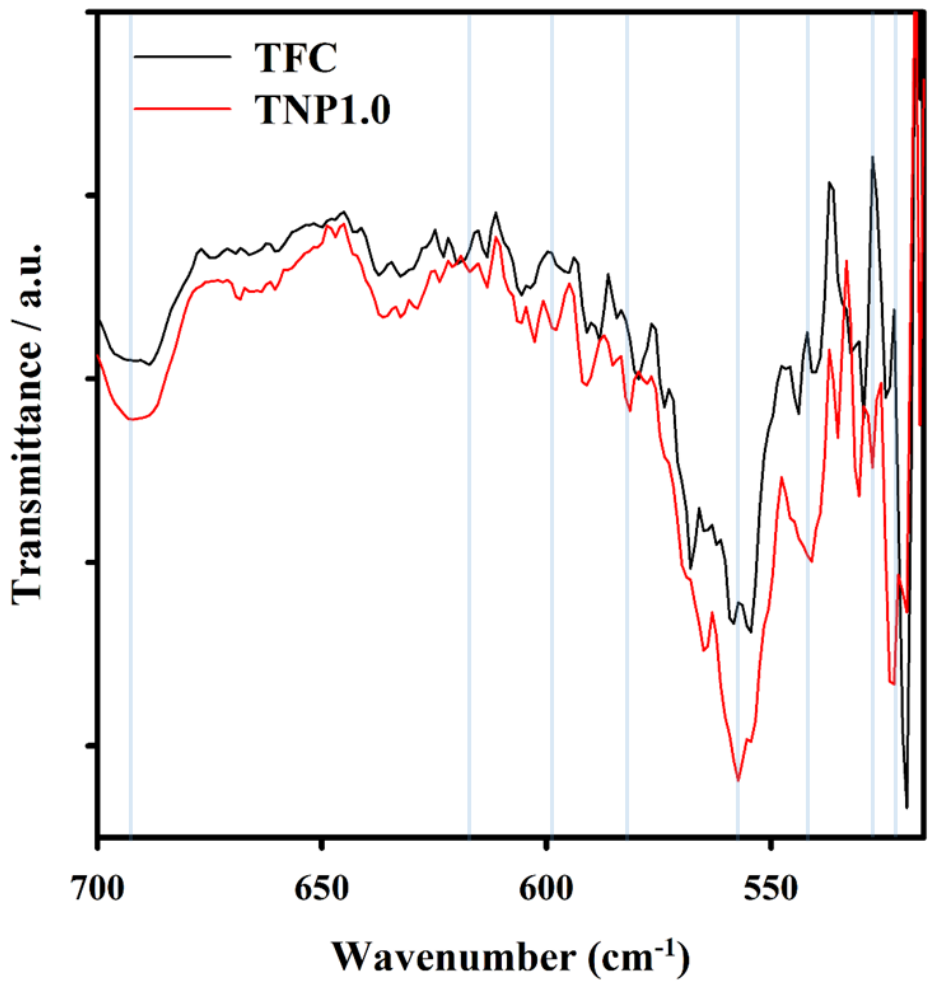

Fig. 3-21. ATR-FTIR spectra of TNP1.0 and TFC membranes (note that TNP1.0 indicates 1 mL of TiO_2 sol sprayed on a TFC membrane).

3.3.3.3. Surface properties of TNP coated membrane

Table 3-1 shows the water contact angle and zeta potential measurements of the TNP-coated membranes (TNP0.1, TNP0.5, and TNP1.0) and the TFC membrane. The membrane surface of the TNP-coated membranes were more hydrophilic than the TFC membrane. For example, the average water contact angles of the TNP0.1, TNP0.5 and TNP1.0 membranes were 27.4°, 16.6° and 16.4°, respectively, while the water contact angle of the TFC membrane was 78°, indicating the TNP-coated membranes were more hydrophilic than the TFC membrane. The zeta potential measurements confirm this observation. The zeta potentials of the TNP membranes varied from -20.8 mV to -41.9 mV, and the zeta potential of the TFC membrane was -9.31 mV. This significant negative enhancement of the surface charge is attributed to TiO_2, which is usually negatively charged in neutral or basic solutions [97-99].

Table 3-1. Water contact angle and zeta potential of TNP coated- and TFC membranes (Note that TNP indicates TiO_2 nanoparticle coated membrane and the number implies the amount of sprayed TiO_2 sol on the TFC membrane)

Membrane	Contact angle (°)	Zeta potential (mV)
TNP0.1	27.4 ± 3.8	-20.8
TNP0.5	16.6 ± 2.9	-25.6
TNP1.0	16.4 ± 1.2	-41.9
TFC	77.8 ± 3.2	-9.3

3.3.3.4. Water flux and reverse salt flux of TNP membranes

Fig. 3-22 compares the water flux and reverse salt flux of TNP-coated (TNP0.1, TNP0.5, and TNP1.0) and TFC membranes. The water fluxes across the TNP0.1, TNP0.5 and TNP1.0 membranes were 22.7 LMH, 23.9 LMH and 26.4 LMH, respectively. The water flux increased as the amount of TNP coating increased. The water flux across the TFC membrane was 21.2 LMH. This result can be explained by the enhanced hydrophilicity of the TNP coatings. Because a hydrophobic surface hinders water transport near the membrane surface and may result in dead spaces in the membrane support layer, it is plausible that a hydrophilic coating can increase the sorption of water into the support layer and enhance the water flux. These results were consistent with those of a previous study [74] wherein a PES-TFC membrane coated with hyperbranched polyglycerol showed an approximately 50% enhanced water flux over a bare PES membrane due to increased membrane wettability. The reverse salt fluxes of the TNP0.1, TNP0.5 and TNP1.0 membranes were much lower than that of the TFC membrane.

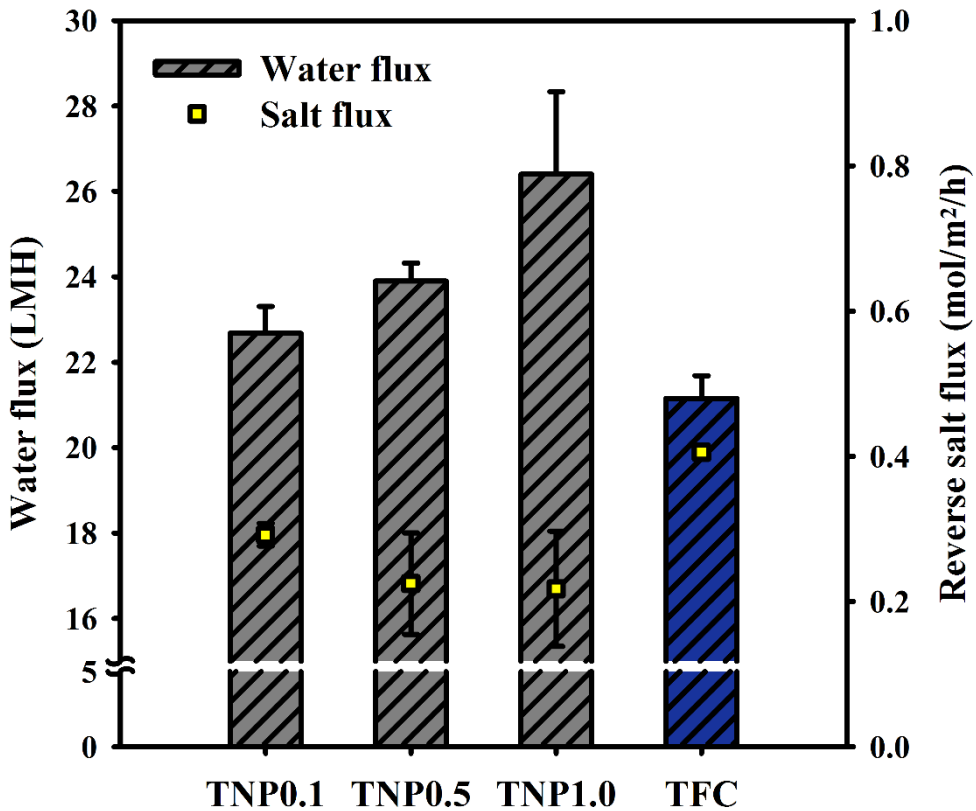

Fig. 3-22. Water flux and reverse salt flux change with the amounts of TNP coating (draw solution: 1 M NaCl; cross-flow velocity: 4 $cm \cdot s^{-1}$; 25°C; note that TNP*X* indicates a membrane with TiO_2 sol (*X* mL) sprayed on a TFC membrane; The permeate flux was measured in PRO mode (active layer facing draw solution) in the condition of no pressure applied; n=3).

Fig. 3-23 compares the water flux and reverse salt flux of the TNP1.0 and TFC membranes for different draw solution concentrations. As illustrated in Fig. 3-23(a), the water flux of the TNP1.0 membrane was higher than that of the TFC membrane for all draw solution concentrations. Furthermore, the flux increased with the draw solution concentration as expected due to the increased osmotic gradient. The reverse salt flux of the TNP-coated membrane was lower than that of the TFC membrane for all draw solution concentrations. The reverse salt flux also increased with the draw solution concentration. The reverse salt flux of the TNP1.0 membrane increased from 0.14 $mol \cdot m^{-2} \cdot h^{-1}$ to 0.32 $mol \cdot m^{-2} \cdot h^{-1}$, while that of the TFC membrane increased from 0.32 $mol \cdot m^{-2} \cdot h^{-1}$ to 0.67 $mol \cdot m^{-2} \cdot h^{-1}$. This indicated that the TNP membrane had a higher selectivity than the TFC membrane. Salt rejection test was carried out for various salt in RO mode using dead-end filtration cell and results are given in Fig. 3-24. The main purpose of this test was to compare the salt rejection performance of TFC and TNP1.0 more accurately. As we can see from Fig. 3-24(a) and (b), TNP1.0 demonstrated higher salt rejection than TFC membrane regardless concentration of feed water and a kind of salt. One explanation for the enhanced salt exclusion of the TNP coated membrane is that negatively charged support layer of TFC membrane resulting from the coating of negatively charged TNPs may have contributed to enhance reverse salt flux by increasing Donnan exclusion phenomenon as a result of electrostatic repulsion between ions and the fixed charge of the membrane (Fig. 3-25) [56, 100, 101].

The reverse salt flux result–measured at pH 4, 7, and 11(Fig. 3-26)–support this explanation. The TNP1.0 showed smaller reverse salt flux than TFC at all pH conditions. Moreover, reverse salt flux decreased as pH increased. Since the surface negative charge of TiO_2 increase with pH, Donnan exclusion phenomenon might be increased at high pH condition, finally, decreasing reverse salt flux.

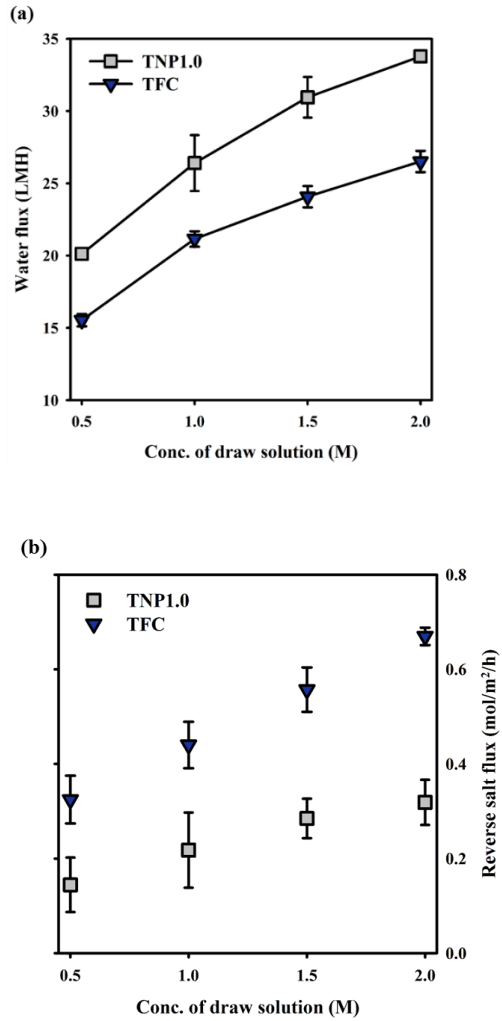

Fig. 3-23. (a) Water flux and (b) reverse salt flux of TNP1.0 and TFC membranes with respect to draw solution NaCl concentration (cross-flow velocity: 4 $cm \cdot s^{-1}$; 25°C; note that TNP1.0 indicates 1 mL of TiO_2 sol sprayed on a TFC membrane; The permeate flux was measured in PRO mode (active layer facing draw solution) in the condition of no pressure applied; n=3)

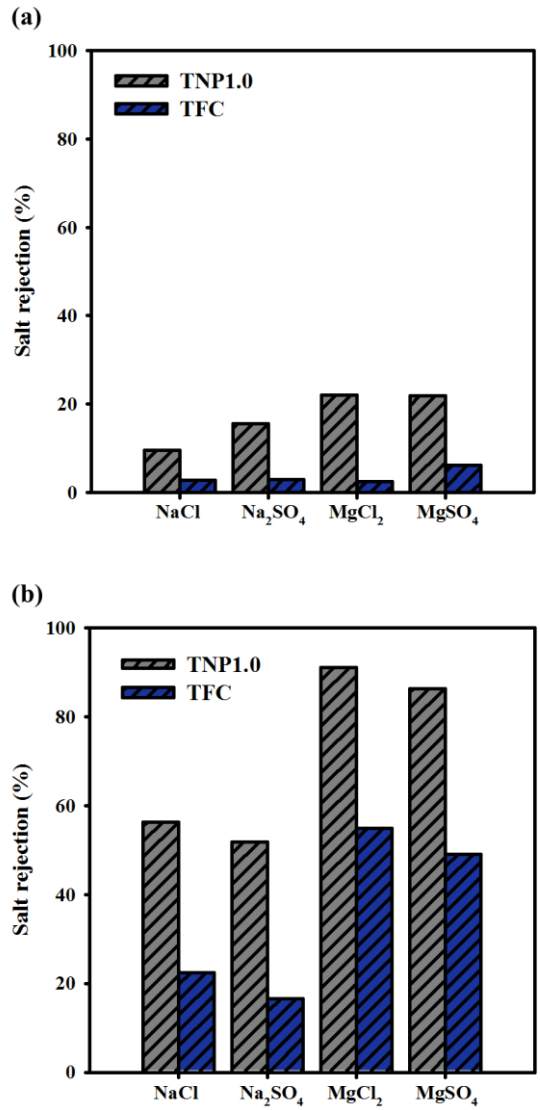

Fig. 3-24. Salt rejection measured for four salt solution (a) 2 mM and (b) 20 mM of TNP1.0 and TFC membranes using dead-end filtration cell (effective area of dead-end filtration cell: 14.6 cm^2; note that TNP1.0 indicates 1 mL of TiO_2 sol sprayed on a TFC membrane).

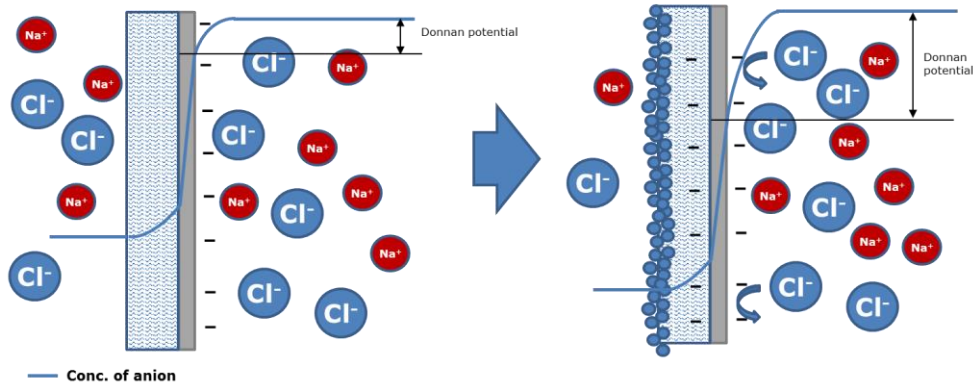

Fig. 3-25. Schematic diagram of reverse salt flux enhancement mechanism by TiO_2 nanoparticle coating of PRO membrane support layer.

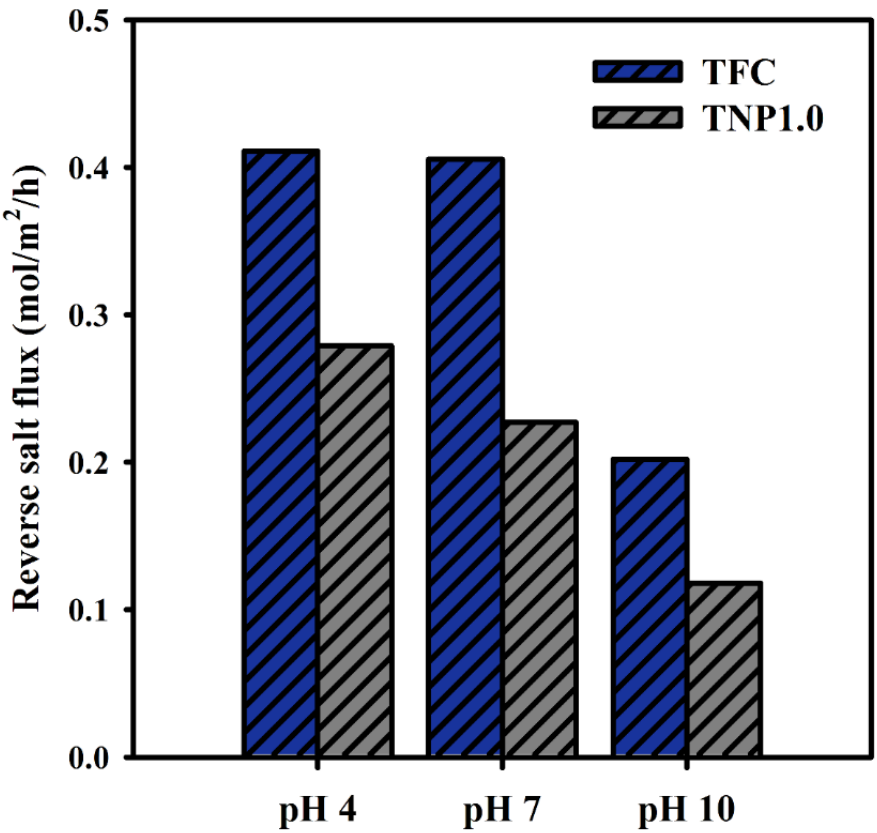

Fig. 3-26. Effect of pH condition on reverse salt flux of TFC and TNP1.0 membranes (draw solution: 1 M NaCl; cross-flow velocity: 4 $cm \cdot s^{-1}$; 25°C; note that TNP*X* indicates a membrane with TiO_2 sol (*X* mL) sprayed on a TFC membrane; The permeate flux was measured in PRO mode (active layer facing draw solution) in the condition of no pressure applied).

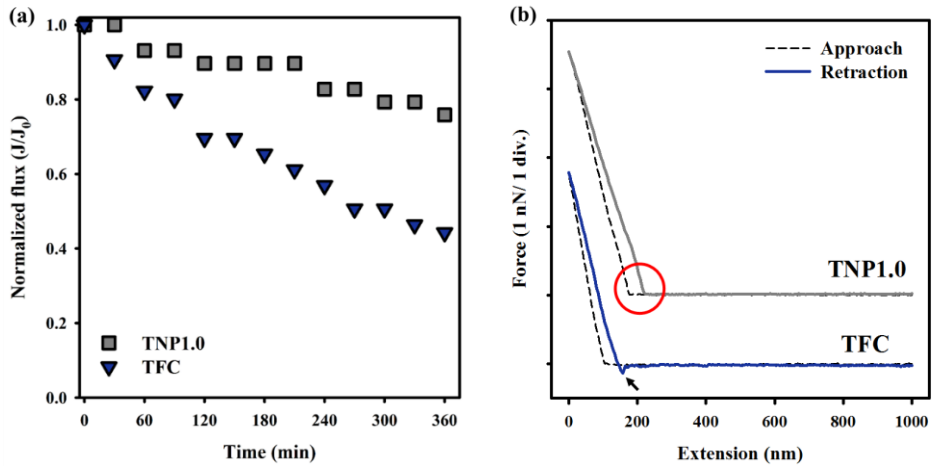

Fig. 3-27. Organic fouling characteristics of 1.0 mL of TiO_2 sol coated and TFC membranes (a) Normalized flux change under humic acid filtration (Time '0' implies the point of humic acid dosage; feed solution: 10 mM NaCl, 1 mM $CaCl_2$ and 100 mg/L humic acid; draw solution: 1 M NaCl; cross-flow velocity: 4 $cm \cdot s^{-1}$; initial water flux: 15 LMH; 25°C), (b) force-extension curve of humic acid-immobilized AFM tip against membrane surface

3.3.3.5. Organic fouling property of TNP coated membrane

Fig. 3-27(a) shows the normalized flux decline of TNP1.0 and TFC membranes over 360 min in the presence of humic acid. The normalized flux of the TFC membrane significantly decreased to 0.44 while that of the TNP1.0 membrane only decreased to 0.76, indicating that the flux reduction of the TNP membrane was 32% less than that of the TFC membrane. Because humic acid is hydrophobic and negatively charged, a less negatively charged (i.e., neutral or positive) and hydrophobic membrane would be vulnerable to organic fouling due to more favorable foulant-membrane interactions [36, 102]. The less favorable foulant-membrane interactions of the TNP-coated membranes were confirmed by the interaction forces between a humic acid-immobilized AFM tip and the membrane surfaces, as shown in Fig. 3-27(b). During the retraction step of the humic acid-immobilized AFM tip, the TNP1.0 membrane indicated no observable pull-off force (red circle), whereas the bare TFC membrane showed 0.14 nN of pull-off force (black arrow). This indicated that the TNP1.0 membrane had a less interactive force with humic acid than the bare TFC membrane.

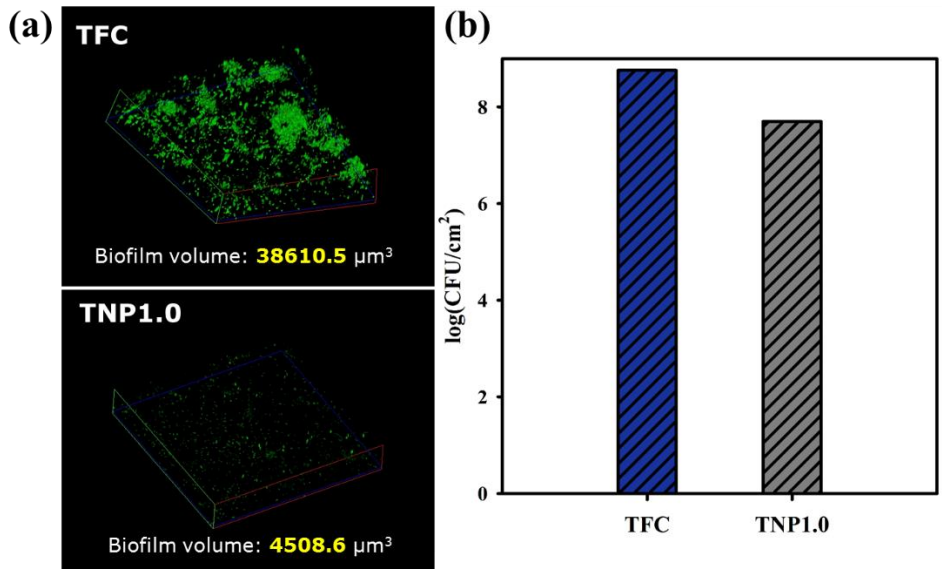

Fig. 3-28. Biofouling characteristics of TFC and TNP-coated membranes (a) CLSM image of TFC and TNP1.0 membranes, (b) amount of PAO1 on TFC and TNP1.0 membrane.

3.3.3.6. Biofouling property of TFC and TNP coated membrane

Fig. 3-28 shows the biofouling property of TFC and TNP coated membrane. The morphology of PAO1 biofilm was observed by CLSM (Fig. 3-28(a)). As can be seen in Fig. 3-28(a), the CLSM image and the calculated biofilm volume show that approximately 9—10 times smaller amount of biofilm was attached and grown on the membrane surface of TNP1.0 compared to that of TFC membrane. It seems that TiO_2 nanoparticle coating layer enhanced hydrophilicity and surface negative charge and these modified surface property hindered the attachment of microorganism on membrane surface.

Table 3-2. Durability test of 1.0 mL TiO_2 sol coated membrane with various operating time (n=3)

Sample	Relative weight concentration (average, %)			
	C	O	S	Ti
Initial	41.4 ± 1.03	38.7 ± 0.68	3.29 ± 0.18	16.7 ± 0.56
1 h	38.6 ± 0.91	41.4 ± 0.53	3.86 ± 0.34	16.4 ± 0.64
12 h	37.8 ± 0.67	42.6 ± 0.82	3.17 ± 0.34	16.4 ± 0.46
48 h	37.5 ± 0.81	43.2 ± 1.11	4.17 ± 0.17	16.6 ± 0.45
168 h	34.5 ± 0.96	45.4 ± 0.16	3.56 0.03	16.4 ± 0.66

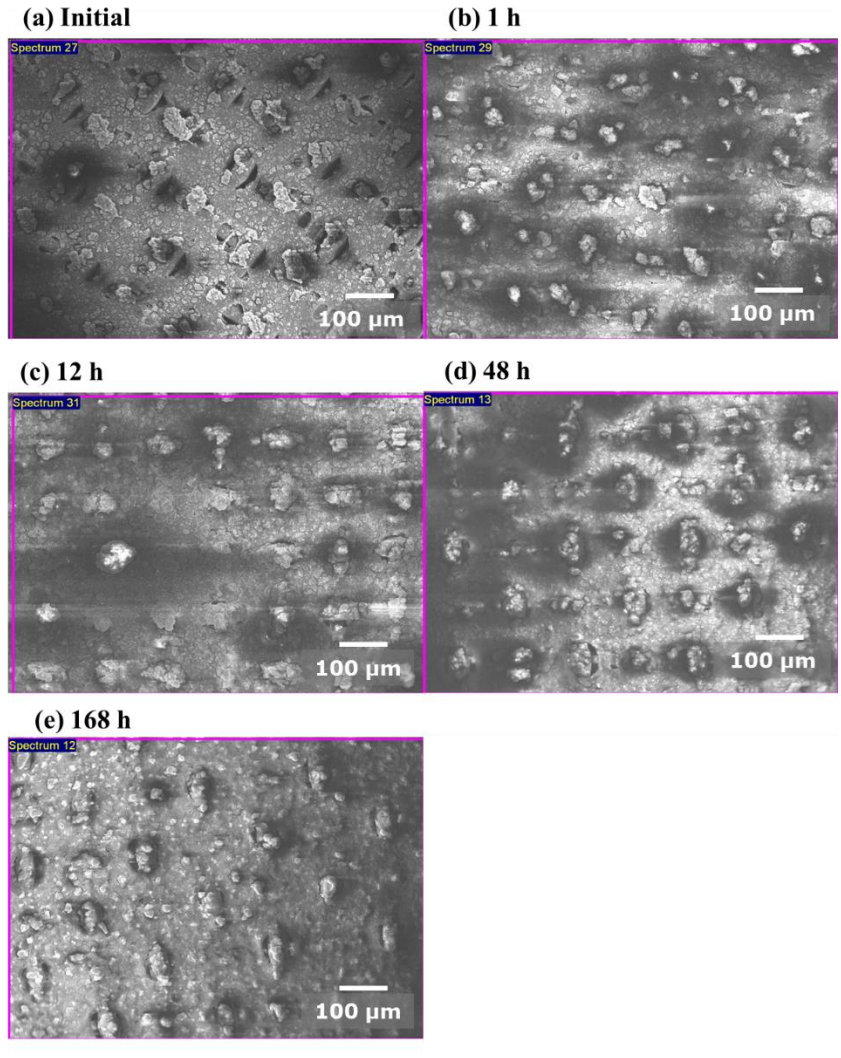

Fig. 3-29. SEM images for surface morphology change observation of TNP1.0 membrane under various operation times (The test was performed using lab scale cross-flow osmotically-driven membrane system; cross-flow velocity: 4 $cm \cdot s^{-1}$; draw solution: 1 M NaCl; note that TNP1.0 indicates 1 mL of TiO_2 sol sprayed on a TFC membrane).

3.3.3.7. Durability of TNP coating layer

The durability of the TNP coating layer was evaluated based on the relative weight percentages of titanium in the TNP1.0 membrane over time (1 h, 12 h, 48 h, and 168 h). The EDS results (Table 3-2) showed that the weight percentage of titanium was maintained within 16%, indicating that the TNPs remained mostly attached for up to 168 h of operation. This result was further supported by the morphology of the TNP coating layer, which showed no distinguishable change over time (Fig. 3-29). This indicated that a strong and stable TNP coating layer was formed via the sol-gel-derived spray coating. The strong and stable interaction of TNP with the TFC membrane [28, 29]. was due to the self-assembly of the TNPs on the membrane surface by a bidentate coordination of a sulfone group, an ether bond to Ti^{4+}, a H-bond between the sulfone group, and an ether bond to a TiO_2 surface hydroxyl group [103]. Additionally, the sol-gel reaction of the residual titanium butoxide in TiO_2 sol on the membrane surface potentially provided extra links between TNPs and between TNPs and the surface and thereby, contributed to a more durable TNP coating layer.

3.3. Facile surface modification of PA TFC RO membrane using TiO_2 sol-gel derived spray coating method to enhance anti-fouling property

3.3.1. Introduction

Membrane fouling is considered as one of the main obstacle for RO process [15, 16]. Membrane fouling causes the reduction of membrane performance (i.e. water flux and salt rejection) resulted from hinder the water transport and cause concentration polarization near the membrane surface, eventually, increase the operating cost [18].

The fouling characteristics of a membrane is affected by its surface property such as hydrophilicity, morphology, and surface charge [35]. In general, hydrophilic, smooth, and negatively charged membranes are known to have resistance to the fouling because foulant (i.e. protein and humic acid) naturally has the hydrophobic and negatively charged surface property [36]. On the basis of these understanding of membrane fouling mechanism, development of anti-fouling RO membrane has been conducted. Hydrophilic modification of RO membrane surface via plasma polymerization [104], graft polymerization [49], and grafting poly(ethylene glycol) (PEG) [105] showed enhanced fouling resistance. PEG- [106], or zwitterionic film coating [107] on RO membrane were

also resulted in improving anti-fouling property by increasing the steric repulsion to foulants.

This study introduced a facile surface modification for a fouling resistant PA RO membrane via TiO_2 sol-gel derived spray coating method. TiO_2 nanoparticle (TNP) was prepared by base catalyzed sol-gel method and coated on the commercial PA RO membrane by spray coating method. The surface properties of TNP coated PA RO membrane were analyzed by using scanning electron microscope, X-ray photoemission spectroscopy, attenuated total reflection Fourier-transform infrared, contact angle analyzer and zeta potential analyzer. The water flux, salt rejection, and organic fouling property of the TNP coated PA RO membrane was evaluated in lab-scale cross-flow RO filtration system.

3.3.2. Materials and methods

3.4.2.1. Materials

Commercial PA RO membrane (RE-SHF) was kindly provided by Toray chemical company (Korea). Titanium butoxide ($Ti(OC_4H_9)_4$, reagent grade, 97%), diethanolamine (DEA, $HN(C_2H_4OH)_2$, reagent grade, ≥ 98%), ammonium hydroxide (NH_4OH, 28% in H_2O), sodium chloride (anhydrous, ≥ 99.0%), humic acid (technical grade) were purchased from Sigma Aldrich. Ethanol (99.9%, Samchun Chemical) was chosen as solvent of TiO_2 sol-gel process.

3.4.2.2. Preparation of TiO_2 sol and TiO_2 nanoparticle coated PA membrane

TiO_2 nanoparticle (TNP) was synthesized by base catalyzed TiO_2 sol-gel reaction. Ammonium hydroxide 100 μL, DI water 1 mL, and ethanol 16 mL were mixed as base catalyst and solvent, respectively. While maintaining vigorous stirring, titanium butoxide 2 mL was injected into ethanol and the solution was changed into white color TiO_2 sol. After 10 min stirring, 1 mL of 10 w/v% DEA/ethanol solution was injected into TiO_2 sol as stabilizer to slow down the hydrolysis and condensation reaction [59]. Finally, TiO_2 sol was sonicated in bath sonicator for 20 min. The prepared TiO_2 sol was deposited onto PA membrane with spray coating method. The PA RO membrane (10 cm × 10 cm) was fixed on stainless plate and certain volume of TiO_2 sol was sprayed using airbrush on PA RO

membrane and each membrane identified TNPROX. Note that TNPRO indicates TiO_2 nanoparticle coated RO membrane and the X implies the amount of sprayed volume of TiO_2 sol on the PA RO membrane. After the sprayed solution evaporated, membrane samples were rinsed with DI water and stored in DI water before tested.

3.4.2.3. Surface characterization of TNP coated membranes

Field emission scanning electron microscope (FE-SEM; JSM-6701F, JEOL, Japan) was used to observe surface morphology of TNP coated and bare PA membrane. To obtain clear SEM image, membrane surface was coated with Pt by sputter coater at 20 mA for 80 s. Electron composition of TNP coated membrane was analyzed using energy dispersive X-ray spectroscopy (EDS, JSM-6701F, JEOL, Japan). Surface hydrophilicity of TNP coated and bare PA membrane were characterized through a sessile drop method by using a contact angle analyzer (DSA100, KRÜSS, Germany) [57]. Zeta potential of TNP coated and bare PA membrane was analyzed by electrophoretic light scattering spectrophotometer (ELS-8000, Otsuka Electronics, Japan). The TNPRO2.0 and bare PA membrane were analyzed by X-ray photoemission spectroscopy (XPS, SIGMA PROBE®, Thermo VG Scientific Co. Ltd.) in terms of carbon, oxygen, sulfur, and titanium. Each elements were scanned in 0.10 eV steps and the element spectrum was fitted to the C1s peak (285.0 eV).

3.4.2.4. Water flux and salt rejection change

Water flux and salt rejection of the TNP coated PA RO membrane was evaluated in a lab-scale cross-flow RO filtration system. More details of the system was described in our previous study [108]. In this study, 6 L feed water containing 2,000 mg/L NaCl was used and an effective membrane area was 22.4 cm^2 (3.3 cm x 6.8 cm) with 0.3 cm of channel height. The membrane performance test was performed with 8 $cm \cdot s^{-1}$ of cross-flow velocity at 25°C. After the membrane compaction for 30 min at 15.5 bar, the permeated water was collected into bottle for 20 min under same pressure. The water flux and salt rejection were calculated according to equation (1) and (2), respectively:

$$J_w = \frac{V}{A \times t} \quad (1)$$

$$R_s = \left[1 - \frac{C_p}{C_f}\right] \times 100 \quad (2)$$

where, equation (1), J_w is the water flux (LMH, $L \cdot m^{-2} \cdot h^{-1}$), V is the permeated volume of water, A is the effective membrane area (m^2), t is measuring time (h). R_s is the NaCl rejection percentage ratio, C_f is the conductivity of feed water ($mS \cdot cm^{-1}$) and C_p is conductivity of permeate ($mS \cdot cm^{-1}$) in equation (2). A conductivity meter (Horiba) was used to evaluate the salt rejection.

3.4.2.5. Organic fouling test of TNP coated membrane compared to bare PA RO membrane

Organic fouling characteristics of TNP coated- and commercial PA RO membrane were evaluated by measuring flux changes. The membrane was mounted in membrane cell of the cross-flow RO filtration system. The operating condition was set up to 35 LMH of initial flux, 4 $cm \cdot s^{-1}$ of cross-flow velocity at 25°C. The feed water consists of 10 mM $CaCl_2$ and 1 mM NaCl. After system was stabilized, 1,200 mg of humic acid was added to feed water tank to adjust humic acid concentration of feed water for 200 $mg \cdot L^{-1}$ of humic acid. The changes of water flux was automatically recorded by computer every 30 min and the fouling was carried out for 19 h.

The atomic force microscope (AFM, Seiko Instrument, SPA-400, Japan) was used to measure the interaction forces between membrane surfaces and humic acid immobilized AFM tips (Nanosensors, CONTR, spring constant = 0.2 $N \cdot m^{-1}$). Similarly to our previous studies [83, 84], the humic acid-immobilized AFM tips were prepared by surface chemical reaction of amine-terminated AFM tip and 100 mM of humic acid solution. A speed of 0.1 $mm \cdot s^{-1}$ was applied to obtain the force–extension curves during approach and retraction of the membrane surfaces from the humic acid-immobilized AFM tip. All experiments were carried out in water at room temperature. Approximately 50 approach/retract cycles were performed for each membrane surface collected.

3.3.3. Results and discussion

3.4.3.1. Characterization of TNP membranes

Fig. 3-30 shows the SEM images of TNP coated and bare PA RO membrane. In Figs 3-30 (a) – (d), TNP coated membranes display that the ridge and alley structure of bare PA membrane (Fig. 3-30 (e)) surface was covered with TNPs and the TNP coated area increased with the amount of sprayed TiO_2 sol. As shown in Fig. 3-30 (f), the size of TNPs, which were deposited on TNP2.0 with sol-gel derived spray coating method, appeared to be 30–50 nm.

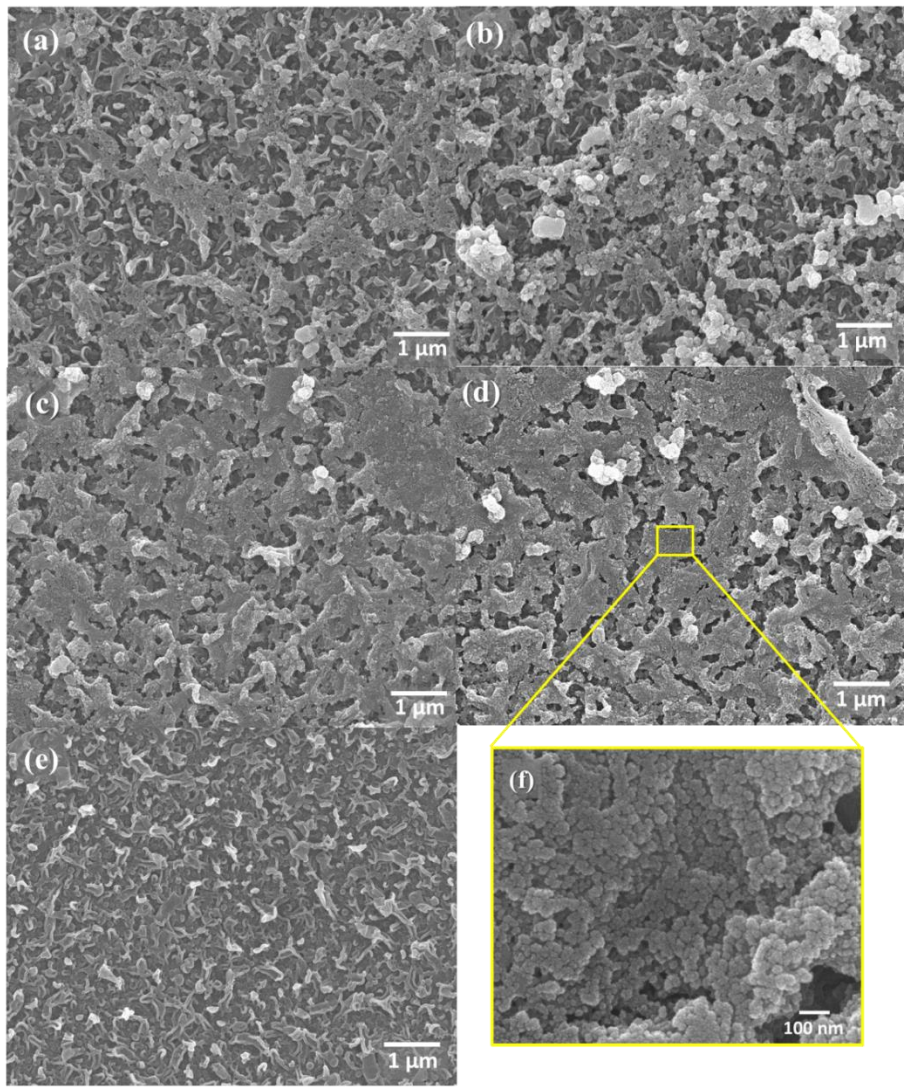

Fig. 3-30. SEM images of (a) TiO_2 nanoparticles on PA membrane (enlarged image of TNPRO2.0), (b) TNPRO0.5, (c) TNPRO1.0, (d) TNPRO1.5, (e) TNPRO2.0 and (f) bare PA (Note that TNPRO indicates TiO_2 nanoparticle coated membrane and the number implies the amount of sprayed TiO_2 sol on the PA RO membrane)

TNP coating layer on the PA RO membrane was also observed by EDS analysis (Fig. 3-31). Fig. 3-31(a) shows the titanium weight concentration change of TNP coated membranes as function of TNP coating amount on PA RO membrane. The titanium weight concentration of TNP coated membranes gradually increased from 1.2% to 5.1% as increased coating amount of TiO_2 sol while commercial PA RO membrane showed no titanium. EDS mapping analysis also reveals the observed coating layer consist of TiO_2. Figs 3-31(c)–(e) displayed carbon, titanium and oxygen elemental mapping of TNPRO2.0. Note that red, green, and yellow color indicate carbon, titanium, and oxygen, respectively and brightness difference of color implies the amount of each element. While the carbon signal (Fig. 3-31(c)) was detected uniformly with no difference of brightness, titanium and oxygen signal (Figs 3-31(d) and (e)) showed various intensity of signal and its morphology was very similar with coating layer on TNPRO2.0 observed by SEM image (Fig. 3-31(b)).

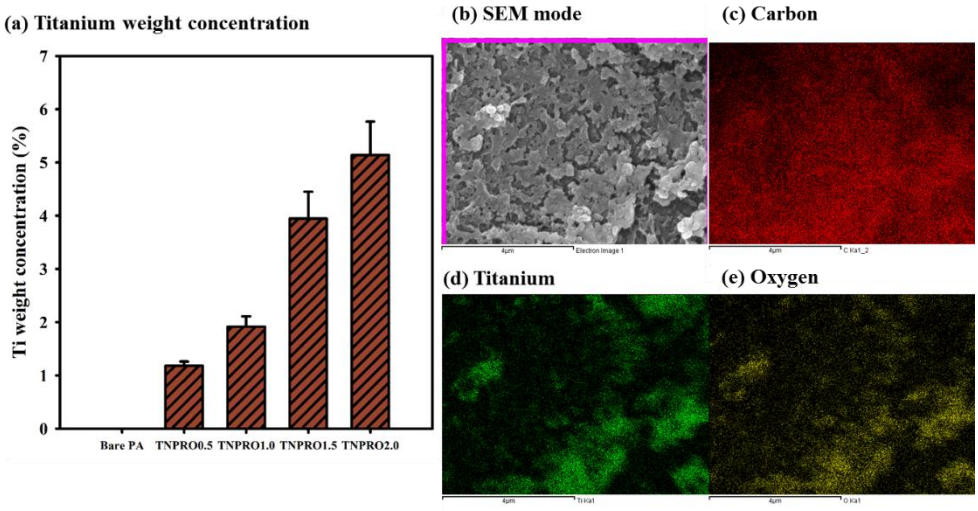

Fig. 3-31. EDS analysis results; (a) titanium weight concentration of TNP membranes, (b) SEM image of TNPRO2.0 membrane and its elemental mapping in terms of (c) carbon, (d) titanium, and (e) oxygen (Note that TNPRO indicates TiO_2 nanoparticle coated membrane and the number implies the amount of sprayed TiO_2 sol on the PA RO membrane)

Fig. 3-32 illustrates the XPS spectrum of TNPRO2.0 in comparison with bare PA RO membrane. As shown in Fig. 3-29, two main change was observed in XPS spectrum. First, Ti and Ti-O peak was detected in TNPRO2.0 after TNP coating. The titanium spectrum of TNP2.0 represented four titanium peaks as follows: Ti 2p3/2 (457 – 459 eV), Ti 2p1/2 (463 – 464 eV), Ti^{3+} (457.0 eV & 462.8 eV), and Ti^{4+} (458.3 eV & 464.1 eV) [87, 88]. In oxygen spectrum, Ti-O peaks at 529.9 eV and 531.3 eV were found after TNP coating [90, 109]. These formation of Ti and Ti-O peaks obviously indicates that TiO_2 was synthesized from titanium butoxide via base catalyzed sol-gel method. In order to confirm this result, ATR-FTIR analysis was performed (Fig. 3-33). In the range of 450-700 cm^{-1}, several peaks, which might be attributed to the Ti-O-Ti bond, were detected and this also support the formation of TiO_2 [95, 96] . On the other hand, the TiO_2 layer coated on PA surface blocks the XPS signal from PA layer or makes the peak intensity of PA layer weakened. The C-O peaks (285.6 eV), C-N peak (287.7 eV), C=O peak (533.5 eV), and aromatic ring peak (290.9 eV) was disappeared and the peak intensity of C-C (284.5 eV), C-O (532.4 eV), and C-N (399.7 eV) was reduced after TiO_2 coating [110-113]. It seems that deposition of TiO_2 coating layer reduce or hide the XPS signal of PA layer owing to the low XPS penetration depth. The peaks at 285.8 eV and 401.5 eV corresponding to the $C\text{-}N^+$ bond was generated in TNP2.0 [113, 114]. This might be a reason that the basic TiO_2 sol leads to the release of protons from amide group of PA layer.

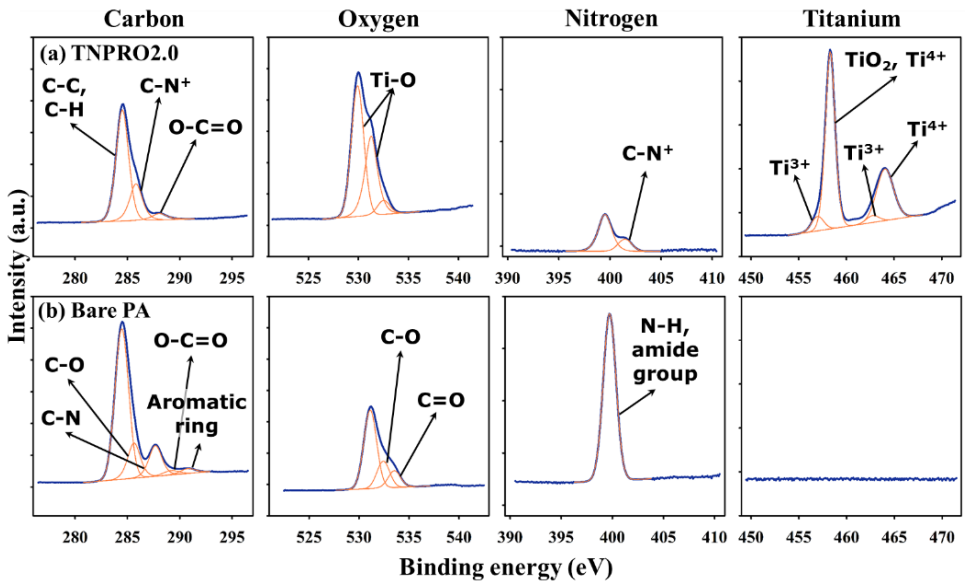

Fig. 3-32. The comparison of X-ray photoelectron spectroscopy spectrum for (a) TNPRO2.0 and (b) bare PA membrane in terms of carbon, oxygen, nitrogen, and titanium (Note that TNPRO indicates TiO_2 nanoparticle coated membrane and the number implies the amount of sprayed TiO_2 sol on the PA RO membrane)

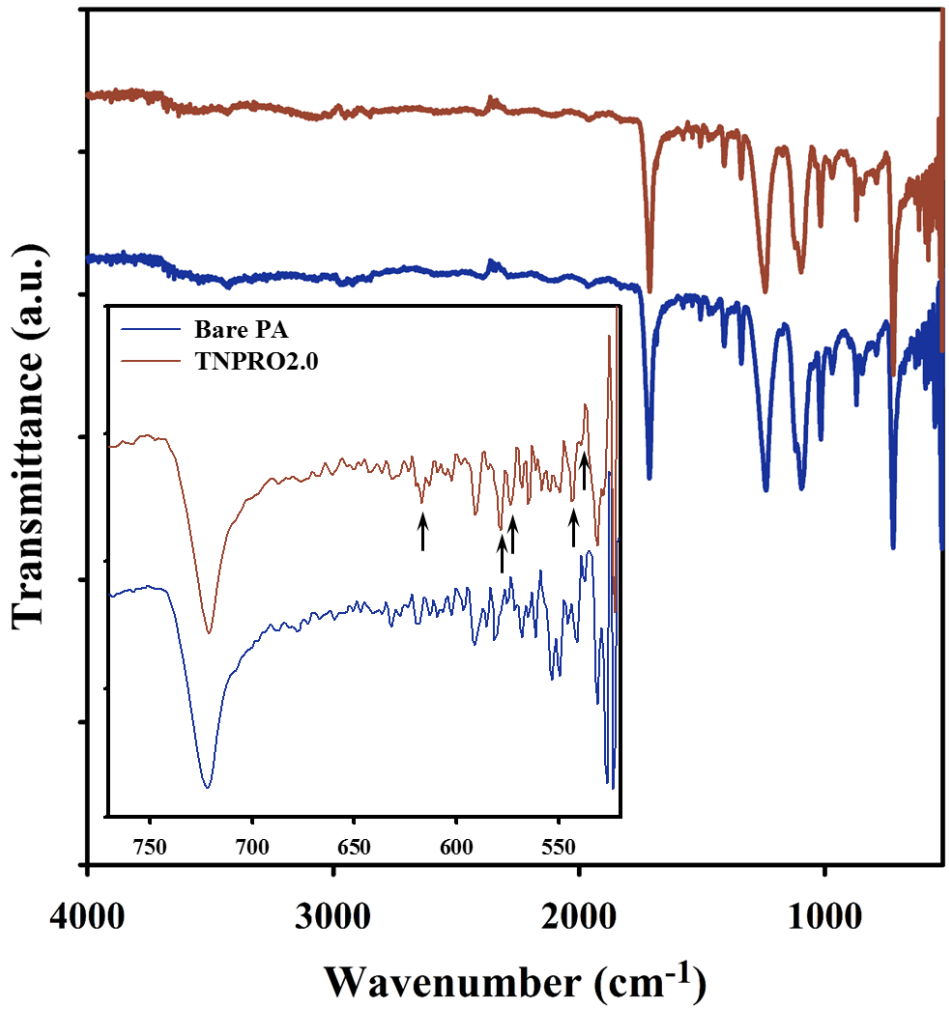

Fig. 3-33. Attenuated total reflectance fourier transform infrared (ATR-FTIR) spectroscopy of TNPRO2.0 and bare PA membrane

Table 3-3 represent the contact angle and zeta potential of TNP coated membranes. Average contact angle of TNP membranes gradually decreased from 23.6° to 5.8° as increased coating amount of TNP while that of bare PA was 43.6°. This results apparently indicate that TNP coating made more hydrophilic surface of the TNP membrane. In terms of zeta potential, zeta potentials of TNPRO0.5, TNPRO1.0, TNPRO1.5, and TNPRO2.0 was -25 mV, -29.8 mV, -30.9 mV, and -40.1 mV, respectively. TNP coated membranes showed greatly increased negative charge than bare PA (-10.6 mV) and as TiO_2 coating amount increased, surface zeta potential is gradually reduced. This result is consistent with the previous study showing that surface charge of TiO_2 is negative in neutral or base condition [97-99]. Therefore, it could be interpreted that the surface coating of TNP changed the charge of PA RO membrane surface into negative due to this negative charge of TiO_2.

Table 3-3. Sessile drop contact angle and surface zeta potential of TNP coated membranes in comparison with bare PA membrane **(**Note that TNPRO indicates TiO_2 nanoparticle coated membrane and the number implies the amount of sprayed TiO_2 sol on the PA RO membrane)

Membrane	Contact angle (°)	Zeta potential (mV)
TNPRO0.5	23.6 ± 0.9	-25.0
TNPRO1.0	16.3 ± 2.7	-29.8
TNPRO1.5	7.8 ± 2.4	-30.9
TNPRO2.0	5.8 ± 2.2	-40.1
Bare PA	43.6 ± 1.2	-10.6

3.4.3.2. Water flux and salt rejection change of TNP coated PA RO membrane

Fig. 3-34 displays the effect of TNP coating on water flux and salt rejection of PA membrane. In our cross-flow RO membrane system, the water flux and salt rejection of bare PA membrane was 27.6 LMH (blue dashed line) and 98.2% (gray dotted line), respectively. As shown in Fig. 3-34, while till 2.0 mL of TNP coating on membrane demonstrated only negligible difference of membrane performance (i.e. water flux and salt rejection) compare with bare PA membrane, TNPRO4.0 showed decreased performance. It could be explained by external concentration polarization (ECP) caused by deposited TNP on PA membrane [115-117]. It seems that the large amount of TNPs on TNPRO4.0 caused accumulation of salt on membrane surface and increased osmotic pressure, consequently, decrease the water flux and salt rejection rate, whereas appropriate coating amount of TNPRO2.0 keep its performance.

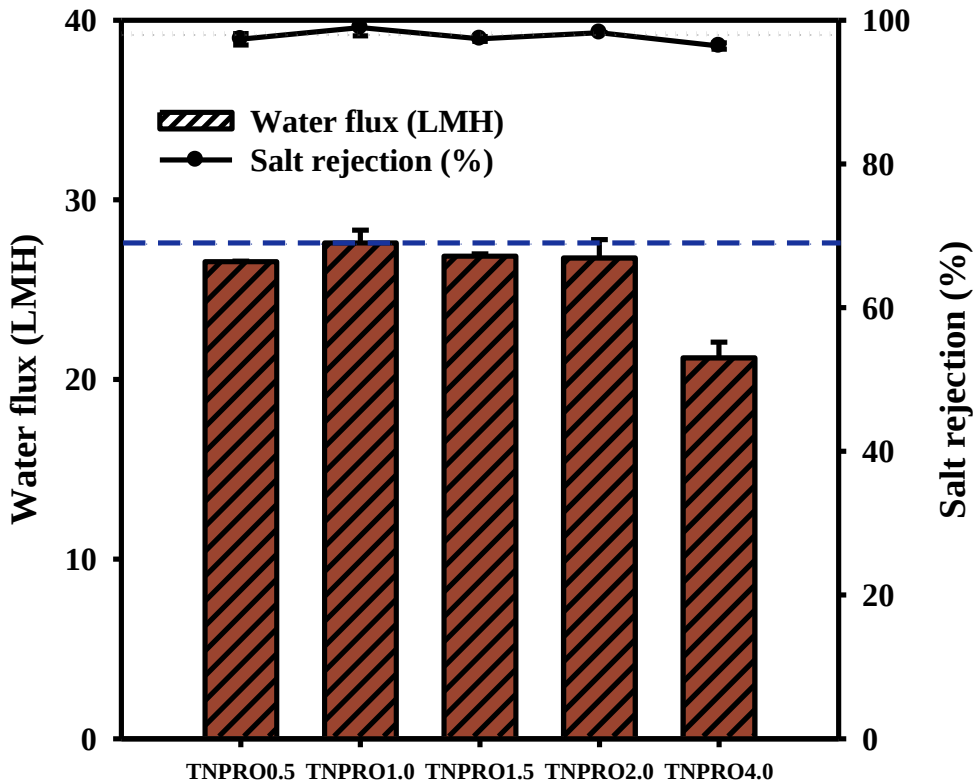

Fig. 3-34. Water flux and salt rejection change of TNP coated membranes as function of the TNP coating amount on PA membrane (gray dotted line: salt rejection of bare PA; blue dashed line: water flux of bare PA; the test was carried out in cross-flow filtration system; cross-flow velocity and temperature: 8 $cm \cdot s^{-1}$ and 25°C; feed water: 2,000 mg/L NaCl; Note that TNPRO indicates TiO_2 nanoparticle coated membrane and the number implies the amount of sprayed TiO_2 sol on the PA RO membrane; n=3)

3.4.3.3. Anti-fouling property of TNP coated PA RO membrane

Anti-fouling performance of TNPRO2.0 in comparison with bare PA was evaluated under humic acid filtration condition and displayed in Fig. 3-32(a). As can be seen in Fig. 3-35(a), TNPRO2.0 demonstrated only 6% of flux decline for 5 h, while bare PA showed 28% of reduced flux. The normalized flux gap between TNPRO2.0 and bare PA was 26% at the end of experiment (19 h). Since the accumulation of humic acid cause a water flux decline, Fig. 3-35(a) indicates less quantity of humic acid was deposited on TNPRO2.0 than bare PA membrane. It is reported that hydrophobic and less negatively charged membrane is easily fouled with humic acid due to the negative and hydrophobic surface property of humic acid [102]. As represented in Table 3-3, the surface property of membrane became more hydrophilic and more negatively charged, which consequently reduced foulant-membrane interaction [36]. The interactive forces between humic acid tethered AFM tip and membrane surface of TNPRO2.0 and bare PA membranes clearly show this correlation (Fig. 3-35(b)). As shown in Fig. 3-35(b), during retraction, no interactive force (red circle) was found on TNPRO2.0, while bare PA showed 0.15 nN of pull-off force (black arrow). This result implies that TNP coating on PA membrane reduced attraction force to humic acid. Therefore, the enhanced membrane surface property could be attributed to fouling resistance against humic acid. This result is consistent with previous study [105]. The surface

modified RO membrane via grafting poly(ethylene glycol) exhibited fouling resistance due to increased hydrophilicity and negative charge.

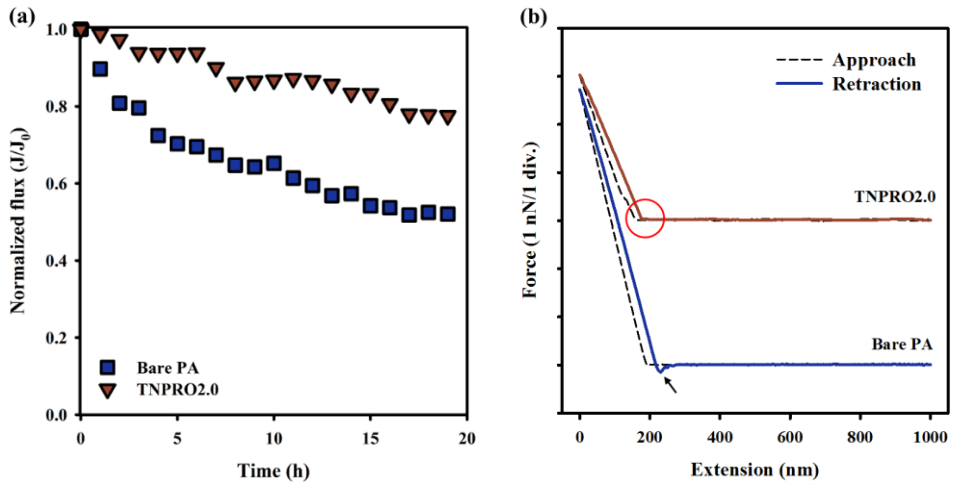

Fig. 3-35. Organic fouling property of TNPRO2.0 membrane compared to bare PA membrane (a) normalized flux change under humic acid filtration condition (Initial water flux: 35 LMH; Feed water: 10 mM NaCl, 1 mM $CaCl_2$ and 200 mg/L humic acid; Cross-flow velocity and temperature: 4 $cm \cdot s^{-1}$ and 25°C; time '0' means the dosing point of humic acid into feed water; Note that TNPRO indicates TiO_2 nanoparticle coated membrane and the number implies the amount of sprayed TiO_2 sol on the PA RO membrane) (b) interaction force between humic acid tethered AFM tip and membrane surface.

3.4. Summary

In this part, we report a novel surface coating method to increase the water flux and organic fouling resistance of PA TFC membranes. The surface of PA TFC membrane was coated with TiO_2 nanoparticles (TNPs) via a sol-gel-derived spray coating method. The optimum TiO_2 nanoparticle coating layer, which is dense and durable without blocking the pore or surface, was formed by base-catalyzed (ammonium hydroxide 0.2 mL) TiO_2 sol-gel-derived spray coating. The support layer of a commercial TFC was coated with TiO_2 nanoparticles (TNPs) via a sol-gel-derived spray coating method for PRO application. This TNP coating imparted hydrophilic properties and a negative charge to the membrane surface. A TNP-coated membrane (TNP1.0) showed a 25% increase in water flux and a 50% decrease in reverse salt flux in PRO process. The flux reduction of the TNP membrane was 32% less than that of a commercial TFC membrane in the presence of humic acid foulants. The less favorable foulant-membrane interaction of the TNP-coated membrane was confirmed by a lower interaction force between a humic acid-tethered AFM tip and the membrane surface. The TNP-coated PA active layer also exhibited enhanced hydrophilicity and negative charge. These modified surface property reduced the interaction force between humic acid and membrane surface and resulted in the enhancement of fouling resistance of the RO membrane without the losses in membrane performances such as water flux and salt rejection when the proper amounts of TiO_2 sol was coated.

4. Evaluation of thin-film nanocomposite reverse osmosis membranes using TiO_2 nanotubes and TiO_2 nanoparticles

4.1. Introduction

Reverse osmosis (RO) has been widely used in desalination processes and requires relatively low energy consumption [8]. Currently, polyamide (PA) thin-film composite (TFC) RO membranes comprise over 90% of the market for RO membranes due to their high water permeability and high selectivity [50]. Along with the wide applicability of PA TFC RO membranes, efforts are being made to reduce the energy consumption of the RO process to produce water at lower costs [118]. To this end, various nanomaterials have been used to improve membrane performance [119]. Thin-film nanocomposite (TFN) RO membranes, fabricated by embedding nanomaterials in polymeric selective layers (e.g., PA), have been developed to improve the performance of RO membranes, including increasing water flux and antifouling properties [120]. These improvements depend on the characteristics of the embedded nanomaterials [19].

Table 4-1 summarizes the various nanomaterials that have been used as embedded materials and their corresponding effects in TFN RO membranes. The nanomaterials can be classified as nanoparticles (e.g., TiO_2, zeolites, SiO_2, and Ag)

and nanotubes (e.g., carbon nanotubes (CNTs) and TiO_2 nanotubes (TNTs)). In terms of nanoparticles, Jeong et al. [52] first reported embedding zeolite A into a PA layer. This zeolite A PA TFN RO membrane showed an approximately 80% enhanced water flux and maintained a high level of salt rejection. Similarly, PA-TiO_2 nanocomposite membranes displayed a 95% rejection of $MgSO_4$ and a 9.1 LMH water flux, i.e., levels higher than those of PA TFC membranes [25]. SiO_2 and Ag nanoparticle-based TFN RO membranes also showed enhanced water flux [121, 122]. Furthermore, nanotube-based TFN RO membranes exhibited superior performance compared with PA TFC RO membranes. For example, a TNT TFN RO membrane was synthesized by a hydrothermal method using silane coupled, amino-functionalized TiO_2 nanoparticles [24]. This TNT TFN RO membrane showed an approximately 93% enhanced water permeability and an anti-organic fouling property. In the same manner, a CNT TFN RO membranes, which was fabricated by the deposition of oxidized CNTs on a PA layer covered with polyvinyl alcohol, showed an approximate 30% enhanced water flux while maintaining salt rejection [23]. These enhanced membrane performances can be explained in two ways. First, the increased hydrophilicity on the membrane surface was due to the embedded hydrophilic nanomaterials, including pre-treated CNTs [52, 121-123, 126, 127]. Second, the inner void spaces of nanotubes [124-126, 128, 129] or gaps between the polyamide layers and nanomaterials provided for fast diffusion rates [125, 127, 130].

Table 4-1. Summary of various nanomaterials as embedded materials and their effects on membrane performance for TFN RO membranes.

Nanomaterial		Water flux enhancement percentage (LMH)[a]	Reference
Nanoparticle	Zeolite A	80% (17)	[52]
	TiO_2	35% (23)	[123]
	SiO_2	64% (47)	[121]
	Ag	24% (31)	[122]
Nanotube	TiO_2	93% (37)	[24]
	Carbon nanotubes	32% (51)	[124]
		27% (44)	[23]
		319% (29)	[125]

[a] Reported water flux.

However, the effects of structural properties on membrane performance has yet to be verified. Furthermore, the effects of the embedded nanomaterials and their hydrophilic and void space contributions on performance enhancement in TFN RO membranes have to be identified. Most studies have only evaluated the performances of TFN RO membranes relative to those of TFC RO membranes; comparative studies between nanotube-based TFN RO membranes and nanoparticle-based TFN RO membranes have not been conducted.

The aim of this study was to compare the effect of embedded nanomaterials in TFN RO membrane by using TNT and TNP, which are same material that have different structure. By using a same material, both the TNT and TNP TFN RO membranes might have similar hydrophilicity which could independently evaluate the effect of the nanomaterial structure on the performance of the TFN RO membrane. TNT was synthesized via the anodic oxidation of Ti foil, and TNP was supplied from a commercial source. The morphology of the TNT and TNP structures were analyzed by SEM and TEM. The TNT and TNP TFN RO membranes were fabricated by interfacial polymerization. The surface properties of these TFN RO membranes were analyzed by SEM, EDS, and contact angle measurement. Water flux and salt rejection were measured in a lab-scale cross-flow RO filtration system.

4.2. Materials and methods

4.2.1. Synthesis of TiO_2 nanotube

A TiO_2 nanotube (TNT) array was synthesized in an electrochemical cell consisting of a 2 cm × 3 cm Ti foil (Sigma-Aldrich) as an anode, a 2 cm × 3 cm Pt foil (Sigma-Aldrich) as a cathode, and an ethylene glycol solution containing 2.5 wt.% H_2O and 0.2 wt.% NH_4F (Sigma-Aldrich) as an electrolyte. The voltage was provided by a DC power supply (UDP-150I, Unicorn Tech Co., Korea). After anodization, the TNT array was annealed at 450°C for 1 h under atmospheric pressure and detached from the Ti foil. Additional details on the synthesis of the TNT array was described in our previous report [131].

4.2.2. Characterization of TiO_2 nanotube and TiO_2 nanoparticle

The TNT array was analyzed by a field emission scanning electron microscope (FE-SEM; JSM-6701F, JEOL, Japan). The as-grown TNT array was cut into a 3 mm × 3 mm sample size and attached on carbon tape. The specimen was washed with ethanol and dried at room temperature.

The morphologies of TNT and TNP were observed by transmission electron microscope (TEM, Libra 120, Carl Zeiss). TiO_2 nanoparticles (TNPs; Aeroxide® P-25) were purchased from Evonik. The TNT array was dispersed in *n*-hexane (Sigma-Aldrich) by using an ultrasonic bath (UCP-10, Jeio Tech Co., Korea) for 1 h and a tip type sonicator (VCX500, Sonics and Materials, Inc., USA) for 10 min, consecutively. A 0.02 wt.% TNT solution and a 0.02 wt.% TNP solution in *n*-hexane were prepared. A few drops of each suspension were deposited onto 3-mm diameter carbon-coated grids. The TEM analyses were conducted at 120 kV acceleration voltage.

4.2.3. Fabrication of TiO_2 nanotube and TiO_2 nanoparticle embedded thin-film nanocomposite membrane

Fig. 4-1 describes the synthesis procedure of the TNT and TNP TFN RO membranes. First, a poly(sulfone) (PSf) support membrane was prepared by phase inversion with 20 wt.% PSf (Mw 22,000 Da, Sigma-Aldrich) in *N*-methyl-2-pyrrolidinone (Sigma-Aldrich) and stabilized in deionized (DI; Millipore) water for 4 h. The PSf support membrane was positioned on a stainless plate with aluminum tape and soaked in a 2 wt.% *m*-phenylenediamine (MPD; >99%, Sigma-Aldrich) aqueous solution for 1 h. Excess MPD aqueous solution was removed using a rubber roller. The MPD-saturated PSf membrane was reacted with a 0.1 wt.% trimesoyl chloride (TMC; >98.5%, Sigma-Aldrich) solution in *n*-hexane for 1 min. The TMC solution was prepared by dispersing 0.01 and 0.02 wt.% TNT and 0.02 wt.% TNP by sonication (as mentioned in section 2.1). These fabricated membranes were rinsed with *n*-hexane and cured in a dry oven at 75°C for 4 min. A PA TFC RO membrane was synthesized by the same procedure without adding the nanomaterials in the TMC solution. The fabricated RO membranes were identified as TFC, TNT0.01, TNT0.02 and TNP0.02. TFC, TNT and TNP, respectively, indicate a plain PA RO membrane, a TNT TFN RO membrane and a TNP TFN RO membrane; the numbers indicate the embedded nanomaterial weight percentages.

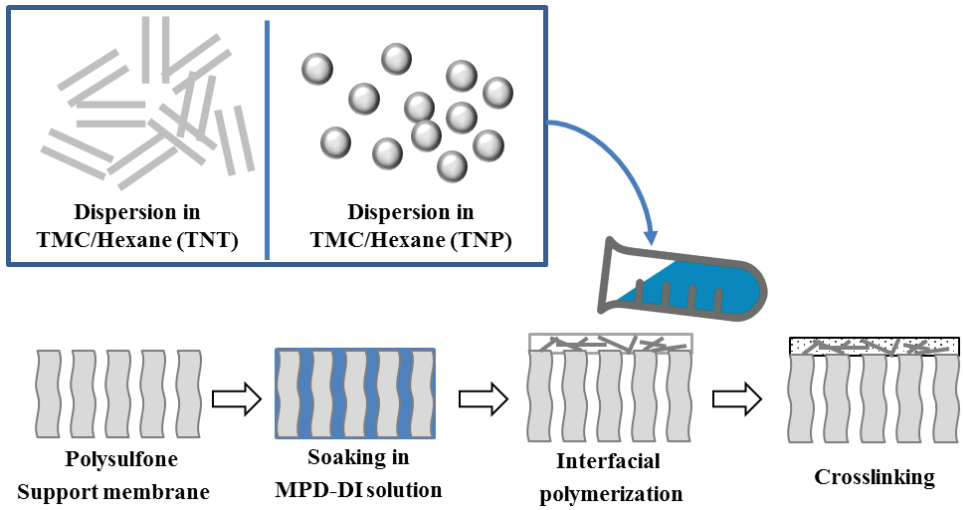

Fig. 4-1. Schematic of the interfacial polymerization procedure for fabrication of the thin-film nanocomposite (TFN) RO membrane by using TiO_2 nanotube (TNT) or TiO_2 nanoparticle (TNP).

4.2.4. Characterization of TiO_2 nanotube and TiO_2 nanoparticle embedded thin-film nanocomposite membrane

The surface morphologies of the TNT and TNP TFN RO membranes were analyzed by FE-SEM. The membrane surface conductivity was enhanced by Pt sputtering at 10 mA for 120 s. Energy dispersive spectroscopy (EDS, JSM-6701F, JEOL, Japan) was used to detect the titanium in PA layer at 20 kV acceleration voltage. The membrane surface hydrophilicity was analyzed by a contact angle analyzer (DSA100, KRÜSS, Germany) using the captive bubble method [132]. Briefly, membrane samples were attached to a glass support and immersed in DI water at room temperature. Ten microliters of an air bubble droplet were formed at the end of a 'J'-shaped syringe needle and slightly attached onto the membrane surface. At least five measurements were made for reproducibility and the average value with standard deviation was reported for each sample.

4.2.5. Membrane performance test

Membrane performances, such as water flux and salt rejection, were measured in a lab-scale cross-flow filtration system [108]. The system consisted of a 6-L feed water tank and a membrane cell with a 22.4 cm^2 (3.3 cm × 6.8 cm) effective membrane area and 0.3 cm channel height. For membrane performance tests, 2,000 mg/L NaCl solution was fed into the system at a 7 cm/s cross-flow velocity at 30°C. After membrane compaction for 30 min at 15.5 bar, the water flux was measured under the same pressure by maintaining the permeate weight for 20 min. Water flux (J_w) was calculated by Eq. (1):

$$J_w = \frac{V}{a \times t} \quad (1)$$

where J_w is the water flux (LMH, $L \cdot m^{-2} \cdot h^{-1}$), V is the permeate volume (L), a is the effective membrane area (m^2), and t is the operation time (h).

Salt rejection (R_s) was evaluated by measuring the conductivity difference between the feed water and the permeate (Eq. (2)):

$$R_s = \left[1 - \frac{C_p}{C_f}\right] \times 100 \quad (2)$$

where R_s is the percentage ratio of the NaCl rejection, C_f is the conductivity of the feed water (mS/cm) and C_p is the conductivity of the permeate (mS/cm).

The water permeability (A; LMH/bar) and salt permeability (B; LMH) were

calculated using Eq. 3 and Eq. 4, respectively from the solution-diffusion model [24]:

$$A = J_w / \Delta P \quad (3)$$

where J_w is water flux and ΔP is the difference between hydraulic pressure and osmotic pressure (π);

$$B = J_s / (C_p - C_f) \quad (4)$$

where J_s is the salt flux attained by $J_w \times C_f$.

4.3. Results and discussion

4.3.1. Characteristics of TiO_2 nanotube and TiO_2 nanoparticle

Figs 4-2(a)-(c) show the SEM images of the fabricated TNT array. As shown in Fig. 4-2(a), the TNT array was densely packed and perpendicularly aligned on the Ti foil. The ends of the TNT array were opened, indicating that the shapes of individual TNTs were either round or oval and had pore sizes ranging from 70 to 80 nm with an approximately 10 nm-thick wall. In the cross-section SEM image shown in Fig. 4-2(b), the average length of the TNT array was approximately 10 μm.

Fig. 4-2(d) and (e) show the TEM images of the morphology of the dispersed TNT and TNP, respectively. As shown in Fig. 4-2(d), the length of individual TNTs ranged from 0.1 μm to 1 μm, which was shorter than the average length of the TNT array (10 μm, Fig. 4-2(b)). The treatment of TNT by sonication likely separated individual TNTs from the TNT array and also shortened the length of the TNTs. The black particles in Fig. 4-2(d) may be broken residues of TNTs due to excessive sonication. However, the size of TNPs ranged from 10 nm to 50 nm, as shown in Fig. 4-2(e).

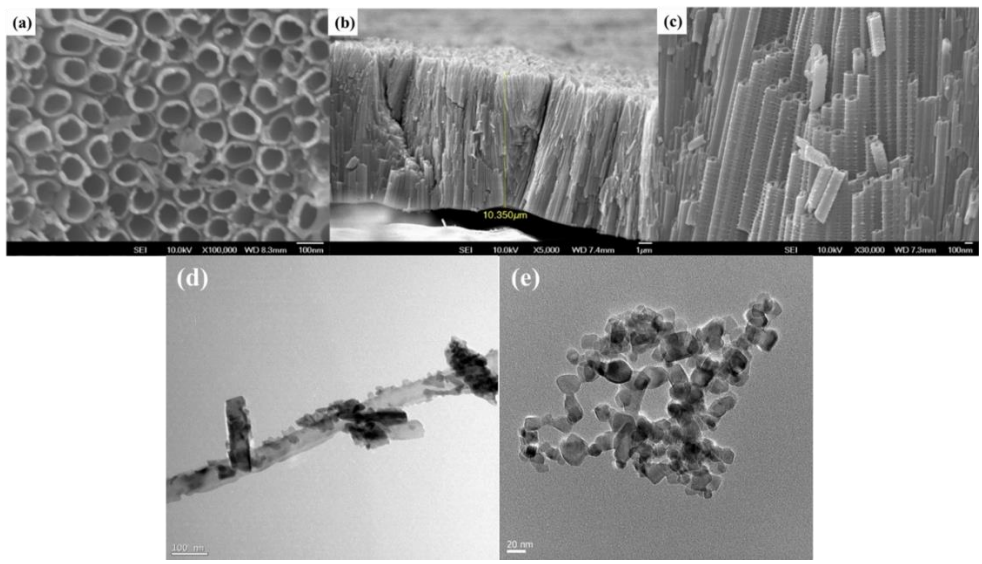

Fig. 4-2. SEM images of fabricated TNT array on Ti foil; (a) surface, (b) cross-section, and (c) enlarged image of (b). TEM images of (d) TNT and (e) TNP.

4.3.2. Characteristics of TiO_2 nanotube and TiO_2 nanoparticle embedded thin-film nanocomposite membrane

Fig. 4-3 shows the surface morphology of the TNT and TNP TFN RO membranes. Figs 4-3(a), (b) and (c) present TNT0.02, TNP0.02 and TFC, respectively. As shown in Fig. 4-3(a), a cylindrically-shaped TNT covered by a PA layer was observed on the TNT0.02 membrane. In the upper right corner of Fig. 4-3(b), well-dispersed TNPs were found on the surface of the TNP0.02 membrane, while the TFC membrane showed a typical surface morphology without any particles (Fig. 4-3(c)). The element weight percentage of the TNT0.02, TNP0.02 and TFC membranes were analyzed by energy dispersive spectroscopy (EDS; Table 4-2). Similar weight percentages of titanium were detected in the TNT PA TFN RO membrane (0.2 ± 0.1%) and the TNP TFN RO membrane (0.3 ± 0.1%) while the PA TFC RO membrane only presented carbon, oxygen and sulfur.

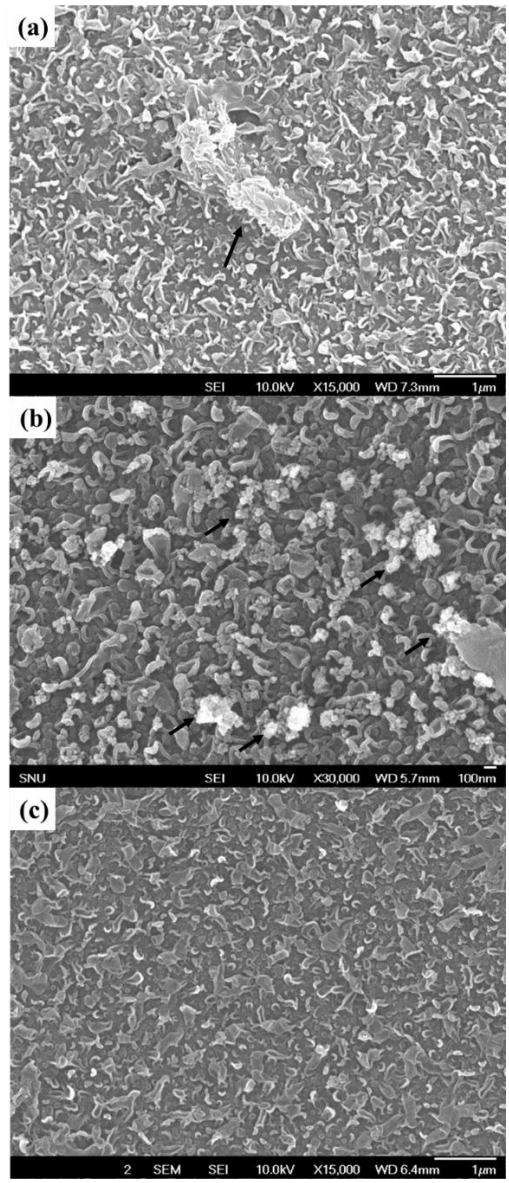

Fig. 4-3. Surface morphology of (a) 0.02 wt.% TNT TFN RO membrane, (b) 0.02 wt.% TNP TFN RO membrane, and (c) PA TFC RO membrane.

Table 4-2. EDS data of 0.02 wt% of TNT TFN RO membrane and TNP TFN RO membrane compared to PA TFC RO membrane (n=3).

Membrane	Carbon (K)	Oxygen (K)	Sulfur (K)	Titanium (K)
0.02 wt% TNT PA TFN RO	77.7 ± 0.1%	15.2 ± 0.4%	6.9 ± 0.2%	0.2 ± 0.06%
0.02 wt% TNP PA TFN RO	78.0 ± 0.3%	14.1 ± 0.3%	7.5 ± 0.04%	0.3 ± 0.08%

The contact angles of TNT0.01 and TNT0.02, TNP0.02, and TFC are listed in Table 4-3. As shown in Table 4-3, the contact angle of TNT0.01 was 38.9°. TNT0.02 and TNP0.02 had the lowest contact angles (37.1° and 37.3°, respectively) while the TFC membrane showed the highest contact angle (45.9°). This result implied that the embedded TiO_2 nanomaterials modified the membrane surface property to be more hydrophilic. This result was consistent with previous studies wherein hydrophilic nanomaterials, such as TiO_2 nanoparticle, zeolite A and silver nanoparticle-embedded TFN RO membranes had more hydrophilic surfaces [52, 122, 133].

Table 4-3. Contact angles of TNT0.01, TNT0.02, TNP0.02, TFC membranes (n=5).

Membrane	TNT0.01	TNT0.02	TNP0.02	TFC
Contact angle (°)[a]	38.9 ± 1.3	37.1 ± 1.2 (40)[b]	37.3 ± 0.7	45.9 ± 1.0 (70)[b]

[a]: Measured by captive bubble method [132].

[b]: Sessile drop contact angle data from literature corresponding to TFN0.1 and TFC membranes, [24].

4.3.3. Performance of TiO_2 nanotube and TiO_2 nanoparticle embedded thin-film nanocomposite membrane

Fig. 4-4 illustrates the water flux and the salt rejection of the TNT0.01, TNT0.02, TNP0.02, and TFC membranes. As shown in Fig. 4-4, the water flux of TNT0.01 and TNT0.02 were enhanced to 43.0 LMH and 54.7 LMH, respectively, as the amount of embedded TNT increased from 0.01 wt.% to 0.02 wt.% compared with the 37.0 LMH water flux of the PA TFC RO membrane. The TNP0.02 membrane showed a lower enhanced water flux (44.9 LMH) than that of the TNT0.02 membrane; however, the TNP0.02 membrane had a similar hydrophilicity. The salt rejection rates of the TNT0.01, TNT0.02, TNP0.02, and TFC membranes were 91.8%, 92.6%, 95.4% and 94.9%, respectively. As the TNT amount increased, the salt rejection slightly reduced for all membranes except TNP0.02.

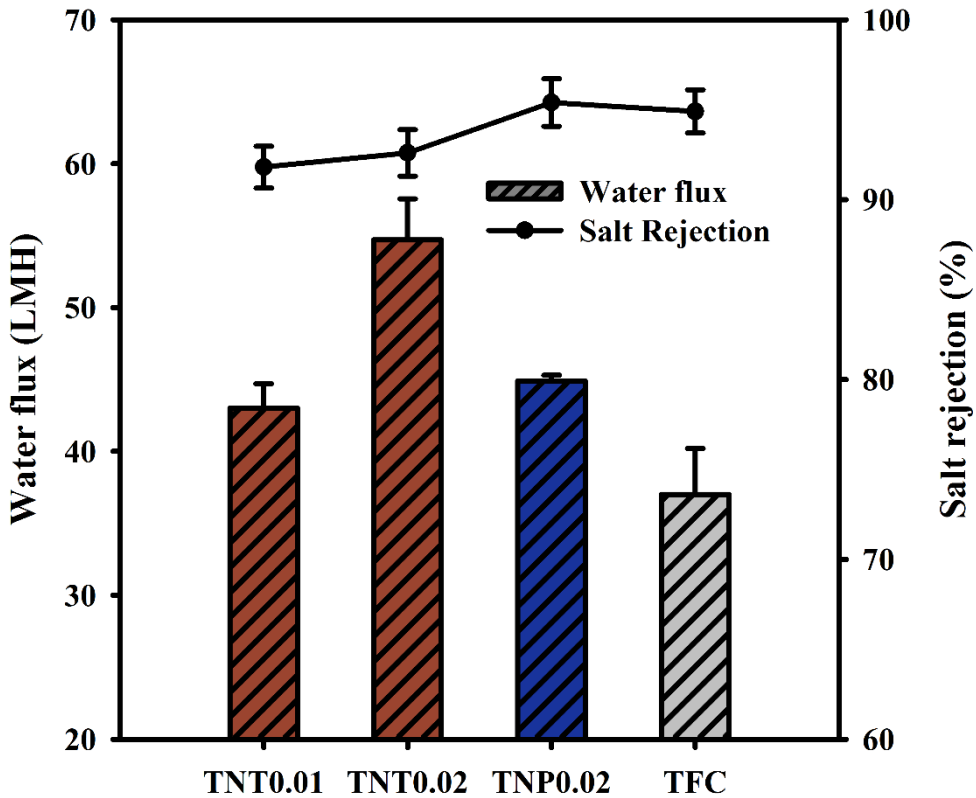

Fig. 4-4. Water flux and NaCl rejection of TNT0.01, TNT0.02, TNP0.02, and TFC membranes (n=3).

Fig. 4-5 shows the correlations between the contact angle and the enhancements to water permeability and salt permeability. As shown in Fig. 5, both water permeability and salt permeability were enhanced as the membrane surface became more hydrophilic. This improved hydrophilicity enhanced the water flux. This result was consistent with previous studies of TiO_2-based TFN RO membranes [25, 126]. Interestingly, the TNP0.02 membrane (square) showed lower water and salt permeability enhancements than those of the TNT0.02 membrane. This indicated that the nanotube structure significantly enhanced the permeability, while the nanoparticle structure only slightly affected the permeability. The larger pore size of TNTs (approximately 80 nm) may have increased the sorption capacity of the RO membrane, which resulted in the greater permeability enhancement, whereas the TNP had no internal pores. This result correlated with the findings of a previous study of silica-based TFN RO membranes. In the past study, a non-porous silica-embedded TFN membrane showed 25% enhanced water flux while a porous silica-embedded TFN membrane exhibited 64% enhanced water flux [121]. Moreover, the enhanced salt permeability was higher than that of water permeability in the TNT TFN RO membrane. As shown in Figs 4-5(a) and (b), the water permeability of the TNT0.02 membrane increased 48% while the salt permeability increased 120%. The larger pores of the TNTs contributed to higher salt and water permeability.

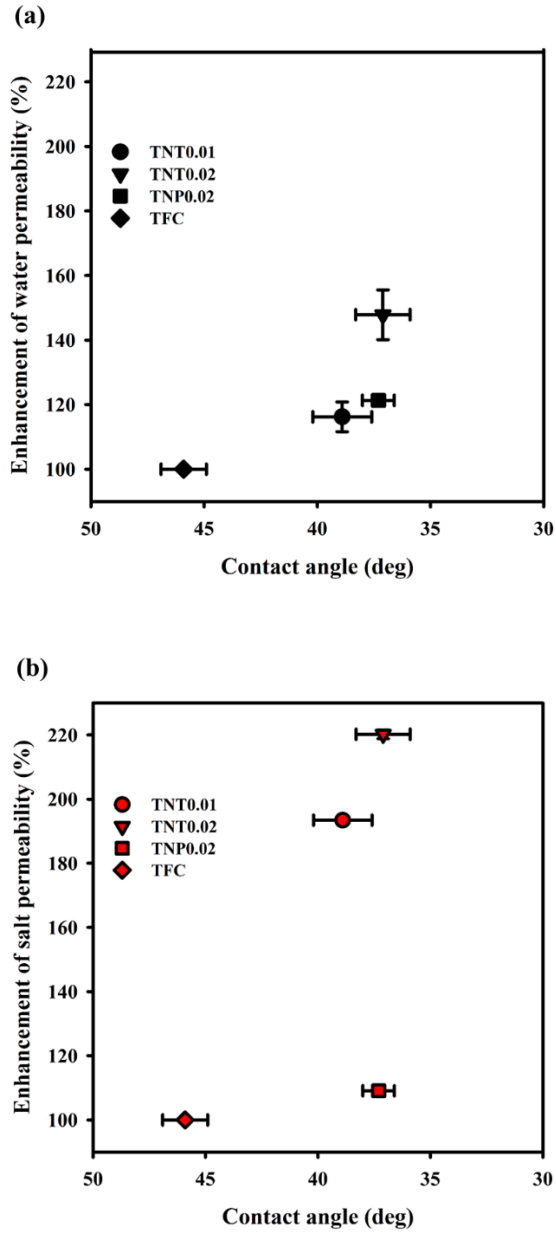

Fig. 4-5. Correlations between contact angle and (a) enhancement of water permeability and (b) enhancement of salt permeability.

In order to confirm the water flux enhancement of TiO_2 nanomaterial embedded PA TFN, the water flux and salt rejection of PA TFN membranes were compared with upper bound consist of plain TFC membrane (Fig. 4-6). In Fig. 4-6, the red slash represent the upper bound of plain TFC membranes. As shown in Fig. 4-6, all PA TFN membranes (Purple Triangle Down, Gray square, Dark gray square) are placed on right side of upper bound and this imply that the water flux enhancement of TiO_2 nanomaterial embedded PA TFN overcame the trade-off relation of permeate flux and salt rejection. On the other hand, the performance of literature result and commercial membrane were compared with this study. As can be seen in Fig. 4-6, one commercial membrane (Green square) showed high salt rejection with moderate water flux, while another commercial membrane (Sky blue circle)—containing nanomaterial in its polyamide layer—exhibited high salt rejection with 41 LMH of water flux at 15.5 bar. The yellow diamond and dark green hexagon represent CNT and GO/CNT embedded membranes, respectively. The CNT embedded TFN membrane showed 44 LMH water flux and 96% salt rejection and GO/CNT embedded demonstrated highly increased water flux (58 LMH) due to enhanced dispersibility after GO embedding. The silicate-1 zeolite embedded TFN membrane showed extremely high water flux (66 LMH).

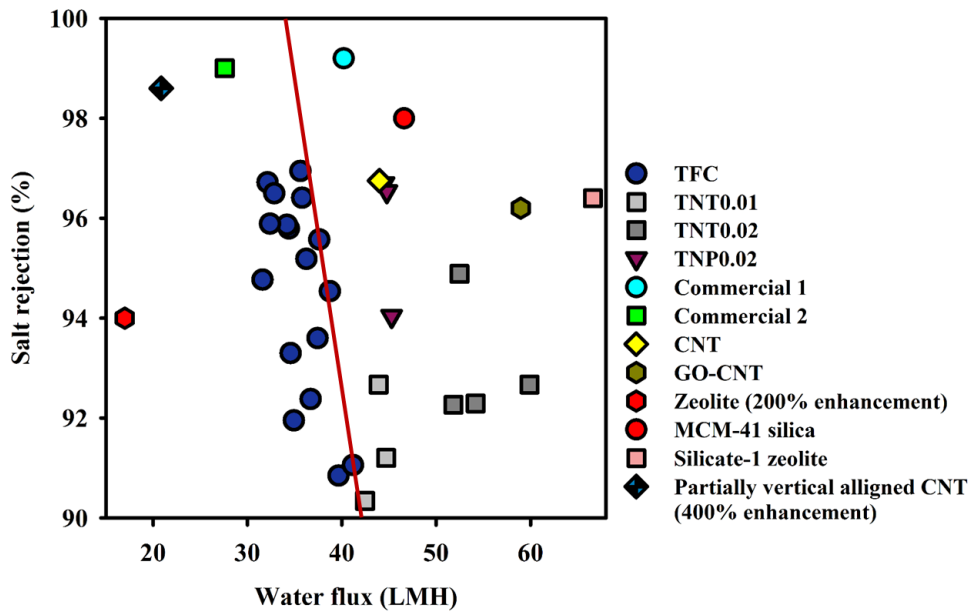

Fig. 4-6. Comparison of nanomaterials embedded PA TFN membranes and commercial PA TFC membrane with upper bound of hand-cast TFC membrane (The water flux and salt rejection of TFC, TNT, TNP, and commercial membrane were evaluated at 15.5 bar with 2,000 mg/L NaCl; CNT [53], GO-CNT [55], zeolite A [52], MCM-41 silica [121], silicate-1 zeolite [134], zwitterion functionalized CNT [56]).

4.4. Summary

In this part, the performances of TNT TFN RO membranes and TNP TFN RO membranes were compared to evaluate the effect of embedded nanomaterials in TFN RO membranes. The hydrophilicity of the membrane surface was increased as the concentration of the TiO_2 nanomaterials increased in the TFN RO membranes, which resulted in high water and salt permeability. Under the same conditions, the TNT0.02 membrane showed a 48% higher water permeability and a 120% higher salt permeability than the TFC RO membrane, while the TNP0.02 membrane showed a 21% higher water permeability and a 9% higher salt permeability. These results indicated that the large pores (approximately 80 nm) of the TNTs significantly affected membrane permeability, whereas the TNPs, which had no pores but had a gap between the TNP and PA layers, only slightly affected membrane permeability. The permeability of TFN RO membranes could be affected by the hydrophilicity and the structure of embedded nanomaterials. Further studies are necessary to determine the effect of the size of embedded nanomaterials on membrane performance.

5. Conclusions

In this dissertation, the development of high-performance and fouling resistance PA TFC membrane was implemented through addition of TiO_2 nanomaterials.

In the first part, the surface of PA TFC membrane was coated with TiO_2 nanoparticles (TNPs) via a sol-gel-derived spray coating method. The optimum TiO_2 nanoparticle coating layer, which is dense and durable without blocking the pore or surface, was coated on PA TFC membrane via base-catalyzed (ammonium hydroxide) TiO_2 sol-gel-derived spray coating. For pressure retarded osmosis application, the support layer of a commercial TFC was coated with TiO_2 nanoparticles (TNPs) via a sol-gel-derived spray coating method. This TNP coating imparted hydrophilic properties and a negative charge to the membrane surface. A TNP-coated membrane (TNP1.0) demonstrated increased water flux while reducing reverse salt flux in PRO process. The surface property change of membrane resulted in enhancement of fouling resistance. The flux reduction of the TNP membrane was 32% less than that of a commercial TFC membrane in the presence of humic acid foulants. The less favorable foulant-membrane interaction of the TNP-coated membrane was confirmed by a lower interaction force between a humic acid-tethered AFM tip and the membrane surface. The TNP-coated PA active layer also exhibited enhanced hydrophilicity and negative charge. These modified surface property reduced the interaction force between humic acid and membrane surface and resulted in the enhancement of fouling resistance of the

RO membrane without the losses in membrane performances such as water flux and salt rejection when the proper amounts of TiO_2 sol was coated.

In the second part, TiO_2 nanomaterials embedded polyamide thin-film nanocomposite membrane was fabricated for enhancement of water flux and fouling resistance. In addition, the effect of structure and surface property of nanomaterial on water flux was evaluated by comparison of TiO_2 nanotube (TNT) and TiO_2 nanoparticle (TNP) embedded PA TFN membrane. The TFN RO membranes containing TNT or TNP exhibited similarly high hydrophilicities and enhanced water permeability compared with a conventional RO membrane. Although TNP TFN RO membrane has similar surface hydrophilicity with TNT TFN RO membrane when the same amount of TNP and TNT are embedded, the TNT TFN RO membranes had better water permeability than the TNP TFN RO membranes. Compared with non-porous TNP, the nanochannels of TNT contributed to enhancement of water permeability by serving as water transport passageways. From these results, it is expected that the addition of TiO_2 nanomaterials in PA TFC membrane can enhance the performance and fouling resistance in RO and PRO process.

References

[1] International Energy Agency, World Energy Outlook, OECD/IEA, Paris (2011) Available from: http://www.iea.org/publications/freepublications/publication/weo-2011.html (accessed 24.02.16)

[2] BP Statistical Review of World Energy, British Petroleum Company (2015) Available from: https://www.bp.com/content/dam/bp/pdf/energy-economics/statistical-review-2015/bp-statistical-review-of-world-energy-2015-full-report.pdf (accessed 24.02.16)

[3] F. Helfer, C. Lemckert, Y.G. Anissimov, Osmotic power with Pressure Retarded Osmosis: Theory, performance and trends – A review, Journal of Membrane Science, 453 (2014) 337-358.

[4] M.D. Kaminski, S.D. Lee, M. Magnuson, Wide-area decontamination in an urban environment after radiological dispersion: A review and perspectives, Journal of Hazardous Materials, 305 (2016) 67-86.

[5] J.B. Bomanji, F. Novruzov, S. Vinjamuri, Radiation accidents and their management: Emphasis on the role of nuclear medicine professionals, Nuclear Medicine Communications, 35 (2014) 995-1002.

[6] M. Elimelech, W.A. Phillip, The future of seawater desalination: energy, technology, and the environment, science, 333 (2011) 712-717.

[7] R.L. McGinnis, M. Elimelech, Global Challenges in Energy and Water Supply: The Promise of Engineered Osmosis, Environmental Science & Technology, 42

(2008) 8625-8629.

[8] M. Elimelech, W.A. Phillip, The future of seawater desalination: energy, technology, and the environment, Science, 333 (2011) 712-717.

[9] S. Loeb, Energy production at the Dead Sea by pressure-retarded osmosis: challenge or chimera?, Desalination, 120 (1998) 247-262.

[10] V.S. Frenkel, Seawater Desalination: Trends and Technologies, INTECH Open Access Publisher, 2011.

[11] L.F. Greenlee, D.F. Lawler, B.D. Freeman, B. Marrot, P. Moulin, Reverse osmosis desalination: water sources, technology, and today's challenges, Water research, 43 (2009) 2317-2348.

[12] B.E. Logan, M. Elimelech, Membrane-based processes for sustainable power generation using water, Nature, 488 (2012) 313-319.

[13] J. Wu, Z. Wang, W. Yan, Y. Wang, J. Wang, S. Wang, Improving the hydrophilicity and fouling resistance of RO membranes by surface immobilization of PVP based on a metal-polyphenol precursor layer, J. Membr. Sci., 496 (2015) 58-69.

[14] A. Altaee, A. Sharif, Pressure retarded osmosis: advancement in the process applications for power generation and desalination, Desalination, 356 (2015) 31-46.

[15] D. Potts, R. Ahlert, S. Wang, A critical review of fouling of reverse osmosis membranes, Desalination, 36 (1981) 235-264.

[16] X. Zhu, M. Elimelech, Colloidal Fouling of Reverse Osmosis Membranes: Measurements and Fouling Mechanisms, Environmental Science & Technology, 31

(1997) 3654-3662.

[17] A. Zhu, P.D. Christofides, Y. Cohen, Effect of Thermodynamic Restriction on Energy Cost Optimization of RO Membrane Water Desalination, Industrial & Engineering Chemistry Research, 48 (2009) 6010-6021.

[18] E.M. Hoek, M. Elimelech, Cake-enhanced concentration polarization: a new fouling mechanism for salt-rejecting membranes, Environmental science & technology, 37 (2003) 5581-5588.

[19] W.J. Lau, S. Gray, T. Matsuura, D. Emadzadeh, J. Paul Chen, A.F. Ismail, A review on polyamide thin film nanocomposite (TFN) membranes: History, applications, challenges and approaches, Water Res., 80 (2015) 306-324.

[20] P. Roy, S. Berger, P. Schmuki, TiO_2 nanotubes: synthesis and applications, Angewandte Chemie International Edition, 50 (2011) 2904-2939.

[21] X. Gao, B. Zhou, R. Yuan, Doping a metal (Ag, Al, Mn, Ni and Zn) on TiO_2 nanotubes and its effect on Rhodamine B photocatalytic oxidation, Environmental Engineering Research, 20 (2015) 329-335.

[22] C. Andriantsiferana, E.F. Mohamed, H. Delmas, Sequential adsorption - photocatalytic oxidation process for wastewater treatment using a composite material TiO2/activated carbon, Environmental Engineering Research, 20 (2015) 181-189.

[23] C. Kim, S. Kim, J. Choi, J. Lee, J.S. Kang, Y.E. Sung, J. Lee, W. Choi, J. Yoon, Blue TiO_2 nanotube array as an oxidant generating novel anode material fabricated by simple cathodic polarization, Electrochimica Acta, 141 (2014) 113-119.

[24] D. Emadzadeh, W.J. Lau, M. Rahbari-Sisakht, A. Daneshfar, M. Ghanbari, A. Mayahi, T. Matsuura, A.F. Ismail, A novel thin film nanocomposite reverse osmosis membrane with superior anti-organic fouling affinity for water desalination, Desalination, 368 (2015) 106-113.

[25] H.S. Lee, S.J. Im, J.H. Kim, H.J. Kim, J.P. Kim, B.R. Min, Polyamide thin-film nanofiltration membranes containing TiO_2 nanoparticles, Desalination, 219 (2008) 48-56.

[26] D. Emadzadeh, W. Lau, T. Matsuura, M. Rahbari-Sisakht, A. Ismail, A novel thin film composite forward osmosis membrane prepared from PSf–TiO_2 nanocomposite substrate for water desalination, Chemical Engineering Journal, 237 (2014) 70-80.

[27] S.-Y. Kwak, S.H. Kim, S.S. Kim, Hybrid Organic/Inorganic Reverse Osmosis (RO) Membrane for Bactericidal Anti-Fouling. 1. Preparation and Characterization of TiO_2 Nanoparticle Self-Assembled Aromatic Polyamide Thin-Film-Composite (TFC) Membrane, Environmental Science & Technology, 35 (2001) 2388-2394.

[28] S.S. Madaeni, N. Ghaemi, Characterization of self-cleaning RO membranes coated with TiO_2 particles under UV irradiation, Journal of Membrane Science, 303 (2007) 221-233.

[29] S.H. Kim, S.-Y. Kwak, B.-H. Sohn, T.H. Park, Design of TiO_2 nanoparticle self-assembled aromatic polyamide thin-film-composite (TFC) membrane as an approach to solve biofouling problem, Journal of Membrane Science, 211 (2003) 157-165.

[30] Y. Takahashi, Y. Wada, Dip-Coating of Sb-Doped SnO_2 Films by Ethanolamine-Alkoxide Method, Journal of The Electrochemical Society, 137 (1990) 267-272.

[31] R.S. Sonawane, B.B. Kale, M.K. Dongare, Preparation and photo-catalytic activity of Fe-TiO_2 thin films prepared by sol–gel dip coating, Materials Chemistry and Physics, 85 (2004) 52-57.

[32] D.J. Kim, S.H. Hahn, S.H. Oh, E.J. Kim, Influence of calcination temperature on structural and optical properties of TiO_2 thin films prepared by sol–gel dip coating, Materials Letters, 57 (2002) 355-360.

[33] Q. She, R. Wang, A.G. Fane, C.Y. Tang, Membrane fouling in osmotically driven membrane processes: A review, Journal of Membrane Science, 499 (2016) 201-233.

[34] D.I. Kim, J. Kim, H.K. Shon, S. Hong, Pressure retarded osmosis (PRO) for integrating seawater desalination and wastewater reclamation: Energy consumption and fouling, Journal of Membrane Science, 483 (2015) 34-41.

[35] G.D. Kang, Y.M. Cao, Development of antifouling reverse osmosis membranes for water treatment: A review, Water Res., 46 (2012) 584-600.

[36] D. Rana, T. Matsuura, Surface modifications for antifouling membranes, Chemical reviews, 110 (2010) 2448-2471.

[37] Y. Baek, J. Yu, S.H. Kim, S. Lee, J. Yoon, Effect of surface properties of reverse osmosis membranes on biofouling occurrence under filtration conditions, Journal of Membrane Science, 382 (2011) 91-99.

[38] G.-d. Kang, Y.-m. Cao, Development of antifouling reverse osmosis membranes

for water treatment: A review, Water Research, 46 (2012) 584-600.

[39] M. Elimelech, Z. Xiaohua, A.E. Childress, H. Seungkwan, Role of membrane surface morphology in colloidal fouling of cellulose acetate and composite aromatic polyamide reverse osmosis membranes, Journal of Membrane Science, 127 (1997) 101-109.

[40] K. Riedl, B. Girard, R.W. Lencki, Influence of membrane structure on fouling layer morphology during apple juice clarification, Journal of Membrane Science, 139 (1998) 155-166.

[41] Y.S. Li, L. Yan, C.B. Xiang, L.J. Hong, Treatment of oily wastewater by organic–inorganic composite tubular ultrafiltration (UF) membranes, Desalination, 196 (2006) 76-83.

[42] M.C. Wilbert, J. Pellegrino, A. Zydney, Bench-scale testing of surfactant-modified reverse osmosis/nanofiltration membranes, Desalination, 115 (1998) 15-32.

[43] J.S. Louie, I. Pinnau, I. Ciobanu, K.P. Ishida, A. Ng, M. Reinhard, Effects of polyether–polyamide block copolymer coating on performance and fouling of reverse osmosis membranes, Journal of Membrane Science, 280 (2006) 762-770.

[44] I.-C. Kim, K.-H. Lee, Dyeing process wastewater treatment using fouling resistant nanofiltration and reverse osmosis membranes, Desalination, 192 (2006) 246-251.

[45] A. Kulkarni, D. Mukherjee, W.N. Gill, Flux enhancement by hydrophilization of thin film composite reverse osmosis membranes, Journal of Membrane Science,

114 (1996) 39-50.

[46] S. Belfer, Y. Purinson, R. Fainshtein, Y. Radchenko, O. Kedem, Surface modification of commercial composite polyamide reverse osmosis membranes, Journal of Membrane Science, 139 (1998) 175-181.

[47] S. Belfer, R. Fainshtain, Y. Purinson, J. Gilron, M. Nyström, M. Mänttäri, Modification of NF membrane properties by in situ redox initiated graft polymerization with hydrophilic monomers, Journal of Membrane Science, 239 (2004) 55-64.

[48] V. Freger, J. Gilron, S. Belfer, TFC polyamide membranes modified by grafting of hydrophilic polymers: an FT-IR/AFM/TEM study, Journal of Membrane Science, 209 (2002) 283-292.

[49] J. Gilron, S. Belfer, P. Väisänen, M. Nyström, Effects of surface modification on antifouling and performance properties of reverse osmosis membranes, Desalination, 140 (2001) 167-179.

[50] R.J. Petersen, Composite reverse osmosis and nanofiltration membranes, Journal of Membrane Science, 83 (1993) 81-150.

[51] E.M. Van Wagner, A.C. Sagle, M.M. Sharma, Y.-H. La, B.D. Freeman, Surface modification of commercial polyamide desalination membranes using poly (ethylene glycol) diglycidyl ether to enhance membrane fouling resistance, Journal of Membrane Science, 367 (2011) 273-287.

[52] B.-H. Jeong, E.M.V. Hoek, Y. Yan, A. Subramani, X. Huang, G. Hurwitz, A.K. Ghosh, A. Jawor, Interfacial polymerization of thin film nanocomposites: A new

concept for reverse osmosis membranes, Journal of Membrane Science, 294 (2007) 1-7.

[53] H.J. Kim, K. Choi, Y. Baek, D.-G. Kim, J. Shim, J. Yoon, J.-C. Lee, High-performance reverse osmosis CNT/polyamide nanocomposite membrane by controlled interfacial interactions, ACS applied materials & interfaces, 6 (2014) 2819-2829.

[54] J.K. Holt, H.G. Park, Y. Wang, M. Stadermann, A.B. Artyukhin, C.P. Grigoropoulos, A. Noy, O. Bakajin, Fast mass transport through sub-2-nanometer carbon nanotubes, Science, 312 (2006) 1034-1037.

[55] H.J. Kim, M.-Y. Lim, K.H. Jung, D.-G. Kim, J.-C. Lee, High-performance reverse osmosis nanocomposite membranes containing the mixture of carbon nanotubes and graphene oxides, Journal of Materials Chemistry A, 3 (2015) 6798-6809.

[56] W.-F. Chan, H.-y. Chen, A. Surapathi, M.G. Taylor, X. Shao, E. Marand, J.K. Johnson, Zwitterion functionalized carbon nanotube/polyamide nanocomposite membranes for water desalination, Acs Nano, 7 (2013) 5308-5319.

[57] C. Kim, J. Lee, S. Kim, J. Yoon, TiO_2 sol–gel spray method for carbon electrode fabrication to enhance desalination efficiency of capacitive deionization, Desalination, 342 (2014) 70-74.

[58] C.J. Brinker, G.W. Scherer, Sol-gel science: the physics and chemistry of sol-gel processing, Academic press, 2013.

[59] S. Kahraman, S. Çetinkaya, H.A. Çetinkara, H.S. Güder, Effects of

diethanolamine on sol–gel–processed Cu_2ZnSnS_4 photovoltaic absorber thin films, Materials Research Bulletin, 50 (2014) 165-171.

[60] M. Guglielmi, G. Carturan, Precursors for sol-gel preparations, Journal of Non-Crystalline Solids, 100 (1988) 16-30.

[61] K. Murugan, T.N. Rao, G.V.N. Rao, A.S. Gandhi, B.S. Murty, Effect of dehydration rate on non-hydrolytic TiO_2 thin film processing: Structure, optical and photocatalytic performance studies, Materials Chemistry and Physics, 129 (2011) 810-815.

[62] H.J. Chen, L. Wang, W.Y. Chiu, Chelation and solvent effect on the preparation of titania colloids, Materials Chemistry and Physics, 101 (2007) 12-19.

[63] Y. Djaoued, M. Thibodeau, J. Robichaud, S. Balaji, S. Priya, N. Tchoukanova, S.S. Bates, Photocatalytic degradation of domoic acid using nanocrystalline TiO_2 thin films, Journal of Photochemistry and Photobiology A: Chemistry, 193 (2008) 271-283.

[64] J. Yu, M. Zhou, H. Yu, Q. Zhang, Y. Yu, Enhanced photoinduced super-hydrophilicity of the sol-gel-derived TiO_2 thin films by Fe-doping, Materials Chemistry and Physics, 95 (2006) 193-196.

[65] H.S. Jung, J.K. Lee, J.Y. Kim, K.S. Hong, Synthesis of nano-sized MgO particle and thin film from diethanolamine-stabilized magnesium-methoxide, Journal of Solid State Chemistry, 175 (2003) 278-283.

[66] C. Sanchez, J. Livage, M. Henry, F. Babonneau, Chemical modification of alkoxide precursors, Journal of Non-Crystalline Solids, 100 (1988) 65-76.

[67] Y. Takahashi, Y. Matsuoka, Dip-coating of TiO_2 films using a sol derived from Ti(O-i-Pr)4-diethanolamine-H_2O-i-PrOH system, Journal of Materials Science, 23 (1988) 2259-2266.

[68] Y. Takahashi, K. Yamaguchi, Dip-coating conditions and modifications of lead titanate and lead zirconate titanate films, Journal of Materials Science, 25 (1990) 3950-3955.

[69] Y. Ohya, H. Saiki, Y. Takahashi, Preparation of transparent, electrically conducting ZnO film from zinc acetate and alkoxide, Journal of Materials Science, 29 (1994) 4099-4103.

[70] N.Y. Yip, A. Tiraferri, W.A. Phillip, J.D. Schiffman, L.A. Hoover, Y.C. Kim, M. Elimelech, Thin-film composite pressure retarded osmosis membranes for sustainable power generation from salinity gradients, Environ Sci Technol, 45 (2011) 4360-4369.

[71] D. Stillman, L. Krupp, Y.-H. La, Mesh-reinforced thin film composite membranes for forward osmosis applications: The structure–performance relationship, Journal of Membrane Science, 468 (2014) 308-316.

[72] S. Zhang, F. Fu, T.-S. Chung, Substrate modifications and alcohol treatment on thin film composite membranes for osmotic power, Chemical Engineering Science, 87 (2013) 40-50.

[73] J.R. McCutcheon, M. Elimelech, Influence of membrane support layer hydrophobicity on water flux in osmotically driven membrane processes, Journal of Membrane Science, 318 (2008) 458-466.

[74] X. Li, T. Cai, T.S. Chung, Anti-fouling behavior of hyperbranched polyglycerol-grafted poly(ether sulfone) hollow fiber membranes for osmotic power generation, Environ Sci Technol, 48 (2014) 9898-9907.

[75] J.T. Arena, B. McCloskey, B.D. Freeman, J.R. McCutcheon, Surface modification of thin film composite membrane support layers with polydopamine: Enabling use of reverse osmosis membranes in pressure retarded osmosis, Journal of Membrane Science, 375 (2011) 55-62.

[76] N.N. Bui, J.R. McCutcheon, Hydrophilic nanofibers as new supports for thin film composite membranes for engineered osmosis, Environ Sci Technol, 47 (2013) 1761-1769.

[77] N.N. Bui, J.R. McCutcheon, Nanofiber supported thin-film composite membrane for pressure-retarded osmosis, Environ Sci Technol, 48 (2014) 4129-4136.

[78] S. Chou, R. Wang, A.G. Fane, Robust and High performance hollow fiber membranes for energy harvesting from salinity gradients by pressure retarded osmosis, Journal of Membrane Science, 448 (2013) 44-54.

[79] L.A. Hoover, J.D. Schiffman, M. Elimelech, Nanofibers in thin-film composite membrane support layers: Enabling expanded application of forward and pressure retarded osmosis, Desalination, 308 (2013) 73-81.

[80] R. Patel, W.S. Chi, S.H. Ahn, C.H. Park, H.-K. Lee, J.H. Kim, Synthesis of poly(vinyl chloride)-g-poly(3-sulfopropyl methacrylate) graft copolymers and their use in pressure retarded osmosis (PRO) membranes, Chemical Engineering Journal, 247 (2014) 1-8.

[81] A. Nguyen, S. Azari, L. Zou, Coating zwitterionic amino acid l-DOPA to increase fouling resistance of forward osmosis membrane, Desalination, 312 (2013) 82-87.

[82] H. Yoon, Y. Baek, J. Yu, J. Yoon, Biofouling occurrence process and its control in the forward osmosis, Desalination, 325 (2013) 30-36.

[83] H.J. Kim, D.G. Kim, H. Yoon, Y.S. Choi, J. Yoon, J.C. Lee, Polyphenol/FeIII Complex Coated Membranes Having Multifunctional Properties Prepared by a One-Step Fast Assembly, Advanced Materials Interfaces, 2 (2015).

[84] D.-G. Kim, H. Kang, S. Han, J.-C. Lee, The increase of antifouling properties of ultrafiltration membrane coated by star-shaped polymers, Journal of Materials Chemistry, 22 (2012) 8654-8661.

[85] W. Lee, C.H. Ahn, S. Hong, S. Kim, S. Lee, Y. Baek, J. Yoon, Evaluation of surface properties of reverse osmosis membranes on the initial biofouling stages under no filtration condition, Journal of Membrane Science, 351 (2010) 112-122.

[86] J. Yu, G.-A. Shin, B.S. Oh, J.-I. Kye, J. Yoon, N-chlorosuccinimide as a novel agent for biofouling control in the polyamide reverse osmosis membrane process, Desalination, 357 (2015) 1-7.

[87] J.D. Grunwaldt, U. Göbel, A. Baiker, Preparation and characterization of thin TiO_2-films on gold/mica, Fresenius J Anal Chem, 358 (1997) 96-100.

[88] C. Chen, H. Bai, C. Chang, Effect of Plasma Processing Gas Composition on the Nitrogen-Doping Status and Visible Light Photocatalysis of TiO_2, The Journal of Physical Chemistry C, 111 (2007) 15228-15235.

[89] G. Hopfengärtner, D. Borgmann, I. Rademacher, G. Wedler, E. Hums, G.W. Spitznagel, XPS studies of oxidic model catalysts: Internal standards and oxidation numbers, Journal of Electron Spectroscopy and Related Phenomena, 63 (1993) 91-116.

[90] P.Y. Jouan, M.C. Peignon, C. Cardinaud, G. Lempérière, Characterisation of TiN coatings and of the TiN/Si interface by X-ray photoelectron spectroscopy and Auger electron spectroscopy, Applied Surface Science, 68 (1993) 595-603.

[91] S.D. Gardner, C.S.K. Singamsetty, G.L. Booth, G.-R. He, C.U. Pittman Jr, Surface characterization of carbon fibers using angle-resolved XPS and ISS, Carbon, 33 (1995) 587-595.

[92] D.W. Zeng, K.C. Yung, C.S. Xie, XPS investigation of the chemical characteristics of Kapton films ablated by a pulsed TEA-CO_2 laser, Surface and Coatings Technology, 153 (2002) 210-216.

[93] L. Ren, F. Yang, C. Wang, Y. Li, H. Liu, Z. Tu, L. Zhang, Z. Liu, J. Gao, C. Xu, Plasma synthesis of oxidized graphene foam supporting Pd nanoparticles as a new catalyst for one-pot synthesis of dibenzyls, RSC Advances, 4 (2014) 63048-63054.

[94] T. Laiho, J.A. Leiro, M.H. Heinonen, S.S. Mattila, J. Lukkari, Photoelectron spectroscopy study of irradiation damage and metal–sulfur bonds of thiol on silver and copper surfaces, Journal of Electron Spectroscopy and Related Phenomena, 142 (2005) 105-112.

[95] W. Zhang, J. Shi, X. Wang, Z. Jiang, X. Song, Q. Ai, Conferring an adhesion layer with mineralization-inducing capabilities for preparing organic–inorganic

hybrid microcapsules, Journal of Materials Chemistry B, 2 (2014) 1371-1378.

[96] N. Nakayama, T. Hayashi, Preparation and characterization of poly(l-lactic acid)/TiO2 nanoparticle nanocomposite films with high transparency and efficient photodegradability, Polymer Degradation and Stability, 92 (2007) 1255-1264.

[97] G. Parfitt, The surface of titanium dioxide, Prog. Surf. Membr. Sci, 11 (1976) 181-226.

[98] T. Hanawa, M. Kon, H. Doi, H. Ukai, K. Murakami, H. Hamanaka, K. Asaoka, Amount of hydroxyl radical on calcium-ion-implanted titanium and point of zero charge of constituent oxide of the surface-modified layer, J. Mater. Sci. Mater. Med., 9 (1998) 89-92.

[99] K. Suttiponparnit, J. Jiang, M. Sahu, S. Suvachittanont, T. Charinpanitkul, P. Biswas, Role of Surface Area, Primary Particle Size, and Crystal Phase on Titanium Dioxide Nanoparticle Dispersion Properties, Nanoscale Research Letters, 6 (2011) 1-8.

[100] S. Bason, Y. Oren, V. Freger, Characterization of ion transport in thin films using electrochemical impedance spectroscopy: II: Examination of the polyamide layer of RO membranes, Journal of Membrane Science, 302 (2007) 10-19.

[101] T. Tsuru, M. Urairi, S.-I. Nakao, S. Kimura, Proceedings of the Twelfth International Symposium on Desalination and Water Re-useNegative rejection of anions in the loose reverse osmosis separation of mono- and divalent ion mixtures, Desalination, 81 (1991) 219-227.

[102] J. Cho, G. Amy, J. Pellegrino, Membrane filtration of natural organic matter:

comparison of flux decline, NOM rejection, and foulants during filtration with three UF membranes, Desalination, 127 (2000) 283-298.

[103] M.-L. Luo, J.-Q. Zhao, W. Tang, C.-S. Pu, Hydrophilic modification of poly(ether sulfone) ultrafiltration membrane surface by self-assembly of TiO_2 nanoparticles, Applied Surface Science, 249 (2005) 76-84.

[104] L. Zou, I. Vidalis, D. Steele, A. Michelmore, S.P. Low, J.Q.J.C. Verberk, Surface hydrophilic modification of RO membranes by plasma polymerization for low organic fouling, Journal of Membrane Science, 369 (2011) 420-428.

[105] G. Kang, M. Liu, B. Lin, Y. Cao, Q. Yuan, A novel method of surface modification on thin-film composite reverse osmosis membrane by grafting poly(ethylene glycol), Polymer, 48 (2007) 1165-1170.

[106] A.C. Sagle, E.M. Van Wagner, H. Ju, B.D. McCloskey, B.D. Freeman, M.M. Sharma, PEG-coated reverse osmosis membranes: desalination properties and fouling resistance, Journal of Membrane Science, 340 (2009) 92-108.

[107] R. Yang, J. Xu, G. Ozaydin-Ince, S.Y. Wong, K.K. Gleason, Surface-tethered zwitterionic ultrathin antifouling coatings on reverse osmosis membranes by initiated chemical vapor deposition, Chemistry of Materials, 23 (2011) 1263-1272.

[108] Y. Baek, J. Yu, S.-H. Kim, S. Lee, J. Yoon, Effect of surface properties of reverse osmosis membranes on biofouling occurrence under filtration conditions, J. Membr. Sci., 382 (2011) 91-99.

[109] M.Z. Atashbar, H.T. Sun, B. Gong, W. Wlodarski, R. Lamb, XPS study of Nb-doped oxygen sensing TiO_2 thin films prepared by sol-gel method, Thin Solid Films,

326 (1998) 238-244.

[110] K. Yamamoto, Y. Koga, S. Fujiwara, XPS studies of amorphous SiCN thin films prepared by nitrogen ion-assisted pulsed-laser deposition of SiC target, Diamond and Related Materials, 10 (2001) 1921-1926.

[111] L. Matuana, J. Balatinecz, R. Sodhi, C. Park, Surface characterization of esterified cellulosic fibers by XPS and FTIR spectroscopy, Wood Science and Technology, 35 (2001) 191-201.

[112] S. Delpeux, F. Beguin, R. Benoit, R. Erre, N. Manolova, I. Rashkov, Fullerene core star-like polymers—1. Preparation from fullerenes and monoazidopolyethers, European polymer journal, 34 (1998) 905-915.

[113] J. Charlier, V. Detalle, F. Valin, C. Bureau, G. Lecayon, Study of ultrathin polyamide-6, 6 films on clean copper and platinum, Journal of Vacuum Science & Technology A, 15 (1997) 353-364.

[114] V. Wiertz, P. Bertrand, Identification of the N-containing functionalities introduced at the surface of ammonia plasma treated carbon fibres by combined ToF-SIMS and XPS, (1998).

[115] S. Sablani, M. Goosen, R. Al-Belushi, M. Wilf, Concentration polarization in ultrafiltration and reverse osmosis: a critical review, Desalination, 141 (2001) 269-289.

[116] E.M.V. Hoek, M. Elimelech, Cake-Enhanced Concentration Polarization: A New Fouling Mechanism for Salt-Rejecting Membranes, Environmental Science & Technology, 37 (2003) 5581-5588.

[117] E. Matthiasson, B. Sivik, Concentration polarization and fouling, Desalination, 35 (1980) 59-103.

[118] V.G. Gude, Energy consumption and recovery in reverse osmosis, Desalination and Water Treatment, 36 (2011) 239-260.

[119] M.M. Pendergast, E.M. Hoek, A review of water treatment membrane nanotechnologies, Energy & Environmental Science, 4 (2011) 1946-1971.

[120] K.P. Lee, T.C. Arnot, D. Mattia, A review of reverse osmosis membrane materials for desalination—Development to date and future potential, J. Membr. Sci., 370 (2011) 1-22.

[121] J. Yin, E.-S. Kim, J. Yang, B. Deng, Fabrication of a novel thin-film nanocomposite (TFN) membrane containing MCM-41 silica nanoparticles (NPs) for water purification, Journal of Membrane Science, 423-424 (2012) 238-246.

[122] E.-S. Kim, G. Hwang, M. Gamal El-Din, Y. Liu, Development of nanosilver and multi-walled carbon nanotubes thin-film nanocomposite membrane for enhanced water treatment, Journal of Membrane Science, 394-395 (2012) 37-48.

[123] H.S. Lee, S.J. Im, J.H. Kim, H.J. Kim, J.P. Kim, B.R. Min, Polyamide thin-film nanofiltration membranes containing TiO_2 nanoparticles, Desalination, 219 (2008) 48-56.

[124] H.D. Lee, H.W. Kim, Y.H. Cho, H.B. Park, Experimental Evidence of Rapid Water Transport through Carbon Nanotubes Embedded in Polymeric Desalination Membranes, Small, 10 (2014) 2653-2660.

[125] W.F. Chan, H.Y. Chen, A. Surapathi, M.G. Taylor, X.H. Hao, E. Marand, J.K.

Johnson, Zwitterion Functionalized Carbon Nanotube/Polyamide Nanocomposite Membranes for Water Desalination, Acs Nano, 7 (2013) 5308-5319.

[126] D. Emadzadeh, W. Lau, M. Rahbari-Sisakht, A. Daneshfar, M. Ghanbari, A. Mayahi, T. Matsuura, A. Ismail, A novel thin film nanocomposite reverse osmosis membrane with superior anti-organic fouling affinity for water desalination, Desalination, 368 (2015) 106-113.

[127] S. Roy, S.A. Ntim, S. Mitra, K.K. Sirkar, Facile fabrication of superior nanofiltration membranes from interfacially polymerized CNT-polymer composites, Journal of Membrane Science, 375 (2011) 81-87.

[128] G.N.B. Baroña, J. Lim, M. Choi, B. Jung, Interfacial polymerization of polyamide-aluminosilicate SWNT nanocomposite membranes for reverse osmosis, Desalination, 325 (2013) 138-147.

[129] W.-g. Kim, S. Nair, Membranes from nanoporous 1D and 2D materials: A review of opportunities, developments, and challenges, Chemical Engineering Science, 104 (2013) 908-924.

[130] H. Huang, X. Qu, H. Dong, L. Zhang, H. Chen, Role of NaA zeolites in the interfacial polymerization process towards a polyamide nanocomposite reverse osmosis membrane, RSC Advances, 3 (2013) 8203.

[131] C. Kim, S. Kim, J. Lee, J. Kim, J. Yoon, Capacitive and oxidant generating properties of black-colored TiO_2 nanotube array fabricated by electrochemical self-doping, ACS Applied Materials and Interfaces, 7 (2015) 7486-7491.

[132] Y. Baek, J. Kang, P. Theato, J. Yoon, Measuring hydrophilicity of RO

membranes by contact angles via sessile drop and captive bubble method: A comparative study, Desalination, (2012).

[133] A.-h.M.A. El-Aassar, Improvement of reverse osmosis performance of polyamide thin-film composite membranes using TiO_2 nanoparticles, Desalination and Water Treatment, (2014) 1-12.

[134] H. Huang, X. Qu, X. Ji, X. Gao, L. Zhang, H. Chen, L. Hou, Acid and multivalent ion resistance of thin film nanocomposite RO membranes loaded with silicalite-1 nanozeolites, Journal of Materials Chemistry A, 1 (2013) 11343-11349.

국문초록

폴리아마이드 복합막(polyamide thin-film composite membrane)은 높은 투과수량과 염제거율, 넓은 pH, 온도 운전조건으로 현재 역삼투(reverse osmosis, RO)공정 및 나노여과(nanofiltration, NF) 공정에서 가장 많이 사용되고 있는 분리막이다. 또한, 압력지연 삼투공정(pressure retarded osmosis, PRO)에서도 cellulose acetate막의 대안으로 폴리아마이드 복합막을 사용하기 위해 연구되고 있다. 하지만 고압 운전에 의한 에너지 소비와 막오염 문제는 폴리아마이드 복합막의 해결해야 할 문제로 남아있다. 따라서 본 논문에서는 이러한 폴리아마이드 복합막의 단점을 개선하기 위해 타이타니아 나노물질을 첨가하여 고성능, 내오염성의 막을 개발하고자 하였다.

첫째로, 타이타니아 졸-겔 스프레이 코팅법을 통해 폴리아마이드 복합막의 표면을 타이타니아 나노입자(TiO_2 nanoparticles, TNPs)로 코팅하였다. 먼저 멤브레인에 적합한 코팅 조건을 찾기 위하여 졸-겔 반응의 용매, 티타늄전구체, 첨가제, 그리고 산/염기 촉매의 영향을 알아보았다. 암모늄하이드록사이드가 첨가된 졸-겔 스프레이 코팅이 역삼투막의 투과수량에 영향을 주지 않는 나노입자 사이즈를 형성하면서

내구성 높은 코팅 층을 형성하였다. 최적화된 타이타니아 졸-겔 스프레이 코팅 조건을 이용해 폴리아마이드 복합막을 코팅하여 압력지연삼투공정과 역삼투공정에서의 영향을 연구하였다. 타이타니아 나노입자가 폴리아마이드 복합막의 지지층에 코팅되었을 때 지지층의 표면이 친수화되고 음전하가 강해졌다. 타이타니아 나노입자로 코팅된 막은 PRO공정에서 25% 향상된 물 투과수량 성능을 보였고 염의 역확산을 50% 감소시켰다. Humic acid를 이용해 유기물오염 특성을 평가하였을 때 타이타니아 나노입자가 코팅된 막이 32% 덜 감소된 투과수량을 보였다. 또한, atomic force microscope 분석에서 타이타니아 나노입자로 코팅된 막이 humic acid-타니타니아 사이의 낮은 interaction 에너지를 보여 타이타니아 나노입자의 코팅이 폴리아마이드 복합막의 내오염성을 향상시키는 것으로 관찰되었다. 폴리아마이드 복합막의 활성층에 코팅되었을 때에도 마찬가지로 향상된 친수성과 음전하를 보였으며 RO공정에서 투과수량의 감소 없이 향상된 내오염성을 보였다.

둘째로, 타이타니아 나노물질을 폴리아마이드 복합막의 활성층에 첨가함으로써 RO공정에서의 투과수량 성능과 내오염성을 향상시켰다. 또한 타이타니아 나노튜브와 나노입자를 첨가한 폴리아마이드 복합막의 성능 변화를 비교함으로써 나노물질의 구조와 표면성질이 막의 성능에

미치는 영향을 분석하였다. 타이타니아 나노물질이 첨가된 폴리아마이드 복합막은 모두 향상된 표면 친수성과 투과수량을 보였다. 하지만 동일한 양의 타이타니아 나노튜브와 나노입자를 첨가하였을 때 표면 친수성은 비슷했지만 나노튜브가 첨가된 폴리아마이드가 더 높은 투과수량을 보여 나노튜브의 기공구조가 RO공정에서 폴리아마이드 복합막의 투과수량 향상에 더 기여했을 것으로 보인다.

본 연구의 결과에서 보였듯이, 타이타니아 나노물질의 첨가는 폴리아마이드 복합막의 투과수량 성능과 내오염성을 향상시켜 PRO공정과 RO공정에서 효율을 높일 수 있을 것으로 기대된다.

주요어: 타이타니아 졸-겔 스프레이 코팅; 표면 개질; 타이타니아 나노튜브 나노복합막; 압력지연삼투공정; 역삼투공정

학 번: 2009-23948

김 정 찬